Ann. Henri Poincaré 7 (2006), 1099–1211

1424-0637/061099-113, *published online* 2006-10-03
DOI 10.1007/s00023-006-0278-4

Annales Henri Poincaré

Fractional Hamiltonian Monodromy

Nikolaií N. Nekhoroshev, Dmitrií A. Sadovskií and Boris I. Zhilinskií

Abstract. We introduce fractional monodromy in order to characterize certain non-isolated critical values of the energy–momentum map of integrable Hamiltonian dynamical systems represented by nonlinear resonant two-dimensional oscillators. We give the formal mathematical definition of fractional monodromy, which is a generalization of the definition of monodromy used by other authors before. We prove that the $1{:}(-2)$ resonant oscillator system has monodromy matrix with half-integer coefficients and discuss manifestations of this monodromy in quantum systems.

1. Introduction

Qualitative understanding of the dynamics of classical mechanical systems is largely based on the study of simple completely or partially integrable approximations. Analysis of the corresponding quantum systems also relies on such approximations. Typically, we begin by uncovering universal qualitative features or phenomena in the dynamics of our simple models and then find which of these aspects are stable under transformation to the original complex system and how they can possibly be deformed. Such qualitative characteristics orient our physical intuition and form a basis of understanding, classifying and predicting the behavior of the original complex system.

In this paper we present *fractional monodromy* which is a generalization of "usual" or "integer" monodromy introduced earlier by Duistermaat [22] as the simplest topological obstruction to the existence of global action–angle variables. To our knowledge, we give the first description of this important new qualitative characteristics of classical integrable systems and their quantum analogues. In the announcement of our work [56] we suggested that fractional monodromy occurred in nonlinear resonant oscillators. Here we focus on the detailed mathematical definition of generalized monodromy, and then prove that the phenomenon of fractional monodromy does indeed occur in this important class of classical and quantum mechanical systems.

1.1. Review of related work

Most qualitative characteristics of an integrable Hamiltonian dynamical system are related to the geometry of the integral fibration defined by the first integrals of the system in involution. For a large class of integrable Hamiltonian dynamical systems, the Liouville–Arnol'd theorem [1, 51] says that the fibers are regular tori and the fibration is locally trivial. However, integral fibrations of many important physical systems have singular fibers and their topology is highly nontrivial. This makes the general study of the geometry of certain singular fibrations [61, 52, 44] an important part of the qualitative theory of Hamiltonian dynamical systems. Global topological description of integral fibrations in a general formal way was the subject of many publications by Fomenko and coworkers, see [8, 9] and references therein. A more concrete approach combines geometry and analytical methods and makes broad use of action–angle variables and their generalizations.

The Liouville–Arnol'd integrability leads generically to the existence of local action–angle variables [1, 2, 53, 54] which define period lattices on neighboring regular tori. Global action–angle variables do not always exist. Conditions for the existence of global action–angle variables and their generalizations were formulated in 1972 by Nekhoroshev [53, 54]. In 1980 Duistermaat asked the reciprocal question: what are obstructions to the existence of such variables? He introduced *monodromy* as the simplest topological obstruction [22]. Detailed analysis of monodromy and the corresponding singularities of toric fibrations followed [20, 73, 17], see [15] for more references.

The first concrete example of a simple classical Hamiltonian system with monodromy was the spherical pendulum, whose monodromy was studied by Cushman [14, 15]. *Quantum monodromy*, or the manifestation of monodromy of a classical system in the corresponding quantum system, was analyzed for the first time on the example of quantized spherical pendulum by Cushman and Duistermaat [16].

Subsequently, a number of other examples of classical integrable systems with monodromy was described [6, 37, 7], in particular the Champagne bottle potential and the Lagrange top [15], and more recently – the swinging spring [24]. Some particular examples of singularities, related to model two-degrees-of-freedom Hamiltonian systems with monodromy, i.e., systems with focus–focus singularity, were suggested and analyzed by Lerman [43], Matveev [45, 10, 46] and Zung [73, 74]. Nevertheless, in spite of this series of concrete studies, monodromy remained relatively unnoticed among many other topological properties of integrable dynamical systems. The broader mathematical community considers Hamiltonian dynamical systems with monodromy as a rather specific example of a general case of singular fibrations [9, 61, 52, 44].

Importance of monodromy became apparent to physicists in the mid-90's, when several fundamental systems, such as the hydrogen atom (an atomic Kepler system) perturbed by orthogonal electric and magnetic fields [18], diatomic molecular ion H_2^+ [67], symmetric top dipolar molecules rotating in electric field (molecular analogue of the Lagrange top) [41], rotating quasi-linear molecules, notably

the water molecule near the barrier to linearity [12], systems with several coupled (spin, orbital, vibrational, rotational, etc) angular momenta [60, 31] were shown to have monodromy. These concrete applications were in many ways inspired by Cushman, who made a great effort of introducing and explaining monodromy to physicists.

Of course, all atomic and molecular applications deal with quantum systems, and their monodromy should be analyzed on the basis of the quantum-classical correspondence principle and Einstein–Brillouin–Keller (EBK) quantization theory [64]. Another aspect is that these real physical systems are not integrable and their monodromy and quantization should be studied in the framework of the KAM theory [18, 58].

Manifestation of monodromy in quantum systems can be quite spectacular and simple at the same time. So it often happens that quantum monodromy of simple model quantum mechanical systems [60, 31, 66, 56] helps understanding and analyzing classical monodromy. Integer quantum monodromy is related primarily to *point defects* in the lattice of points in the image of the classical integral map (energy–momentum map) which correspond to regular integer values of local actions. In fact the idea of fractional monodromy [56] was initiated by a generalization of possible defects of such lattices [71].

It was shown more recently in [60, 31] that quantum monodromy is related intrinsically to the qualitative phenomenon of redistribution of the energy levels between quantum energy bands (branches, multiplets) which happens when some physical parameters of the system, such as strict or approximate integrals of motion, or simply, some constants in the potential, are varied. For further examples and analysis of this interesting phenomenon, which is observed frequently in atomic and molecular spectra, see [57, 59, 72, 11, 21, 27, 28, 29].

With our present paper, we hope to give a fresh impulse to the study of Hamiltonian monodromy and its manifestations in physics.

1.2. Organization of the paper

We begin in Sec. 2 by setting up a conceptual framework within which both the "standard" integer monodromy and the generalized fractional monodromy of integrable classical Hamiltonian systems can be naturally defined. Recall that Duistermaat [22] introduced monodromy to characterize a locally regular 2-torus bundle over a closed path (= loop) Γ in the base space of the integrable fibration F defined by two Hamiltonian functions (F_1, F_2) in involution. Thus integer monodromy of F is defined as a mapping between the space of regular closed loops Γ in the base space and the authomorphisms of the first homology group H_1 of regular fibers $\Lambda \sim \mathbb{T}^2$. Note that for regular fibers $\mathbb{T}^2$ instead of first homology group one can equivalently think about the fundamental group. Generalization to fractional monodromy arises when we allow this mapping to be defined for some subgroup of finite index of the homology group rather than for the entire homology group itself and at the same time extend in some special way the class of *admissi-*

ble closed paths Γ. We conclude by defining admissible integral fibrations F which have fractional monodromy.

In Sec. 3 we introduce concrete nonlinear resonant oscillator systems with two degrees of freedom which can have many applications in classical and quantum mechanics and which demonstrate that our requirements for admissible fibrations are quite natural and can be met in many Hamiltonian dynamical systems. We study the integral fibrations defined by the first integrals of our example systems, describe briefly the stratification of the image of the integral map (or the energy–momentum map $\mathcal{EM}$), and determine the topology of all singular fibers. The latter are further described in Appendix A. A more general description of $\mathcal{EM}$ and relevant details of reduction of the dynamical symmetry group S^1 and geometry of corresponding orbit spaces and reduced phase spaces are relegated to Appendix B.

Section 4 gives parallel statements about the standard (integer) monodromy of the $1{:}(-1)$ resonant oscillator and the fractional (half-integer) monodromy of the $1{:}(-2)$ resonant oscillator. We reproduce the known results about the monodromy of the $1{:}(-1)$ oscillator in order to compare it to the general case of the $m_1{:}(-m_2)$ resonance and to demonstrate our technique in the simplest case. Monodromy in the $1{:}(-2)$ case was not, up to our knowledge, studied prior to [56], and not computed explicitly before [25, 26] and our present work. This computation is the main result of our paper.

To our knowledge, there exist several different ways of computing monodromy in Hamiltonian systems with two degrees of freedom. The most "traditional" approach consists of a purely analytical study of the flow of the Hamiltonian vector fields (X_{F_1}, X_{F_2}) [15]. Such study results in an explicit construction of the *period lattice* on the regular tori. The period lattice is then continued along Γ in order to compute monodromy. In this way fractional monodromy of the $1{:}(-2)$ system has been computed recently in [25] after appropriate adaptations. At the same time it has been suggested on several occasions [10, 45, 46, 73, 74] that monodromy of systems with the isolated singular fiber Λ_0 was defined solely by the topology of Λ_0. This was formulated more rigorously in [17] in a form of the geometric monodromy theorem. As a consequence, all we have to do in order to find monodromy is to characterize Λ_0. This theorem does *not* apply in the $1{:}(-2)$ system because there Λ_0 is not isolated. Standard monodromy can be equally computed using the affine structure of the Lagrangian fibration which is closely related to Duistermaat-Heckman measure [23, 74]. But this approach was not yet applied to the case of fractional monodromy.

Our proof of the statements in Sec. 4 is of a different kind. It relies on the geometric (as opposed to dynamical) definition and continuation of cycles representing elements of the first homology group of fibers. Similar proofs are used in the theory of complex monodromy [5, 63]. Section 5 gives the idea of our proof relying on geometry and some intuition. We visualize directly the evolution of cycles representing basis elements of the first homology group $H_1(\Lambda)$ as we move along Γ. Appendices C and D detail the argument and present a number of technical analytical lemmas, which are needed to complete the mathematical

proof of the statements in Sec. 4. Therefore, the formal mathematical part of the paper which gives the proof of the existence of fractional monodromy consists of Secs. 2–5 and Appendices A, C, D. Section 5 gives a general picture of the evolution of cycles using internal charts on toric fibers of the integrable fibration in $\mathbb{R}^4$. A rigorous proof is given in Appendices C, D. It is based on the analysis of the geometry of the embedding of tori Λ in $\mathbb{R}^4$. This geometry is studied in detail using intersections of Λ with the hyper-plane $\sigma \subset \mathbb{R}^4$ which plays the role of the global non-regular Poincaré section.

Section 6 discusses monodromy of the corresponding quantum systems, i.e., resonant quantum oscillators, where monodromy manifests as a defect of the lattice of quantum states formed by the joint spectrum of quantum operators $(\hat{F}_1, \hat{F}_2)$ in the image of the energy–momentum map. The key point here is the correspondence between the transformation of basis elements of the homology group $H_1(\Lambda)$ and the associated transformation of vectors (or elementary cells) which characterize locally the lattice of quantum states.

Further in Sec. 7, we consider briefly and less formally the more general question of the relation between the lattice defects, which are widely studied in solid state physics [39, 47, 48, 42], and the presence of singular fibers in toric fibrations. On the basis of this relation we suggest a simple geometric interpretation of the lattice defects which correspond to the singular toric fibrations with integer and fractional monodromy.

2. Generalized definition of monodromy

In this section we introduce an ensemble of definitions which serves as a foundation of our mathematical analysis of fractional (or rational) monodromy. Consider[1] a Hamiltonian dynamical system with Hamiltonian H defined on a $2n$-dimensional symplectic manifold M. Consider also its open $2n$-dimensional subset $\tilde{\mathsf{M}} \subseteq \mathsf{M}$. *Regular integrability* of this system on $\tilde{\mathsf{M}}$ means that the following conditions are met.

Conditions 2.1.

i. There exists a set $F = (F_1, \dots, F_n)\colon \mathsf{M} \to \mathbb{R}$ of Hamiltonian functions in involution on M that are functionally independent on $\tilde{\mathsf{M}} \subseteq \mathsf{M}$. Specifically, at each point $x \in \tilde{\mathsf{M}}$ the differentials $(dF_1, \dots, dF_n)$ are linearly independent and $\{F_i, F_j\} = 0$ for all $i, j = 1 \dots n$.

ii. The Hamiltonian H can be locally represented on $\tilde{\mathsf{M}}$ as $H = \mathcal{H}(F_1, \dots, F_n)$ where $\mathcal{H}$ is any smooth function $\mathbb{R}^n \to \mathbb{R}$, or, equivalently, all functions $(F_1, \dots, F_n)$ are integrals of the system $\{H, F_i\} = 0$, $i = 1, \dots, n$.

Many important properties of regular and non-regular integrable systems depend only on the set F and on the fibration of the phase space M into common

[1]Unless the contrary is noted explicitly, everywhere below in this paper we assume that all manifolds, functions, and vector fields are C^∞-differentiable.

levels of functions F_i. Consequently, we can forget the concrete form of H and study just F. Note that in this article we mean by fibration the decomposition of the manifold into connected components of common levels of functions F_i. To describe and analyze such fibrations we consider the mapping

$$F\colon \mathsf{M} \to \mathbb{R}^n,$$

defined by functions F, where M and its image $F(\mathsf{M}) \subseteq \mathbb{R}^n$ are the *definition domain* and the *range* of F respectively. With some abuse of language, we will call the mapping F an *integrable map* or in some cases a (*generalized*) *energy–momentum map* $\mathcal{EM}$. Recall also that the *critical point* of map F is a point $x \in \mathsf{M}$ where the differentials $(dF_1, \ldots, dF_n)$ are linearly dependent; the *critical value* of F is the image $f = F(x) \in \mathbb{R}^n$.

2.1. Integrable fibrations

Consider again the manifolds M and $\tilde{\mathsf{M}} \subseteq \mathsf{M}$, the set of functions F, and the corresponding mapping F discussed above.

Definition 2.1. We call the fibration of M into connected components of the inverse images $F^{-1}(f)$ of points $f \in F(\mathsf{M}) \subseteq \mathbb{R}^n$ an *integrable fibration defined by* F. Note that for further convenience, we call each connected component of $F^{-1}(f)$, rather than the total inverse image $F^{-1}(f)$ itself, a *fiber* of this fibration. If functions F satisfy Condition i) of 2.1 on $\tilde{\mathsf{M}}$ we call this fibration *regular integrable fibration* of $\tilde{\mathsf{M}}$. Moreover, if all fibers are compact, we call it *regular and toric*.

Note that the manifold M and the range $B = F(\mathsf{M})$ of the integrable map F are the *total space* and the *base* of the integrable fibration F respectively.

Regular toric fibrations were studied from a slightly more general point of view in [54, 22] where, in particular, an arbitrary n-manifold B, rather than $B \subseteq \mathbb{R}^n$, was considered as a base. In this paper we consider only the case $B \subseteq \mathbb{R}^n$ which is sufficient for our purposes. All our definitions given below can be trivially adapted to the more general situation in [54, 22].

Certain singular fibrations were also studied, see for example a series of papers by Gross [32, 33, 34]. However, restrictions imposed on these fibrations, such as the requirement for the singular sets to be of dimension $n-2$, are too strong for our purposes. Below we define a class of admissible generally non-regular integrable fibrations. These fibrations are both relatively simple and quite natural and important from the point of view of possible applications.

2.2. Cellular structure of the phase space

Consider the set $\sigma \subset F(\mathsf{M}) \subseteq \mathbb{R}^n$ of all critical values of map F and the set $\mathsf{M}' := \mathsf{M} \setminus F^{-1}(\sigma)$ of inverse images of all non-critical values of this map.

Definition 2.2. The closure K of each connected component K^0 of the set M' is an *upper cell* of fibration F with regular inner part K^0 and boundary $\partial K^0 := K \setminus K^0$. The image $F(K)$ of the upper cell K is the *lower cell*.

Note that upper cells lie in M and intersect only on their boundaries, while lower cells lie in $\mathbb{R}^n$ and can be superimposed.

We suppose that the union $\cup_i \partial K_i^0$ of all boundaries of all upper cells has the form $\cup_i \partial K_i^0 = \left(\cup_j W_j\right) \cup S$ with sets W_i and S satisfying the following conditions:

Conditions 2.2.

i. S is a subset of the union of smooth manifolds N_k of dimension at most $2n-2$ with piecewise smooth boundary: $S \subseteq \cup N_k$, $\dim N_k \leq 2n-2$.
ii. Each set W_i is a $(2n-1)$-dimensional connected closed manifold with piecewise smooth boundary ∂W_i.
iii. Hypersurfaces W_i can intersect only on ∂W_i, i.e., $W_i \cap W_j = \partial W_i \cap \partial W_j$. If some internal point of W_j belongs to the cell K_i, then the whole hypersurface W_j is part of K_i. There are at most two cells, which can contain the same surface W_j.
iv. Each compact subspace of M intersects only a finite number of cells K_i, and hypersurfaces W_j and N_k.

Definition 2.3. We call fibration F which satisfies Conditions 2.2 *admissible* and we call the hypersurfaces W_i *walls*. Each wall either belongs to a common boundary of two neighboring upper cells or lies inside one cell.

Note that cells, their regular inner parts, and their boundaries are unambiguously defined by F. Furthermore, it is clear that the integrable fibration F is regular in the inner part K^0 of each cell K. In this work we will consider only *toric cells*, i.e., cells K for which F is toric on K^0.

Trivial example of cellular structure. As an example of cellular structure and walls, consider singular fibration F defined by constant level sets of one function of two variables

$$F\colon \mathbb{R}^2 \to \mathbb{R}\colon (x,y) \to x^4 + y^4 - 5^2(x^2+y^2), \tag{2.1}$$

see Fig. 1, left. The total space $\mathbb{R}^2_{x,y}$ of the corresponding fibration is decomposed into six upper cells as shown in Fig. 1, center. The base B of this fibration is a half-line $B = \{f \geq -\frac{1}{2}5^4\} \subset \mathbb{R}$ where the six lower cells are superimposed as shown schematically in Fig. 1, right, in the form of a one-dimensional Reeb graph.

2.3. Admissible paths through walls

Consider two upper cells K_{l} and K_{r}, which we call "left" and "right" respectively, and which are separated by wall W. Let us fix a piece-wise smooth "local" path $\delta\colon [0,1] \to \mathsf{M}$ which goes from K_{l} to K_{r} and intersects W transversally at some inner point ξ_W of W. We suppose that ξ_W is the only point of δ which belongs to a wall and consequently, one part of $\delta \setminus \{\xi_W\}$ belongs to the regular inner part K_{l}^0 of K_{l}, whereas the other part belongs to K_{r}^0. In particular let $\xi_0 := \delta(0) \in K_{\mathrm{l}}^0$ and $\xi_1 := \delta(1) \in K_{\mathrm{r}}^0$ be the initial (left) and the final (right) point of the path δ, respectively. For each $\xi \in \delta$ belonging to K_{l}^0 or K_{r}^0, we denote by $\mathbb{T}^n_\xi \ni \xi$ the torus of the left or the right regular toric fibration which the path δ crosses at point

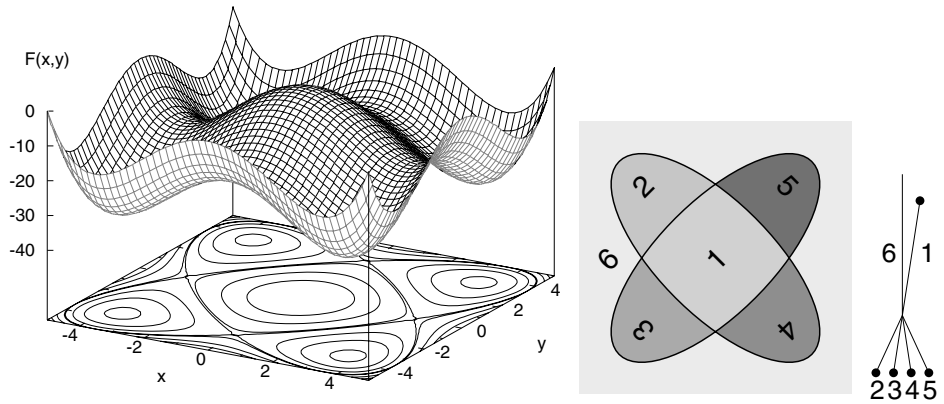

FIGURE 1. Cellular structure in the case of the fibration of the plane $\mathbb{R}^2_{x,y}$ defined by the levels of function (2.1): the 3D-image of the function and its 2D-contour plot (left), the system of upper cells (center), the system of lower cells as a Reeb graph of the base space (right).

$\xi = \mathbb{T}^n_\xi \cap \delta$. We now consider a cycle[2] γ_0 on torus $\mathbb{T}^n_{\xi_0}$ and introduce a deformation of γ_0 along the path δ resulting in the cycle γ_1 on torus $\mathbb{T}^n_{\xi_1}$.

Definition 2.4. We call the *deformation* $\{\gamma_t \subset \mathbb{T}^n_{\delta(t)},\ 0 \le t \le 1\}$ of the cycle γ_0 along the path δ *admissible* and the cycle γ_0 itself *passable*, if

i. For each $\xi \neq \xi_W$, all loops forming γ_t lie on torus $\mathbb{T}^n_\xi$ and vary smoothly and independently from each other with $\xi = \delta(t)$.
ii. At point ξ_W the deformation γ_t should be at least continuous; splitting and fusion of orientable loops are allowed.

For example, the cycle γ_0 which consists of k loops can transform into the cycle γ_1 with k' loops. When γ_t passes across the wall W, the k loops forming cycle γ_t in the left cell break into oriented fragments which are reassembled into new k' loops forming cycle γ_t in the right cell. *The orientation of all fragments is conserved* in this process.

We remind that the classes of homologically equivalent cycles form the first homology group H_1 of the manifold M. The first homology group of the n-dimensional torus $\mathbb{T}^n$ is isomorphic to the regular lattice $\mathbb{Z}^n$ and coincides with the fundamental group of $\mathbb{T}^n$. With this isomorphism in mind, cycles γ_0 and γ_1, which we introduced above, define elements g_0 and g_1 of groups $\mathbb{Z}^n_0 := H_1(\mathbb{T}^n_{\xi_0})$ and $\mathbb{Z}^n_1 := H_1(\mathbb{T}^n_{\xi_1})$ respectively. The admissible deformation γ_t establishes the correspondence between the elements $g_0 \in \mathbb{Z}^n_0$ and $g_1 \in \mathbb{Z}^n_1$.

[2]We call *loop* any closed oriented path and we call *cycle* any finite set of loops.

Definition 2.5. We call a piecewise smooth local path δ *admissible* if

i. All admissible deformations of cycles along δ define the map
$$\mu_\delta \colon \zeta_0^n \to \zeta_1^n, \tag{2.2}$$
which is the isomorphism of some subgroups $\zeta_0^n \subseteq \mathbb{Z}_0^n$ and $\zeta_1^n \subseteq \mathbb{Z}_1^n$.

ii. The subgroups ζ_0^n and consequently ζ_1^n are *complete* subgroups, i.e., they are themselves isomorphic to $\mathbb{Z}^n$.

Notice that δ in the above definition does not necessarily traverse a wall, but if it does, the crossing of the wall is transversal.

Furthermore we like to remind that in a hamiltonian dynamical system, the lattices $\mathbb{Z}^n$ (and their complete sublattices ζ^n) are defined up to an orientation preserving isomorphism which is given by conjugation with elements in $\mathrm{SL}(n,\mathbb{Z})$. So unless specified otherwise, we will refer to such $\mathrm{SL}(n,\mathbb{Z})$ isomorphisms of $\mathbb{Z}^n$ lattices.

Example of non-admissible paths. We illustrate the notion of passable cycles and admissible paths on our example of the singular fibration (2.1) presented in Fig. 1. Consider a path δ_{12} which goes from the upper cell 1 to the upper cell 2 separated by the wall W_{12}. The path δ_{12} crosses W_{12} at ξ_W. With each regular point $\xi \neq \xi_W$, $\xi \in \delta_{12}$ of upper cells 1 and 2 we associate a one-dimensional torus $\mathbb{T}^1_\xi = \mathbb{S}^1_\xi$ of the respective regular toric fibration. The path δ_{12} crosses $\mathbb{T}^1_\xi$ at the point $\xi = \mathbb{T}^1_\xi \cap \delta_{12}$. On each such torus, there are contractible (i.e., homotopic to zero) and non-contractible cycles. It is easy to see that only contractible cycles are passable across W_{12} because any non-contractible cycle undergoes a discontinuous transformation at ξ_W. This means that the subgroup formed by classes of homotopically equivalent passable cycles is not complete and the path δ_{12} is not admissible.

2.4. Definition of monodromy

In order to introduce monodromy we associate mapping μ_δ in (2.2) with a *closed* path δ.

Definition 2.6. We call a closed path δ in the phase space *admissible* if

i. It is piece-wise smooth.

ii. It can be split into fragments in such a way that each fragment is an admissible local path which may or may not cross a wall.

iii. Each point of the intersection of δ with the union of boundaries of all upper cells belongs to the inner part of one of the walls.

Notice that it is possible for some boundary points of a cell to be not part of any wall.

We now consider an admissible closed path δ formed by s fragments δ_i and denote regular points which separate δ into these fragments as $\xi_0, \ldots, \xi_{s-1}$ and $\xi_s = \xi_0$. Each fragment $\delta_i := [\xi_{i-1}, \xi_i] \subset \cup_{i=1}^s \delta_i = \delta$ is an admissible path. We denote the homology group $H_1(\mathbb{T}^n_{\xi_i})$ for each $i = 0, \ldots, s-1$ as $\mathbb{Z}_i^n$ and we let $\mathbb{Z}_s^n \equiv \mathbb{Z}_0^n$. Each fragment δ_i defines the map $\mu_i \colon \zeta_{i-1} \to \zeta_i'$, where for each $i = 0, \ldots, s-1$, groups ζ_i and ζ_i' are some complete subgroups of $\mathbb{Z}_i^n$ while ζ_0 and ζ_s'

are some complete subgroups of $\mathbb{Z}_0^n$. Using the known fact that the intersection of complete subgroups of $\mathbb{Z}^n$ is again a complete subgroup, we can easily prove that there exist two complete subgroups $\zeta \subseteq \zeta_0$ and $\zeta' \subseteq \zeta'_s$ of $\mathbb{Z}_0^n$ such that the composition of maps $\mu := \mu_s \circ \mu_{s-1} \circ \cdots \circ \mu_1$ is defined on ζ and maps ζ to ζ'. Moreover, the map $\mu\colon \zeta \to \zeta'$ defines an isomorphism of these two complete subgroups of $\mathbb{Z}_0^n$.

Definition 2.7. We call the constructed map $\mu\colon \zeta \to \zeta'$ of a complete subgroup ζ of the homology group $H_1(\mathbb{T}^n_{\xi_0})$ to a complete subgroup ζ' of the same homology group the *monodromy map* associated with the admissible closed path δ with marked point ξ_0.

Notice that the endpoints ξ_i of fragments δ_i are regular points of δ and the fragments can be smoothly deformed if we move the endpoints on δ without crossing any walls. Furthermore, we can take any such endpoint as $\xi_0 \equiv \xi_s$ to mark the start on δ. In fact, the following property of the monodromy map μ can be easily verified.

Proposition 2.1. *The monodromy map μ depends on the orientation of the path δ, but does not depend on the parameterization of δ or on the choice of the marked endpoint ξ_0 in the following sense. For any other regular endpoint $\tilde{\xi}_0 \in \delta$, which we can choose instead of ξ_0, the map μ remains the same up to the conjugation given by an isomorphism of lattices $H_1(\mathbb{T}^n_{\xi_0})$ and $H_1(\mathbb{T}^n_{\tilde{\xi}_0})$.*

2.4.1. Matrix of monodromy. Let δ be some admissible closed path with marked point ξ_0 and corresponding lattice $\mathbb{Z}_0^n := H_1(\mathbb{T}^n_{\xi_0})$, and let $\mu_{(\delta,\xi_0)}\colon \zeta \to \zeta'$, where $\zeta \subseteq \mathbb{Z}_0^n$ and $\zeta' \subseteq \mathbb{Z}_0^n$ are complete sublattices, be the corresponding monodromy map. Let us consider a natural canonical inclusion of $\mathbb{Z}_0^n$ into a linear space $\mathbb{R}^n$ where $\mathbb{Z}_0^n$ becomes a subgroup of $\mathbb{R}^n$. Since ζ and ζ' are complete, the map $\mu_{(\delta,\xi_0)}$ can be *extended* to a non-degenerate linear operator $\mu\colon \mathbb{R}^n \to \mathbb{R}^n$ defined on the whole $\mathbb{R}^n$. By taking an arbitrary basis on $\mathbb{Z}_0^n$ we can construct the matrix M of the map μ.

Definition 2.8. We call M *generalized* or *extended monodromy matrix*. It represents the monodromy map $\mu_{(\delta,\xi_0)}$ in a given basis of the group $H_1(\mathbb{T}^n_{\xi_0})$.

Let $\mathbb{Q}$ denote the field of rational numbers. It is not hard to prove

Proposition 2.2. *Monodromy matrix M has rational coefficients: $M \in \mathrm{GL}(n, \mathbb{Q})$.*

Using Proposition 2.1 we obtain

Proposition 2.3. *For a different basis on $\mathbb{Z}_0^n$, or the endpoint ξ_0 on δ, the monodromy matrix M remains the same up to conjugation $A^{-1}MA$ with matrices $A \in \mathrm{SL}(n, \mathbb{Z})$.*

We will define different kinds of monodromy using certain properties of monodromy map μ and corresponding matrix M. Let $\mathrm{GL}(n, \mathbb{Z})$ denote a group of n-dimensional matrices over integers with determinant ± 1.

Definition 2.9. We call matrices from $\mathrm{GL}(n,\mathbb{Z})$ and $\mathrm{GL}(n,\mathbb{Q})\setminus\mathrm{GL}(n,\mathbb{Z})$ *integer* and *fractional* matrices respectively.

The following simple facts about integer and fractional matrices are useful in order to distinguish integer and fractional monodromy.

Proposition 2.4. *If M is fractional, then either M itself or its inverse M^{-1} has at least one non-integer coefficient. If M is integer (fractional) and A is integer then any conjugated matrix $A^{-1}MA$ is also integer (fractional).*

Definition 2.10. We call the monodromy map $\mu_{(\delta,\xi_0)}$ *trivial*, *integer*, or *fractional*, if in some (and consequently in any) basis of the homology group $H_1(T^n_{\xi_0})$ it is represented by the identity matrix, an integer matrix, or a fractional matrix, respectively.

Notice that being integer or fractional is property of the map $\mu_{(\delta,\xi_0)}$ rather than of the monodromy matrix M. This property depends neither on the parameterization or the orientation of the path δ, nor on the choice of the basis in $H_1(\mathbb{T}^n_{\xi_0})$ and of the point $\xi_0 \in \delta$ (see Propositions 2.1, 2.3, and 2.4). Thus we can give a basis-independent definition of integer monodromy.

Definition 2.11. The monodromy map $\mu_{(\delta,\xi_0)}$ is called *integer* if it can be extended linearly to an automorphism of the whole lattice $H_1(\mathbb{T}^n_{\xi_0}) \sim \mathbb{Z}^n$ onto itself.

Recall that in Definition 2.7 we have associated the monodromy map $\mu = \mu_{\delta,\xi_0}$ (and the corresponding matrix $M = M_{\delta,\xi_0}$) with a particular admissible closed path δ and a marked endpoint ξ_0 on it. We then showed (Proposition 2.1) that μ did not depend essentially, i.e., up to the usual conjugation with elements in $\mathrm{SL}(n,\mathbb{Z})$, on the choice of ξ_0 and on the fragmentation and parameterization of δ. We assume now that μ also has the natural property to remain essentially invariant under certain deformations of δ. To specify the class of such admissible deformations we first study deformations of open admissible local paths (see Def. 2.5). Let $\delta\colon [0,1] \to \mathsf{M} \subseteq \mathbb{R}^{2n}\colon t \to \delta(t)$ be such path which goes through a wall W at an internal point ξ_W of W. We consider deformation $\delta_\tau\colon [0,1] \to \mathsf{M}$ of $\delta := \delta_\tau\big|_{\tau=0}$, which depends continuously on τ when $0 \le \tau \le 1$, and we require the path δ_τ to remain admissible for all $0 \le \tau \le 1$.

Definition 2.12. We call such deformation of the admissible local path δ *W-continuous.*

Notice that the local path δ_τ goes across W from the left cell to the right cell at point $\xi_{W,\tau}$. Since δ_τ depends continuously on τ, points $\xi_{W,\tau}$ for all $0 \le \tau \le 1$ belong to the interior of the same wall W.

Let $\gamma \subset \mathbb{T}^n_{\delta(0)}$ be a cycle which is passable through the wall W. By Definition 2.4, we can find an admissible deformation $\{\gamma_t,\, t \in [0,1]\}$ of $\gamma = \gamma_0 = \gamma_t\big|_{t=0}$ along the path $\delta\colon [0,1] \to \mathsf{M}\colon t \to \delta(t)$. Let us assume additionally that our deformation can be extended continuously in τ for any $0 \le \tau \le 1$ to the admissible deformation $\{\gamma_{(t,\tau)}; t \in [0,1]\}$ of the cycle $\gamma_{(0,\tau)}$ along the path δ_τ. We thus ob-

tain a two-parameter family $\big\{\{\gamma_{(t,\tau)};\tau\in[0,1]\};t\in[0,1]\big\}$ of cycles. The point $\xi=\delta_\tau(t)\in\mathsf{M}$ and the cycle $\gamma_{(t,\tau)}$ on the torus $\mathbb{T}^n_\xi\ni\xi$ change continuously when (t,τ) varies within the region $\{\tau\in[0,1],t\in[0,1]\}$.

Definition 2.13. We call such deformation of the admissible local path δ^0 *acceptable.*

Definition 2.14. We call the wall W *semi-permeable* if any W-continuous deformation of any admissible path through this wall is acceptable.

Notice that all walls in our example (2.1) are not semi-permeable. In fact, it is quite likely that no semi-permeable walls exist in the case of one degree of freedom.

We now come back to the admissible closed path δ and corresponding monodromy map μ_δ in Definitions 2.6 and 2.7.

Definition 2.15. Continuous deformation $\{\delta_\tau;0\le\tau\le1\}$ of the initial admissible closed path $\delta=\delta_\tau\big|_{\tau=0}$ is *acceptable* if

i. The path δ_τ is an admissible closed path for each $0\le\tau\le1$.
ii. The path δ and, consequently, all its deformations δ_τ with $0\le\tau\le1$ can cross cell boundaries only at internal points of semi-permeable walls.

Since cycles $\gamma_{(t,\tau)}$ depend continuously on (t,τ) the following proposition is evident.

Proposition 2.5. *The monodromy map μ_δ is conserved under given acceptable deformations of the admissible closed path δ.*

From this and Proposition 2.2 we also obtain

Corollary 2.1. *Under any acceptable deformations of δ, the monodromy matrix $M_0=M_{\delta_0}$ transforms into a matrix $M_\tau=M_{\delta_\tau}=B_\tau^{-1}M_0B_\tau$ conjugated with matrices B_τ from $\mathrm{SL}(n,\mathbb{Z})$ for all $0\le\tau\le1$. In particular, the monodromy map μ_δ persists to be either trivial, integer, or fractional.*

2.4.2. Local monodromy. Let $\delta=\delta_0$ be an admissible closed path. Suppose that there exists such deformation $\{\delta_\tau;0\le\tau\le1\}$ of δ that the final path $\delta_1=\{\xi_0\}$ coincides with a point $\xi_0\in\mathsf{M}$, and that for any $\kappa\in[0,1)$ deformation $\{\delta_{\kappa\tau};0\le\tau\le1,\kappa\tau\in[0,1)\}$ is admissible.

Definition 2.16. In this case, we call the monodromy map $\mu=\mu_\delta$ corresponding to the path δ *local.* We call ξ_0 the *central point of local monodromy.*

It is easy to see that if at least one central point of a local monodromy map μ belongs to the inner part W^0 of a wall W then μ is trivial. On the other hand, if local monodromy map μ_δ is nontrivial, then the set X of all its central points belongs to the union $\cup\partial K_i$ of boundaries of all upper cells of the fibration, but does not belong to the union $\cup W^0$ of the inner parts of all walls: $X\subset\cup\partial K_i\setminus\cup W^0_j$.

3. Concrete example of integrable fibrations with monodromy

We consider a particular class of integrable Hamiltonian systems with two degrees of freedom defined on the domain M of the linear symplectic space $\mathbb{R}^4_{p,q}$ with coordinates $(p,q)=(p_1,q_1,p_2,q_2)$ and standard symplectic structure $dq_1\wedge dp_1+dq_2\wedge dp_2$. Let

$$F_1 = m_1\tfrac{1}{2}(p_1^2+q_1^2) - m_2\tfrac{1}{2}(p_2^2+q_2^2) + R_1(q,p), \tag{3.1a}$$

$$F_2 = \operatorname{Im}\big[(q_1+ip_1)^{m_2}(q_2+ip_2)^{m_1}\big] + R_2(q,p), \tag{3.1b}$$

with values $(f_1,f_2)\in\mathbb{R}^2$ be the two first integrals of this system; (f_1,f_2) will be also denoted as (m,h). Note that parameters m_1 and m_2 in (3.1a), and (3.1b) are positive integers with largest common divisor equal 1. In what follows we will limit ourselves mainly to two important cases, namely $m_1=m_2=1$ and $m_1=1, m_2=2$. Furthermore, the "vector function" $R(p,q)=\big(R_1(p,q),R_2(p,q)\big)$ is chosen so that $R(p,q)$ and $F(p,q)=\big(F_1(p,q),F_2(p,q)\big)$ satisfy the following conditions

Conditions 3.1.

1. The connected component Λ_0 of $F^{-1}(0)$ contains $0\in\mathbb{R}^4$, is compact in $\mathbb{R}^4$, and R is defined in some neighborhood $U\subseteq\mathbb{R}^4$ of $\Lambda_0\subset U$.
2. F_1 and F_2 are in involution in U, i.e., $\{F_1,F_2\}=0$ in U.
3. All points $\xi\in\Lambda_0\setminus 0$ are regular, i.e., $\operatorname{rank}F(\xi)=2$ at any point $\xi\in\Lambda_0\setminus 0$; point $\xi=0$ is singular with $\operatorname{rank}F(0)=0$.
4. Compared to the first terms of F_1 in (3.1a) and F_2 in (3.1b) R_1 and R_2 are small in U. More precisely, $\deg R_1\geq 3$ and $\deg R_2\geq(m_1+m_2+1)$ in their respective Taylor series at 0.

We study the integral map $F\colon\mathbb{R}^4_{p,q}\to\mathbb{R}^2\colon(p,q)\to(m,h)$ defined by (3.1) and the corresponding integral fibration F whose fibers $F^{-1}(m,h)$ are mutual common level sets of functions (F_1,F_2) in (3.1). The following proposition can be easily proven.

Proposition 3.1. *When F satisfies Conditions* 3.1*, all connected components $\Lambda\subset U$ of $F^{-1}(m,h)$ which lie near Λ_0 are compact.*

It thus follows that the main purpose of the choice of R specified by Conditions 3.1 is to *compactify* the sets Λ.

Remark 3.1. The system with Hamiltonian F_1 in (3.1a) which satisfies Conditions 3.1 represents a nonlinear perturbation of the harmonic 2-oscillator in $m_1{:}(-m_2)$ resonance. This is why we say that integrable maps defined by equations (3.1) and Conditions 3.1 correspond to the $m_1{:}(-m_2)$ resonant nonlinear oscillator systems.

3.1. Concrete choice of the compactifier R

We will consider a particular continuous family

$$R = R^{(\tau,s)} = \Big(R_1^{(\tau)}, R_2^{(\tau,s)}\Big)$$

of functions satisfying Conditions 3.1 and choose its first member as

$$R_1^{(0)}(p,q) \equiv 0, \tag{3.2a}$$

$$R_2^{(0,s)}(p,q) = \left[m_1 \tfrac{1}{2}(p_1^2+q_1^2) + m_2 \tfrac{1}{2}(p_2^2+q_2^2)\right]^s, \text{ with } s > \tfrac{1}{2}(m_1+m_2). \tag{3.2b}$$

It can be easily verified that R in (3.2) satisfies Conditions 3.1 in $U \subset \mathbb{R}^4_{p,q}$. Furthermore, computing the phase flow of the system with Hamiltonian F_1 gives the following lemma.

Lemma 3.1. *The phase flow $g^t_{F_1^{(0)}} : \mathbb{R} \times \mathbb{R}^4_{q,p} \to \mathbb{R}^4_{q,p}$ of the system with Hamiltonian F_1 defined in* (3.1a) *with $R_1 = 0$ is periodic. The point $0 \in \mathbb{R}^4_{q,p}$ is the only fixed point of this flow; other points lie on $\mathbb{S}^1$ orbits.*

Extended versions of this lemma for the concrete cases of resonances $1{:}(-1)$ and $1{:}(-2)$ are proven, respectively, in Appendices C and D as Lemmas C.1 and D.1.

Corollary 3.1. *The integrable map $F^{(0)}$ defined by* (3.1) *and* (3.2) *with $R_1 = 0$ has an S^1 Lie symmetry whose action is defined by the flow $g^t_{F_1^{(0)}}$. The Hamiltonian vector field $X_{F_1^{(0)}}$ is the infinitesimal generator of this S^1 action.*

Remark 3.2. The map $F^{(0)} : \mathbb{R}^4_{p,q} \to \mathbb{R}^2 : (p,q) \to (m,h)$ defined by (3.1) and (3.2) is a particular case of an integrable map which is often called the *energy–momentum map* $\mathcal{EM}$, and which can also be considered as an extension of the momentum mapping defined by $F_1^{(0)}$, see Chap. B.3 in [15]. In our case one can interpret $F_1^{(0)}$ as momentum and $F_2^{(0)}$ as energy. In a general situation of eqs. (3.1) and (3.2) we have no Lie symmetry S^1 and neither of the two integrals (F_1, F_2) defining the integrable fibration has a periodic flow and can be considered as momentum. At the same time, any smooth function $H(F_1, F_2)$ can be considered as energy.

3.2. Energy–momentum mapping $\mathcal{EM}^{(0)}_{m_1:(-m_2)}$

Before formulating in Sec. 4 the monodromy theorems for the two particular important cases with $m_1 = m_2 = 1$ and $m_1 = 1$, $m_2 = 2$ which constitute the main topic of our work, we discuss briefly the structure of the energy–momentum map $\mathcal{EM}^{(0)}_{m_1:(-m_2)} := F^{(0)}$ for these two cases, $m_1 = 1$, $m_2 = 1, 2$. We draw attention to several rather evident and useful properties of this map and of the corresponding integrable fibration in the neighborhood of the singular fiber $\Lambda_0 \in \mathbb{R}^4$ and the corresponding singular value $0 \in \mathbb{R}^2$.

We recall that points $\xi \in R^4_{q,p}$ at which the rank of the Jacobian matrix $\partial F/\partial(q,p)$ is less than 2 are *critical points* of $\mathcal{EM}$, and the corresponding values $c = \mathcal{EM}(\xi) \in R^2_{m,h}$ are *critical values*. The inverse images $\mathcal{EM}^{-1}(c)$ of the critical values c are *singular fibers* (in more general situation they are union of singular and possibly regular fibers). Specific singular fibers of dimension 2, the *pinched torus* and the *curled torus*, which occur in our example of integrable fibrations are discussed in Appendix A. If (m,h) is a *regular value* then $\operatorname{rank}\big(\partial F/\partial(q,p)\big) = 2$

at all points $(q,p) \in \mathcal{EM}^{-1}(m,h)$. We call c an *isolated critical value* if all values in a sufficiently small neighborhood of c in $\mathbb{R}^2$ are regular.

Proposition 3.2. *The point $0 \in \Lambda_0 \subset \mathbb{R}^4$ is the critical point of rank 0 of the map $\mathcal{EM} = \mathcal{EM}^{(0)}_{m_1:(-m_2)}$ both in the case $m_1 = m_2 = 1$ and in the case $m_1 = 1$, $m_2 = 2$. In the case $m_1 = m_2 = 1$ it is the isolated critical point.*

Proposition 3.3. *When $m_1 = 1$ and $m_2 = 2$, the set Σ_0 of all critical points of $\mathcal{EM}$ in the small neighborhood U_0 of $0 \in \Lambda_0 \subset \mathbb{R}^4_{q,p}$ includes the intersection of U_0 with the two-dimensional plane $\{p_1 = q_1 = 0\}$. The intersection $\Lambda_0 \cap \Sigma_0$ consists of one single point $0 \in \mathbb{R}^4$. All points of the two-dimensional surface $\Sigma_0 \setminus 0 \subset U_0$ are critical points of rank 1 of the $\mathcal{EM}$ map. The surface $\Sigma_0 \setminus 0$ is filled by periodic trajectories γ_c of the system with Hamiltonian $F_1^{(0)}$. These trajectories γ_c are singular orbits of the S^1 group action where S^1 is the group in Corollary 3.1. Orbits γ_c have nontrivial discrete isotropy group $Z_2 \subset S^1$. Specifically, 2π being the period of the regular orbit of the S^1 action, orbits γ_c are of period π.*

Proposition 3.4. *The value $\mathcal{EM}(0) = 0 \in \mathbb{R}^2_{m,h}$ is the critical value of $\mathcal{EM}$. In the case of $1{:}(-1)$ resonance and only in this case the critical value 0 is isolated. When $m_1 = 1, m_2 = 2$, there is a continuous family of other critical values $\mathcal{C}_- = \{m < 0, h = h_-(m)\}$ of $\mathcal{EM}$ such that $h_-(0) = 0$.*

Definition 3.1. We call the set $\Sigma_0 \subset U_0 \subset \mathbb{R}^4_{q,p}$ in Proposition 3.3 and the set $\mathcal{C}_- \subset \mathbb{R}^2_{m,h}$ in Proposition 3.4 *plane of critical points* and *line of weak critical values* respectively.

Remark 3.3. The function $h_-(m)$ defining the line of critical values $\mathcal{C}_- \subset \mathbb{R}^2_{m,h}$ depends on the choice of "basic" functions $\{F_1, F_2\}$. In this work we will use $\{F_1, F_2\}$ with F_2 defined in (3.1b) and R_2 in (3.2b). In this case $h_-(m) = m^s$ for $m < 0$ with $s = 2$ in the case of $1{:}(-2)$ resonance, see Fig. 2 and Appendices B and D. In the same situation the authors of [25] use $F_1' = F_1$ and $F_2' = F_2 - F_1^2$, so that their critical line is part of $\{h = 0\}$.

Proposition 3.5. *The fiber $\Lambda_0 \ni 0$ of the integrable fibration defined by $\mathcal{EM}$ is a singular 2D variety called* pinched torus. *This fiber coincides with $\mathcal{EM}^{-1}(0)$, its inner topological type is the same for $m_1 = m_2 = 1$ and $m_1 = 1, m_2 = 2$. The fiber Λ_0 has one single critical point $0 \in \mathbb{R}^4_{q,p}$ of rank 0.*

All other fibers $\Lambda_{m,h}$ which lie near Λ_0 are connected and compact and coincide with $\mathcal{EM}^{-1}(m,h)$. When $m_1 = m_2 = 1$, and only in this case, all such fibers are regular 2-tori. When $m_1 = 1, m_2 = 2$, we find singular fibers $\Lambda_- = \mathcal{EM}^{-1}(m,h)$ with $(m,h) \in \mathcal{C}_-$ which lie arbitrarily close to Λ_0. The topology of each singular fiber $\Lambda_{m,h} \subset \Lambda_-$ is that of an 2-curled torus. *Each fiber $\Lambda_{m,h} \subset \Lambda_-$ has a circle $\Lambda_{m,h} \cap \Sigma_0$ of critical points of rank 1.*

Propositions 3.2, 3.4, and 3.5 formulated above can be proven directly by studying equations $\{F_1 = m,\ F_2 = h\}$ which define the combined (m,h)-level sets

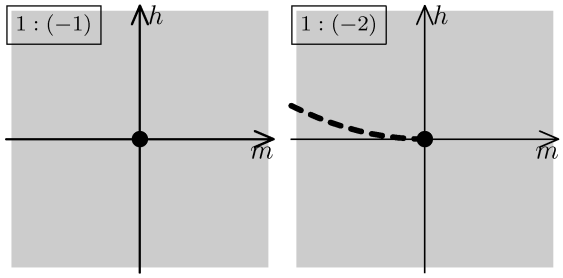

FIGURE 2. Left to right. Images of the energy–momentum map $\mathcal{EM}^{(0)}_{m_1:(-m_2)}$ for the 1:(−1) and 1:(−2) nonlinear resonant oscillator systems near the critical value $0 \in \mathbb{R}^2_{m,h}$ shown by black dot. Dashed line shows the critical value line which corresponds to curled tori, shaded area represents regular values.

of F_1 and F_2 in $\mathbb{R}^4$ and the rank of the Jacobian matrix $\partial F/\partial(q,p)$. We prove similar propositions in Appendices C and D in the form of more detailed technical Lemmas C.1, C.3, D.1, and D.6. Discussion of singular fibers and their possible graphical representations in $\mathbb{R}^3$ is relegated to Appendix A.

Alternatively, the above propositions can be easily proven within the framework of the analysis and reduction of the action of the dynamical Lie symmetry group $g^t_{F_1^{(0)}} \sim S^1$ on $\mathbb{R}^4_{q,p}$ introduced in Corollary 3.1. Such analysis is detailed in Appendix B, where the orbit space of this group action is represented in terms of invariant polynomials and is used for an explicit geometrical description of the integrable fibrations defined by the map $\mathcal{EM}^{(0)}_{m_1:(-m_2)}$.

We conclude with a conjecture which extends our description of basic properties of the integrable fibration $F^{(0)}$ defined by (3.1) and (3.2) to the general class of integrals F in (3.1) with compactifier R satisfying Conditions 3.1.

Conjecture 0. *Let $R^{(1)}$ be a function obtained from $R^{(0)} = R^{(0,s)}$ in* (3.2) *by a deformation $\{R^{(\tau)},\ 0 \le \tau \le 1\}$ which depends smoothly on τ while $R^{(\tau)}$ satisfies Conditions* 3.1 *for each $\tau \in [0,1]$. Then our Propositions* 3.2*,* 3.4*, and* 3.5 *can be reformulated for $R = R^{(1)}$.*

We believe that Conditions 3.1 should be sufficient for this conjecture to be true.

4. Main statements about classical monodromy

We now turn to the nontrivial property of integrable fibrations (F_1, F_2) introduced in Sec. 3 [see (3.1), (3.2) and Conditions 3.1], namely to their monodromy. The standard definition of Hamiltonian monodromy for two degree of freedom integrable systems deals with toric fibrations whose integrable map possesses only isolated critical values. Such definition can only be applied to the case with

$m_1 = m_2 = 1$ introduced above. In the case with one or both (m_1, m_2) greater than 1, we cannot choose a nontrivial closed loop in the base space of the fibration which consists only of regular values of the $\mathcal{EM}$ map because by Proposition 3.4 the critical value $0 \in \mathbb{R}^2_{m,h}$ is not isolated. (See Proposition 3.4 in previous section and Lemma D.6 in Appendix D.) Our generalized definition of monodromy in Sec. 2 makes introducing monodromy possible in this latter case.

In this section we formulate our main statements and apply our generalized definition to the particular cases of integrable fibrations defined by functions (F_1, F_2) in (3.1) with $m_1 = m_2 = 1$ and $m_1 = 1, m_2 = 2$, and with the simplest choice of the compactifier $R = R^{(0,s)}$ in (3.2). Since monodromy of these fibrations is of purely topological origin, we conjecture that an appropriate smooth deformation of R will not modify these statements as long as R satisfies Conditions 3.1.

We begin with the "standard" example of the $m_1 = m_2 = 1$ fibration for which we reproduce the well-known results on Hamiltonian monodromy of systems with "focus–focus" singularities. Using the same technique in the more general case of the fibration with $m_1 = 1$ and $m_2 = 2$, we show that this latter has fractional monodromy. We give the idea of the proof of our classical mechanics statements in Sec. 5 and provide more technical details in Appendices C and D. Subsequently, our results are interpreted for the corresponding quantum analogue systems in Sec. 6 and 7, where we introduce fractional quantum monodromy.

4.1. Monodromy theorem for the $1{:}(-1)$ resonance

Consider the integrable fibration defined by $F = (F_1, F_2)$ in (3.1) with $m_1 = m_2 = 1$ and choose the compactifier R to be equal $R^{(0,s)}$ in (3.2) with $s = 2$,

$$F_1 = \tfrac{1}{2}(p_1^2 + q_1^2) - \tfrac{1}{2}(p_2^2 + q_2^2), \tag{4.1a}$$

$$F_2 = p_1 q_2 + p_2 q_1 + \tfrac{1}{4}\big(p_1^2 + q_1^2 + p_2^2 + q_2^2\big)^2. \tag{4.1b}$$

Recall that by Proposition 3.5 the singular fiber $\Lambda_0 \ni 0$ of the fibration F is compact and connected, and coincides with $F^{-1}(0)$. All fibers Λ in the neighborhood of Λ_0 are regular 2-tori; Λ_0 is a *pinched torus* (see Appendix A) with one singular point of rank 0 at $0 \in \mathbb{R}^4$.

Theorem 1. *Fibration* (4.1) *has a nontrivial local integer monodromy map* μ. *Specifically, for any regular fiber* $\Lambda \sim \mathbb{T}^2$ *of this fibration we can find a basis of the homology group* $H_1(\Lambda)$ *in which* μ *is defined by the matrix*

$$\begin{pmatrix} 1 & 0 \\ -1 & 1 \end{pmatrix}. \tag{4.2}$$

All and only points of Λ_0 *can be the central points of this local monodromy.* Λ_0 *lies inside the upper cell* $K \ni 0$ *and is an isolated component of the boundary* ∂K.

Remark 4.1. Integrable fibration defined by the functions (4.1) is equivalent in some sense to that of the 1:1 resonant oscillator system with the axially symmetric "Champagne bottle" potential [6]. These systems are particular representatives of the class of systems with isolated focus–focus singularities [43, 45, 46, 73, 74].

Monodromy for many such systems has been computed analytically before. Furthermore, according to the *geometric monodromy theorem* in [17], this monodromy is defined entirely by the type of the singular fiber Λ_0.

Taking into account the known results for monodromy in systems with isolated focus–focus singularities we can formulate here without proofs the following corollary to Theorem 1 which extends our statement to a much wider class of integrable fibrations.

Conjecture 1 (corollary to Theorem 1). *Let $R^{(1)}$ be any function which can be obtained from $R^{(0,s)}$ in* (3.2) *with $s = 2$ by a deformation $\{R^{(\tau)},\ 0 \le \tau \le 1\}$ which depends smoothly on τ and such that for each $\tau \in [0,1]$ the function $R^{(\tau)}$ satisfies Conditions* 3.1 *formulated in Sec.* 3. *Then the statement of Theorem* 1 *remains valid for $F = (F_1, F_2)$ in* (3.1) *with $m_1 = m_2 = 1$ and compactifier $R = R^1$.*

We believe that Conditions 3.1 imposed on R are sufficient for this corollary to be true.

4.2. Monodromy theorem for the 1:(−2) resonance

Consider now the integrable fibration F defined by functions (F_1, F_2) in (3.1a) and (3.1b) with $m_1 = 1$ and $m_2 = 2$, and choose the compactifier R to be equal $R^{(0,s)}$ in (3.2) with $s = 2$,

$$F_1 = \tfrac{1}{2}(p_1^2 + q_1^2) - (p_2^2 + q_2^2), \tag{4.3a}$$

$$F_2 = 2p_1q_1q_2 + q_1^2p_2 - p_1^2p_2 + \tfrac{1}{4}\big(p_1^2 + q_1^2 + 2p_2^2 + 2q_2^2\big)^2. \tag{4.3b}$$

Note that by Proposition 3.5 the singular fiber $\Lambda_0 \ni 0$ of the fibration F in (4.3) is compact and connected, and coincides with $F^{-1}(0)$. All fibers $\Lambda_{m,h}$ lying close to Λ_0 coincide with $F^{-1}(m,h)$ and are also compact and connected. Furthermore, by Proposition 3.4 the image of the map F in the neighborhood of $0 \in \mathbb{R}^2$ consists of the critical value 0, the *critical value line* $\mathcal{C}_-$, and regular values, see Fig. 2. For the particular choice $H = F_2$ in (4.3) (see Remark 3.3) the critical line $\mathcal{C}_-$ is parameterized by the conditions

$$h = m^2, \quad m < 0, \tag{4.4}$$

where m is sufficiently close to 0. Critical fibers $\Lambda_- = \Lambda_{m,h}$ with $(m,h) \in \mathcal{C}_-$ are *curled tori* while Λ_0 is a *curled pinched torus* (see Appendix A) which has one singular point of rank 0 at $0 \in \mathbb{R}^4$. All other fibers Λ in the neighborhood of Λ_0 are regular 2-tori. Finally recall that, by Proposition 3.2 (see also Lemma D.6) the set Σ_0 of critical points of F in the small neighborhood U_0 of $0 \in \mathbb{R}^4$ is a two-dimensional *critical point plane* $\Sigma_0 = \{p_1 = q_1 = 0\} \cap U_0$.

Theorem 2. *Fibration* (4.3) *has nontrivial local* fractional *monodromy map μ. Specifically, for any regular fiber $\Lambda \sim \mathbb{T}^2$ of this fibration we can find a basis of the homology group $H_1(\Lambda)$ in which the map μ is given by the matrix*

$$\begin{pmatrix} 1 & 0 \\ -\frac{1}{2} & 1 \end{pmatrix}. \tag{4.5}$$

All points of the fiber Λ_0 and only those points are the central points of this local fractional monodromy.

The upper cell which contains regular fibers $\Lambda_{m,h}$ for (m,h) close to $0 \in \mathbb{R}^2$ is simply connected. This cell has an internal wall W, which partly intersects the inner part of the cell and includes the union $W_0 = \Lambda_0 \cup \Lambda_- \subset W$ of Λ_0 and all non-regular fibers Λ_- in the neighborhood of Λ_0.

Like in the 1:(−1) case we believe that the monodromy Theorem 2 can be extended to a more general class of integrable fibrations F whose compactifier R satisfies some reasonable conditions, such as Conditions 3.1 formulated in Sec. 3. By Conjecture 2, the corresponding integrable fibration near $0 \in \mathbb{R}^4$ and the image of the integrable map (which may no longer be an energy–momentum map) near $0 \in \mathbb{R}^2$ will remain qualitatively the same as described in the beginning of this section, though of course, the definition (4.4) of the critical value line C_- will be modified.

Conjecture 2 (corollary to Theorem 2). *Let $\{R^{(\tau)},\ 0 \le \tau \le 1\}$ be a deformation which depends smoothly on τ and such that for each $\tau \in [0,1]$ the function $R^{(\tau)}$ satisfies Conditions* 3.1*. Let $R^{(1)}$ be any function which can be obtained by such deformation from $R^{(0,s)}$ in* (3.2) *with $s = 2$. Then the statement of Theorem* 2 *can be reformulated for $F = (F_1, F_2)$ in* (3.1) *with $m_1 = 1$, $m_2 = 2$ and compactifier $R = R^1$.*

We leave the proof of this corollary open.

5. Idea of the proof. Representation of cycles on torus charts

The proof of our two monodromy theorems formulated in Sec. 4 follows the general discussion in Sec. 2.3 and 2.4. Computing monodromy of the integrable fibration F begins with defining an admissible closed path δ in the phase space $\mathbb{R}^4_{q,p}$. We make immediate use of the fact that each constant level set of the concrete integrable map F in Sec. 3 consists of only one connected component (fiber) Λ. Due to this simplifying property we can first fix the image $\Gamma = F(\delta)$ of δ in the base of the integrable fibration F and then construct $\delta = \delta_\Gamma$.

Closed path Γ in $\mathbb{R}^2$. The map $F\colon \mathbb{R}^4 \to \mathbb{R}^2$ with $F = (F_1, F_2)$ introduces coordinates on $\mathbb{R}^2$ which we denote by (m,h). Let us denote by Γ the boundary of a sufficiently small rectangular region D in $\mathbb{R}^2 = \mathbb{R}^2_{m,h}$ centered at the origin $(m,h) = (0,0)$,

$$D := \{(m,h),\quad |m| \le m_{\max},\quad |h| \le h_{\max},\quad 0 < m_{\max} \ll h_{\max} \ll 1\}.$$

We call $\Gamma \subset \mathbb{R}^2_{m,h}$ a *contour*. We will go along Γ (see Fig. 3) in the counterclockwise direction starting at the regular point $\Gamma_0 = (0, -h_{\max}) \in \Gamma$; other points on Γ will be denoted Γ_1, Γ_2, etc. The points are placed so that the resulting pieces of Γ, such as (Γ_1, Γ_2), are smooth. Alternatively, introducing parameter $t \in [0,1]$ along the contour Γ we will refer to these points as $\Gamma_{(t)}$, in particular $\Gamma_0 = \Gamma_{(t)}\big|_{t=0} = \Gamma_{(t)}\big|_{t=1}$.

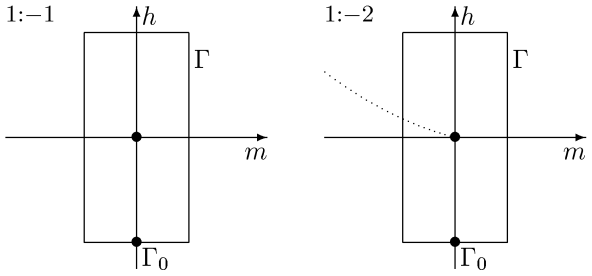

FIGURE 3. Choice of contour Γ in the base of the integrable fibration F introduced in Sec. 3; case $m_1 = m_2 = 1$ (left) and $m_1 = 1, m_2 = 2$ (right). Γ goes around the critical value $(0, 0)$ of the corresponding energy–momentum map (F_1, F_2).

Closed path δ_Γ in $\mathbb{R}^4$. Having chosen the contour Γ, we construct the corresponding closed path $\delta = \delta_\Gamma$ in $\mathbb{R}^4_{q,p}$. To this end we take a regular point $\xi \in \Lambda_0 \setminus \{0\}$ on the singular fiber $\Lambda_0 = \Lambda_{m,h}\big|_{m=h=0}$ and define the Poincaré section σ_ξ at ξ. The surface σ_ξ is transversal to Λ_0 and to all fibers Λ in a neighborhood $U \supset \Lambda_0$ such that $F^{-1}(D) \subset U$. (Since these fibers are two-dimensional, the dimension of σ_ξ is two.) We define the restriction $\mathcal{F} = F\big|_{\sigma_\xi}$ of the map F on σ_ξ. The map $\mathcal{F}\colon \sigma_\xi \to \mathbb{R}^2$ is a diffeomorphism of the Poincaré section σ_ξ on its image $F(\sigma_\xi) \subset \mathbb{R}^2$. As the closed path $\delta_\Gamma \subset \mathbb{R}^4_{q,p}$ we choose the inverse image $\delta_\Gamma = \mathcal{F}^{-1}(\Gamma)$ of the contour $\Gamma \subset \mathbb{R}^2_{m,h}$. Since $\mathcal{F}^{-1}$ is a diffeomorphism, δ_Γ is piecewise smooth and going along δ_Γ is equivalent to going along Γ. Furthermore, we will show that the path δ_Γ is admissible in the sense of Definition 2.6 in Sec. 2.3 both in the 1:(−1) and the 1:(−2) case.

Representation of the basis elements of $H_1(\Lambda_{\Gamma_0})$. Regular fibers $\Lambda_{m,h}$ of F, and in particular the initial fiber Λ_{Γ_0}, are 2-tori (Sec. 3). Their first homology group $H_1(\mathbb{T}^2)$ is isomorphic to $\mathbb{Z}^2$ and has two basis elements, which will be denoted (g_f, e) and will be represented by the cycles $(\gamma_\mathrm{f}, \eta)$. Since $H_1(\mathbb{T}^2)$ is abelian, we write the composition of its elements (and their representatives) as a linear combination, e.g., $2e_0 + g_\mathrm{f}$ and $2\eta_0 + \gamma_\mathrm{f}$. We will give the way to define $(\gamma_\mathrm{f}, \eta_{(t)})$ explicitly and therefore to choose $(g_\mathrm{f}, e_{(t)})$ independently in almost all points $\Gamma_{(t)}$. We begin at the initial point Γ_0 by constructing the basis (g_f, e_0) of the homology group $H_1(\Lambda_{\Gamma_0})$.

Remark 5.1. Both in the case 1:(−1) and 1:(−2) each regular fiber $\Lambda_{m,h} \sim \mathbb{T}^2$ of the integrable fibration $F = (F_1, F_2)$ has one "fixed" element of H_1, g_f, which is *always* represented by the 2π-periodic trajectories γ_f of the system with Hamiltonian F_1 followed to time 2π, see Lemma 3.1 and Corollary 3.1. For all such fibers, g_f remains unchanged after a tour along any admissible closed path δ (Sec. 2.4) and in particular along δ_Γ defined by the contour Γ in the base space of F. Consequently, g_f cannot be the origin of nontrivial monodromy.

Following Remark 5.1 we represent the basic elements g_{f} of $H_1(\Lambda_{\Gamma_0})$ using a 2π-periodic trajectory of the Hamiltonian flow φ_{F_1} of F_1 with orientation induced by φ_{F_1}.

Representation of the basis element e_0 of $H_1(\Lambda_{\Gamma_0})$. We choose the cycle η_0, which represents the second basis element e_0 of $H_1(\Lambda_{\Gamma_0})$, by intersecting Λ_{Γ_0} by a *fixed* three-dimensional hyperspace $\sigma \subset \mathbb{R}^4$. The latter is defined in $\mathbb{R}^4$ by the equation $F_3(q,p) = 0$ so that it is almost everywhere transversal to the flow φ_{F_1}, and in particular σ is transversal to φ_{F_1} on Λ_{Γ_0}. The concrete explicit form of F_3 depends on the concrete (F_1, F_2) under study and will be given in Secs. 5.1 and 5.2 for the 1:(-1) and 1:(-2) systems respectively. We can consider σ as a global non-regular Poincaré section for the system with Hamiltonian F_1 which is regular in the neighborhood of Λ_{Γ_0}. Then the intersection $\lambda_0 = \Lambda_{\Gamma_0} \cap \sigma$ is regular and consists of several disconnected one-dimensional closed curves, which can be *oriented* unambiguously as in the paragraph below. As the cycle η_0, we take one oriented connected component of λ_0. Since by construction η_0 and γ_{f} are transversal, the respective elements e_0 and g_{f} of homology group represented by these cycles form a basis for some complete subgroup of $H_1(\Lambda_{\Gamma_0})$. In order to make sure that (g_{f}, e_0) is a basis for the whole $H_1(\Lambda_{\Gamma_0})$, we will show that (in both the 1:(-1) case and the 1:(-2) case) η_0 intersects any $\gamma_{\mathrm{f}} \subset \Lambda_{\Gamma_0}$ only in one point.

Orientation of components of $\lambda_0 = \Lambda_{\Gamma_0} \cap \sigma$. To define the orientation of the components of λ_0, we recall that regular fibers Λ of the integrable fibration F, and in particular Λ_{Γ_0}, are tori $\mathbb{T}^2$, and are, therefore, orientable. Furthermore, we can orient each $\Lambda_{\Gamma_{(t)}} \sim \mathbb{T}^2$ consistently for all $\Gamma_{(t)} \in \Gamma$ by using the value of the vector fields (X_{F_1}, X_{F_2}) computed at the point $\xi_\delta = \delta_\Gamma \cap \Lambda_{\Gamma_{(t)}}$. We also observe that $F_3(q,p)$ defines a "height" function on $\mathbb{R}^4$, which induces a height function $\mathcal{F} := F_3|_{\Lambda_{\Gamma_0}}$ on Λ_{Γ_0} with zeros on the smooth curve λ_0. Then taking any point $\xi \in \lambda_0$, we consider the tangent plane $T\Lambda_{\Gamma_0}(\xi)$ at ξ spanned by the basis vectors (v_1, v_2), which agree with the orientation of Λ_{Γ_0}. We rotate (v_1, v_2) so that v_1 becomes collinear with the vector $\nabla\mathcal{F}(\xi)$ on $T_\xi\Lambda_{\Gamma_0}$. (Recall that $\mathcal{F}(q,p) = \mathcal{F}(\xi)$ is given explicitly, and in particular, its sign and hence the direction of $\nabla\mathcal{F}(\xi)$ is fixed at all ξ.) Then the second vector v_2 gives the orientation of the closed curve, which passes through ξ and is a part of λ_0.

In this way *all* components of the intersection λ_0 are oriented consistently and become oriented closed curves. All these closed curves together form a cycle, which is homotopic to zero on Λ_{Γ_0}, and which deforms continuously (without changing its homotopy type) as we move along the contour Γ.

Intersections $\lambda_0 \cap \gamma_{\mathrm{f}}$. The intersections of the thus oriented components of λ_0 and the φ_{F_1} orbits γ_{f} can be classified further. Consider an orientable fiber Λ of the integrable map F and an oriented curve (a path) $\kappa \subset \Lambda$, which intersects an orbit $\gamma_{\mathrm{f}} \subset \Lambda$ transversally at a finite number of points $\{\xi_1, \xi_2, \ldots\} = \kappa \cap \gamma_{\mathrm{f}}$. (For example, take $\Lambda = \Lambda_{\Gamma_0}$ and $\kappa \subseteq \lambda_0$.) At each ξ_i, consider $T_{\xi_i}\Lambda$, where the vectors v_{f} and v_κ represent the respective directions of κ and γ_{f} at ξ_i. Take the considered earlier vector basis $(v_1, v_2) = (v_{\mathrm{f}}, v_2)$ in $T_{\xi_i}\Lambda$, which defines the orientation of Λ.

Compute

$$\operatorname{ind}_{\xi_i}(\kappa \cap \gamma_{\mathrm{f}}) := \operatorname{sign}(v_2.v_\kappa) = \pm 1 \quad \text{and} \quad \operatorname{ind}(\kappa \cap \gamma_{\mathrm{f}}) := \sum_{\xi_i} \operatorname{ind}_{\xi_i}(\kappa \cap \gamma_{\mathrm{f}}).$$

Definition 5.1. We call $\operatorname{ind}_{\xi_i}(\kappa \cap \gamma_{\mathrm{f}})$ the *local index* of intersection $\kappa \cap \gamma_{\mathrm{f}}$ at point ξ_i, and we call $\operatorname{ind}(\kappa \cap \gamma_{\mathrm{f}})$ the *index* of $\kappa \cap \gamma_{\mathrm{f}}$.

Note that if κ is a closed path (or a cycle consisting of several closed paths) homotopic to zero, then the index of its intersection with γ_{f} is 0. Thus, $\operatorname{ind}(\lambda_0 \cap \gamma_{\mathrm{f}}) = 0$.

Representing basis elements of $H_1(\Lambda_{\Gamma_{(t)}})$. By Remark 5.1 the choice of the cycle to represent one of the basis elements of $H_1(\Lambda_{\Gamma_{(t)}})$ is fixed: for all t we use as $\gamma_{\mathrm{f}} = \gamma_{\mathrm{f}}(t)$ an oriented 2π-periodic orbit of φ_{F_1}. The choice of the cycle $\eta_{(t)}$ representing the other basis element $e_{(t)}$ can also be made almost at all t in a certain fashion related to our choice of σ. Specifically, we call the intersection $\lambda_{(t)} = \Lambda_{\Gamma_{(t)}} \cap \sigma$ and the point $\Gamma_{(t)} \in \Gamma$ *regular* if

$$\operatorname{rank} \frac{\partial(F_1, F_2, F_3)}{\partial(q, p)} = 3 \quad \text{for all } \xi \in \lambda_{(t)} = \Lambda_{\Gamma_{(t)}} \cap \sigma. \tag{5.1}$$

For all regular $\Gamma_{(t)}$, we construct the cycle $\eta_{(t)}$ similarly to η_0. We begin by taking a cycle $\tilde{\eta}$ composed of one or several connected oriented components of $\lambda_{(t)}$. If – as in the case of Γ_0 – we find that $\operatorname{ind}(\tilde{\eta} \cap \gamma_{\mathrm{f}}) = 1$, then we choose $\eta_{(t)} := \tilde{\eta}$. Otherwise we look for such $\eta_{(t)}$ that

$$\tilde{\eta} + b\gamma_{\mathrm{f}} + a\eta_{(t)} = 0, \qquad \text{where } a, b \in \mathbb{Z} \text{ and } \operatorname{ind}\bigl(\eta_{(t)} \cap \gamma_{\mathrm{f}}\bigr) = 1.$$

Remark 5.2. In practice, to compute monodromy transformation μ_δ for a path δ, we need to know the basis elements $(g_{\mathrm{f}}, e_{(t)})$ only at the end points $t = 0$ and $t = 1$ of δ. So, in the case of the closed path δ_Γ, we only have to know (g_{f}, e_0) for $H_1(\Lambda_{\Gamma_0})$. However, knowing basis elements of the homology group at other points of Γ can be very helpful for constructing the continuous deformation $\gamma_{(t)}$ of the cycle $\gamma_0 = e_0$ (see below), and, of course, is necessary for representing $\gamma_{(t)}$ on the charts $\Lambda_{\Gamma_{(t)}} \to \mathbb{R}^2/\mathbb{Z}^2$.

Nonregular points of intersections $\lambda_{(t)}$. Let us denote by $\Gamma_{(t^*)}$ and ξ^* the nonregular points of the contour Γ and the points of the corresponding nonregular intersection $\lambda_{(t^*)} = \Lambda_{\Gamma_{(t^*)}} \cap \sigma$ at which the rank (5.1) is less than 3. Such nonregular intersections can be described as sets of loops with common points ξ^*, e.g., a "figure eight". To define unambiguously the orientation of all segments of the nonregular intersections $\lambda_{(t^*)}$ which consist only of regular points ξ of the map (F_1, F_2, F_3) we will use the same technique we used above to orient γ_0. Note that nonregularity can arise either because at points ξ^* the surface σ is not transversal to a regular 2-torus $\Lambda_{(t^*)}$ (to the flow of φ_{F_1}) or because $\xi^* = \xi_c$ is also a critical point and $\Gamma_{(t_c)} = \Gamma_{(t^*)}$ is a critical value of $F = (F_1, F_2)$. We will call the latter case as *critical nonregular*. It occurs in the 1:(−2) system when we cross the line of critical values (Proposition 3.4 and Remark 3.3) and $\Lambda_{\Gamma_{(t^*)}}$ is a curled torus.

Continuous deformation of the cycles. Following Sec. 2.4 in the 1:(−1) case we should identify the homology groups $H_1(\Lambda_{\Gamma_{(t)}})$ as $\Gamma_{(t)}$ moves along the contour Γ and makes a complete tour. Specifically, for any regular t_1 and t_2, we define local bases $(g_{\mathrm{f}}, e_{(t_1)})$ and $(g_{\mathrm{f}}, e_{(t_2)})$ and should find the matrix $M = M_{\delta_\Gamma} \in \mathrm{SL}(2,\mathbb{Z})$ that relates these bases. By Remark 5.1 the cycle γ_{f}, represents after a complete tour around contour Γ the same basis element g_{f} of the homology group. The idea of our proof is in the direct construction of the *continuous deformation* $\gamma_{(t)}$ of the cycle

$$\gamma_0 = \gamma_{(t)}\big|_{t=0} := \eta_0$$

representing the second basis element of $H_1(\Lambda_{\Gamma_0})$.

Let us consider the automorphism of the group $H_1(\Lambda_{\Gamma_t})$ induced by the mapping of cycles $\gamma_{\mathrm{f}} \mapsto \gamma_{\mathrm{f}}$, $\gamma_{(t)} \mapsto \eta_{(t)}$. Then the matrix $\mu(t)$ of this automorphism in the basis $(\gamma_{\mathrm{f}}, \gamma_{(t)})$ is constant for any segment of Γ which consists only of regular points.

It is clear that the map μ is represented by the identity matrix for any segment of Γ which consists only of regular points. For example, let $[0, t_1]$ define such a segment. Since different components of the intersection $\Lambda_{\Gamma_{(t)}} \cap \sigma$ remain disconnected for all $t \in [0, t_1]$, we have $\gamma_{(t)} = \eta_{(t)}$ for all $t \in [0, t_1]$. In other words, as long as the intersection remains regular, we continuously associate the second basic element $e_{(t)}$ of the homology groups $\{H_1(\Lambda_{\Gamma_{(t)}});\ t \in [0, t_1]\}$ with the cycle $\gamma_0 := \eta_0$ chosen at the initial point Γ_0. The continuity of the deformation $\gamma_{(t)}$ for $t \in [0, t_1]$ is assured by the use of the same fixed hypersurface σ to define the cycles at all regular points $\Gamma_{(t)} \subset [\Gamma_0, \Gamma_{(t_1)}]$. Arriving at the point $\Gamma_{(t_1)}$ we thus find that $\mu(t_1)$ is the identity matrix.

Consider now $t_1 < t^* < t_2$ and a corresponding smooth segment $[\Gamma_{(t_1)}, \Gamma_{(t_2)}]$ $\subset \Gamma$ which contains one nonregular point $\Gamma_{(t^*)}$. As we pass $\Gamma_{(t^*)}$, the number of disconnected components of the intersection $\Lambda_{\Gamma_{(t)}} \cap \sigma$ changes and each component varies discontinuously. When $t = t^*$ we cannot construct the second basis element of the homology group using the intersection with σ as we normally do before for $t < t^*$ and after for $t > t^*$. Fortunately, we do not need to construct the basis of $H_1(\Lambda_{(t^*)})$. In fact, passing t^* is similar to changing charts in an atlas: as we go to $t > t^*$, we have to specify the relation between the charts. To obtain this relation, we should find a way to continue our original cycle $\gamma_{(t_1)} = \eta_{(t_1)} \subset \sigma$ which represents the basic element $e_{(t_1)}$ of $H_1(\Lambda_{\Gamma_{(t_1)}})$ through point $\Gamma_{(t^*)}$. This continuation depends on the type of nonregularity at $\Gamma_{(t^*)}$.

Nonregular points on regular fibers. If $\Lambda_{\Gamma_{(t^*)}}$ is a regular $\mathbb{T}^2$-fiber of the integrable map $F = (F_1, F_2)$ and ξ^* are regular points of F at which σ and $\Lambda_{\Gamma_{(t^*)}}$ are not transversal, we can replace the cycle $\gamma_{(t_1)} \subset \sigma$ for a homotopically equivalent cycle $\tilde{\gamma}_{(t_1)} \not\subset \sigma$ which can be smoothly continued through the point t^* to $\tilde{\gamma}_{(t_2)}$. We then deform $\tilde{\gamma}_{(t_2)}$ into homotopically equivalent cycle $\gamma_{(t_2)}$, which consists of the oriented component(s) of the regular intersection $\Lambda_{\Gamma_{(t_2)}} \cap \sigma$ and (possibly) of 2π-periodic orbits γ_{f} of φ_{F_1}, i.e., which is a composition of $\eta_{(t_2)}$ and γ_{f}. The possibility for γ_{f} to appear in $\gamma_{(t_2)}$ comes from the necessity to involve parts of these orbits (transversal

to σ in all points except ξ^*) in the homotopies $\gamma_{(t_1)} \to \tilde{\gamma}_{(t_1)}$ and $\tilde{\gamma}_{(t_2)} \to \gamma_{(t_2)}$ in order to move out of σ and bring back to σ small parts of the cycles which would otherwise come to intersect each other at the nonregular points ξ^* of $\Lambda_{\Gamma_{(t^*)}} \cap \sigma$.

Passing critical nonregular points. The specifics of the 1:(−2) case compared to the 1:(−1) case is in the presence of the critical nonregular point $\Gamma_{(t^*=t_c)}$. In this case, there is *no* way in which individual oriented components of the intersection $\Lambda_{\Gamma_{(t_1)}} \cap \sigma$ can be deformed and continued through $\Gamma_{(t_c)}$. However, a cycle constructed as an appropriate composition of these components can be *passable* as a whole, just as outlined in Sec. 2.3. It follows that in the 1:(−2) case the subgroup $\zeta \subset H_1(\Lambda_{\Gamma_0})$ and the cycle γ_0 representing the second basis element of ζ at $t = 0$ should be chosen so that the cycle $\gamma_{(t_c)}$ is passable.

Monodromy. If the cycle $\gamma_{(t)}$ representing element $g_{(t)}$ of the homology group does indeed accumulate one or several φ_{F_1} components when we go around Γ and come back to Λ_{Γ_0} at $t = 1$, then the resulting cycle $\gamma_1 = \gamma_{(t)}\big|_{t=1}$ represents an element g_1 of H_1, which does not coincide with the initial element g_0 but is a composition of g_0 and g_f. After constructing $\eta_{(t)}$, $\gamma_{(t)}$, and $\mu_{(t)}$ explicitly, we compute the nontrivial local monodromy $\mu_{(t)}\big|_{t=1}$ of the integrable fibration F stated in Theorems 1 and 2. We can choose initial elements of the homology group $(g_\mathrm{f}, g_{(t)})$ for $t = 0$ so that they can be expressed as

$$\begin{pmatrix} g_\mathrm{f} \\ g_0 \end{pmatrix} = B \begin{pmatrix} g_\mathrm{f} \\ e_0 \end{pmatrix}, \tag{5.2}$$

where B is a 2×2 matrix with integer coefficients and $\det B \geq 1$, and (g_f, e_0) is the basis of $H_1(\Lambda_{\Gamma_0})$. The monodromy transformation

$$\mu_{(t)}\big|_{t=1} \colon \begin{pmatrix} g_\mathrm{f} \\ g_0 \end{pmatrix} \to \begin{pmatrix} g_\mathrm{f} \\ g_1 \end{pmatrix} = M \begin{pmatrix} g_\mathrm{f} \\ g_0 \end{pmatrix}, \tag{5.3a}$$

is defined by a monodromy matrix $M \in \mathrm{SL}(2, \mathbb{Z})$. Notice that transformation (5.3a) cannot be simply extended to the whole $H_1(\Lambda_{\Gamma_0})$ if $\det B > 1$ because in that case the matrix $B^{-1}MB$ may have rational coefficients and

$$B^{-1}MB \begin{pmatrix} g_\mathrm{f} \\ e_0 \end{pmatrix}. \tag{5.3b}$$

may not necessarily be a basis on $H_1(\Lambda_{\Gamma_1})$. Thus if we use (5.3b) in the case of monodromy $\frac{1}{2}$ (Theorem 2), we would formally obtain $\frac{1}{2}g_\mathrm{f} + e_0$ which can, obviously, only become an element of H_1 after being repeated twice. Using the isomorphism $H_1(\Lambda_{\Gamma_0}) \sim \mathbb{Z}_0^2$ we can illustrate such extension attempt as a formal transformation of the square elementary cell of $\mathbb{Z}_0^2$ shown by shaded area below left

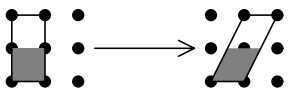

and compare it to the transformation of the double cell. It can be seen that the upper vertices of the transformed elementary cell (shaded area, right) do not match lattice nodes of $\mathbb{Z}_1^2$ and therefore, this transformed cell does not define a basis

in $\mathbb{Z}_1^2$. Consequently, it is more appropriate to think of the extension (5.3b) after including $\mathbb{Z}^2$ canonically in a linear space $\mathbb{R}^2$ (see Def. 2.8 in Sec. 2.4.1) and to consider $B^{-1}MB \in \mathrm{SL}(2,\mathbb{Q})$ as a matrix of transformation of $\mathbb{R}^2$. It is in this sense that we use such matrix in the statement of Theorem 2.

Representation in σ and on the charts of $\Lambda_{\Gamma_{(t)}}$. Construction and continuation of cycles $\gamma_{(t)}$ can be either done directly in $\sigma \subset \mathbb{R}^4$ in natural initial coordinates (q,p) or, alternatively, on the torus charts $\Lambda_{\Gamma_{(t)}} \to \mathbb{R}^2/\mathbb{Z}^2$ with some specially constructed *local* angle coordinates $(\phi_1,\phi) \in [0,2\pi)$. The advantage of the charts is in the possibility to represent more easily the homotopies involved in passing nonregular points t^* when parts of our cycle $\tilde{\gamma}$ remain outside σ. At the same time, finding the image of cycles $\eta_{(t)}$ defined by intersections $\Lambda_{\Gamma_{(t)}} \cap \sigma$ on the torus chart of $\Lambda_{\Gamma_{(t)}}$ presents an additional difficulty for a rigorous proof.

Note that we will use the charts where the angle ϕ_1 (horizontal coordinate) is the conjugate angle of the global action F_1 that gives the coordinate on the fixed element g_{f}. The angle ϕ (vertical coordinate) is the conjugate angle of the second locally constructed action $I(F_1,F_2)$ whose vector field X_I is a linear combination of X_{F_1} and X_{F_2} with periodic flow on $\Lambda_{\Gamma_{(t)}}$. Both X_I and the origin of the torus map will be chosen specially for each particular $(m,h) = \Gamma_{(t)}$ in order to have the clearest representation of $\Lambda_{\Gamma_{(t)}} \cap \sigma$.

In the 1:(−1) case we work directly in σ (see Sec. C.2) and use torus charts in Sec. 5.1 primarily for illustration and for comparison with the more complicated 1:(−2) case. In the latter case we formulate several additional lemmas in Sec. D.2 which define the exact correspondence between the cycles on σ and their images on the torus charts. This enables us to analyze in parallel the deformation of cycles on the torus charts and on σ and to represent this deformation in a much more comprehensive way.

5.1. The $m_1 = m_2 = 1$ case

In the 1:(−1) case each point $\Gamma_{(t)} = (m,h)$ of the contour $\Gamma \subset \mathbb{R}^2$ (Fig. 3, left) and the respective point ξ of the closed path $\delta_\Gamma \subset \mathbb{R}^4$ is associated to a regular 2-torus fiber $\Lambda_{\Gamma_{(t)}} = \Lambda_{m,h}$. We define the hyperspace σ as a hyperplane

$$\sigma := \{F_3 = 0\} \subset \mathbb{R}^4, \quad F_3 = p_1 - q_2. \tag{5.4}$$

Intersections $\lambda_{m,h} = \Lambda_{m,h} \cap \sigma$ are classified by the following statements.

Lemma 5.1. *For all sufficiently small $|m|$ and $|h|$ surfaces $\Lambda_{m,h}$ are smooth everywhere except $\Lambda_{0,0}$, which is not smooth in one point $(p,q) = 0$. All $\Lambda_{m,h}$ intersect the hyperplane σ transversally everywhere except points ξ^* on the axis $\sigma \cap \{q_1 = p_2 = 0\}$. Moreover, at each point $\xi^* \neq 0$ the tangent 2-plane $T_{\xi^*}\Lambda_{m,h}$ lies in σ.*

Analytic proofs of this and related lemmas are given in Sec. C.1.

Corollary 5.1. *The contour Γ has one nonregular point $\Gamma_2 = \Gamma_{(t^*)} = (m = 0, h > 0) \subset \Gamma$ (see Fig. 4). The regular 2-torus Λ_{Γ_2} intersects σ nontransversally in two points $\xi^*_\pm$ with $q_2 = p_1 = \pm p(h)$ which lie on the same φ_{F_1} orbit $\gamma_{\mathrm{f}} \in \sigma$.*

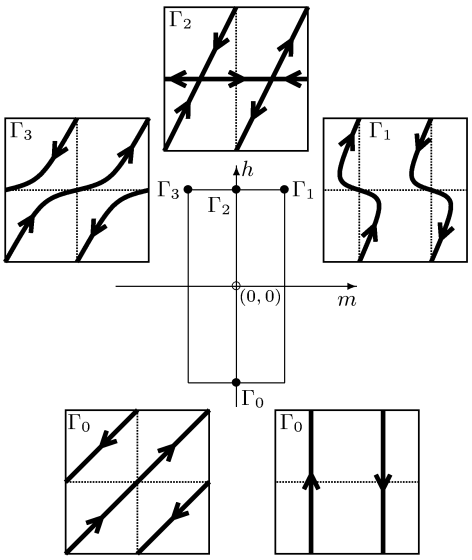

FIGURE 4. Contour Γ in the $m_1 = m_2 = 1$ case and the evolution of the connected components of the intersection $\Lambda_{m,h} \cap \sigma$ which are shown on the torus charts $\Lambda_{m,h} \to \mathbb{R}^2/\mathbb{Z}^2$ computed numerically for $h = \pm 0.05$ and $m = \pm 0.02, 0$.

Further description of $\lambda_{m,h}$ is detailed in Sec. C.2. Images of oriented components of $\lambda_{m,h}$ on the torus charts $\Lambda_{m,h} \to \mathbb{R}^2/\mathbb{Z}^2$ are shown in Fig. 4. We see that any regular $\lambda_{m,h}$, $(m,h) \neq \Gamma_2$ is a union of two non-intersecting smooth closed curves to which we assign opposite orientation. We use one of these oriented curves to represent the second basis element $e_{(m,h)}$ of $H_1(\Lambda_{m,h})$ for all $(m,h) \neq \Gamma_2$. When we pass Γ_2 the two disconnected components of $\lambda_{m,h}$ fuse together in two points and then separate forming two new components. This transformation is *not* continuous for each of the components.

To compute the monodromy map μ, we construct the continuous family of cycles $\gamma_{(m,h)}$ parameterized by $(m,h) \in \Gamma$ starting from $\Gamma_0 = (m = 0, h < 0) \in \Gamma$ where $\gamma_0 = \gamma_{(m,h)}\big|_{(m,h)=\Gamma_0} := \eta_0$ is chosen as one of the oriented connected components of the intersection λ_{Γ_0} and coincides with the cycle η_0 representing the second basis element e_0 of $H_1(\Lambda_{\Gamma_0})$. By Corollary 5.1, $\gamma_{(m,h)}$ deforms continuously (and piecewise smoothly) as we follow any segment of contour Γ (or δ_Γ) which does not contain Γ_2, and in particular the segment from Γ_0 to Γ_1. Hence up until Γ_1 the map $\mu_t \colon H_1(\Lambda_{\Gamma_0}) \mapsto H_1(\Lambda_{\Gamma_{(t)}})$ is trivial.

In order to continue the cycle $\gamma_{(m,h)}$ through the point Γ_2 we replace $\gamma_{\Gamma_1} \subset \sigma$ defined as one oriented component of λ_{Γ_1} by a homotopic cycle $\tilde{\gamma}_{\Gamma_1} \not\subset \sigma$. The new cycle deforms smoothly into $\tilde{\gamma}_{\Gamma_3}$ as we move from Γ_1 to Γ_3 through point Γ_2. We then replace $\tilde{\gamma}_{\Gamma_3}$ for homotopically equivalent γ_{Γ_3} which is a composition of one

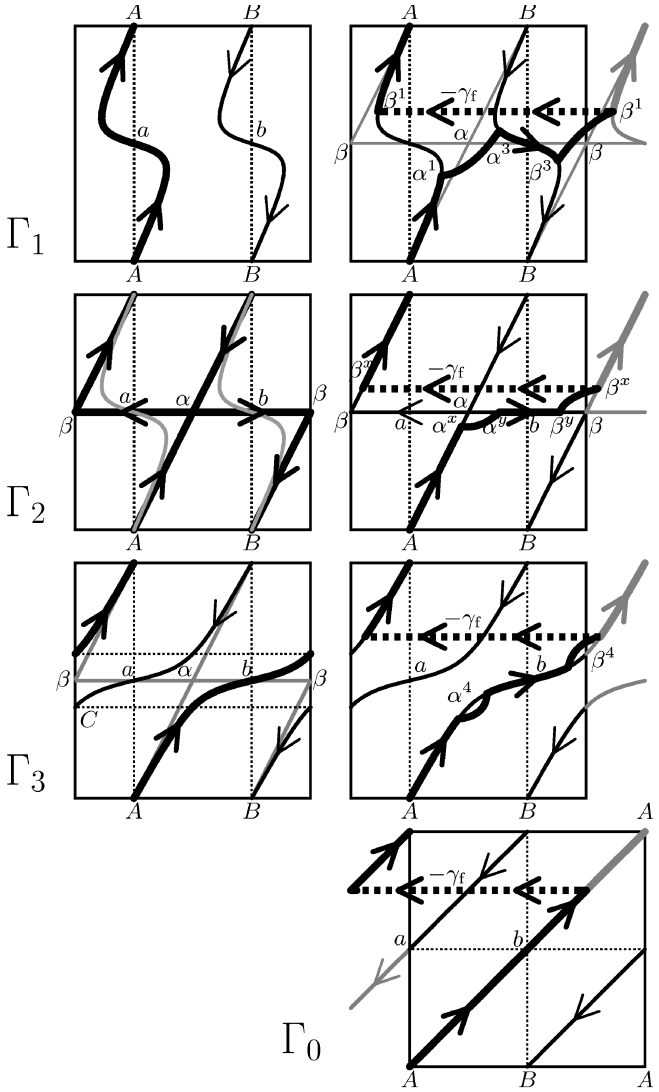

FIGURE 5. Construction of homotopically equivalent cycles on the regular tori $\Lambda_{m,h}$ for $(m,h) \in \Gamma$ near the nonregular point Γ_2 of the 1:(−1) case, cf. Fig. 4. Bold dashed lines show the periodic orbit γ_f of the flow φ_{F_1}. See text for detailed discussion.

oriented connected component of the intersection λ_{Γ_3} and the oriented periodic orbit γ_f of the Hamiltonian flow φ_{F_1}.

The homotopies $\gamma_{\Gamma_1} \to \tilde{\gamma}_{\Gamma_1}$ and $\tilde{\gamma}_{\Gamma_3} \to \gamma_{\Gamma_3}$ are explained in Fig. 5, top and bottom respectively. Realization of the same homotopic modification in σ is

described in Sec. C.2, see Figs. C.4 and C.5, where the same notation is used for corresponding points on σ. In Fig. 5, top left, the cycle $\gamma_{\Gamma_1} = \eta_{\Gamma_1}$ is an oriented connected component of the intersection λ_{Γ_1} labeled AaA. It is replaced by a homotopically equivalent cycle $\tilde\gamma_{\Gamma_1} = A\alpha^1\alpha^3\beta^3\beta^1(-\gamma_{\rm f})\beta^1 A$ (Fig. 5, top right). The new cycle $\tilde\gamma_{\Gamma_1}$ is constructed from the fragments $A\alpha^1$ and $\beta^1 A$ of AaA, the fragment $\alpha^3\beta^3 \subset BbB$ of the second oriented component of λ_{Γ_1}, and two small fragments $\alpha^1\alpha^3$ and $\beta^3\beta^1$. The first three fragments belong to σ and inherit their orientation, the last two fragments lie on the torus Λ_{Γ_1} but do not belong to σ. The orientation of these fragments is chosen to agree with other fragments they connect. At last we add the trajectory of the system with Hamiltonian F_1 as a fragment $\beta^1(-\gamma_{\rm f})\beta^1$. It is easy to see that $\tilde\gamma_{\Gamma_1}$ is homotopic to AaA. The deformation of $\tilde\gamma_{(t)} = A\alpha^1\alpha^3\beta^3\beta^1(-\gamma_{\rm f})\beta^1 A$ for $\Gamma_{(t)} \in [\Gamma_1\Gamma_3]$ proceeds smoothly as we pass Γ_2 (Fig. 5, second row). At point Γ_3, the resulting cycle $\tilde\gamma_{\Gamma_3}$ (Fig. 5, third row, right) is homotopic to the sum $AbA + (-\gamma_{\rm f}) = \gamma_{\Gamma_3}$ of two oriented loops (Fig. 5, third row, left), where $AbA = \eta_{\Gamma_3}$ is one of the oriented connected components of the intersection λ_{Γ_3}, while $-\gamma_{\rm f}$ (bold dashed line in Fig. 5) is a closed trajectory of φ_{F_1} representing element $(-g_{\rm f})$ of the homology group. Here note that cycles $\eta_{\Gamma_1} = AaA$ and $\eta_{\Gamma_3} = AbA$ representing second basis elements e_{Γ_1} and e_{Γ_3} of $H_1(\Lambda_{\Gamma_1})$ and $H_1(\Lambda_{\Gamma_3})$ are shown by bold lines in the top left and bottom left charts of Fig. 5, respectively.

Further deformation of $\gamma_{(t)} = \gamma_{(m,h)}$ as we go from Γ_3 till $\Gamma_{(t)}\big|_{t=1} = \Gamma_0$ is continuous (and piecewise smooth) and does not anymore modify the homotopy type of $\gamma_{(t)}$ in the chart of $\Lambda_{\Gamma_{(t)}}$ which varies smoothly along with deformation of this torus. Arriving at Γ_0 we obtain the cycle $\gamma_1 = \gamma_{(t)}\big|_{t=1}$, which represents an element g_1 of $H_1(\Lambda_{\Gamma_0})$. Expressing g_1 in the original basis $(g_{\rm f}, e_0)$ of $H_1(\Lambda_{\Gamma_0})$ (this basis corresponds to the angle coordinates of the bottom right torus chart of Λ_{Γ_0} in Fig. 4) gives $g_1 = e_0 - g_{\rm f}$. Hence the monodromy map $\mu = \mu_\Gamma = \mu_{\delta_\Gamma}$ is
$\mu\colon H_1(\Lambda_{\Gamma_0}) \to H_1(\Lambda_{\Gamma_0})\colon (g_{\rm f}, e_0) \to (g_{\rm f}, e_0 - g_{\rm f})$,
and the monodromy matrix is $\left(\begin{smallmatrix} 1 & 0 \\ -1 & 1 \end{smallmatrix}\right)$.

5.2. The $m_1 = 1$, $m_2 = 2$ case

In the 1:(−2) case, the proof follows the same general outline. We take the same contour Γ, see Fig. 3, right. The path δ_Γ is constructed as described at the beginning of Sec. 5 and is an admissible closed path. We begin at the same point $\Gamma_0 \in \Gamma$ with $m = 0$ and $h < 0$; the fiber Λ_{Γ_0} is a regular 2-torus. The three-dimensional hyperspace σ is now defined as a hyperplane

$$\sigma := \{F_3 = 0\}, \quad F_3 = p_1 - \sqrt{2}q_2. \tag{5.5}$$

We use (p_1, q_1, p_2) as coordinate functions on σ. (These functions coincide with the restriction on σ of the respective functions defined on the whole $\mathbb{R}^4$.)

Intersections $\lambda_{m,h} = \Lambda_{m,h} \cap \sigma$. Oriented connected components of $\lambda_{m,h}$ are represented in Fig. 6 on the charts $\Lambda_{m,h} \to \mathbb{R}^2/\mathbb{Z}^2$. Direct representation of $\lambda_{m,h}$ in σ is discussed in detail in Sec. D.2. In particular, Lemma D.9 gives the exact

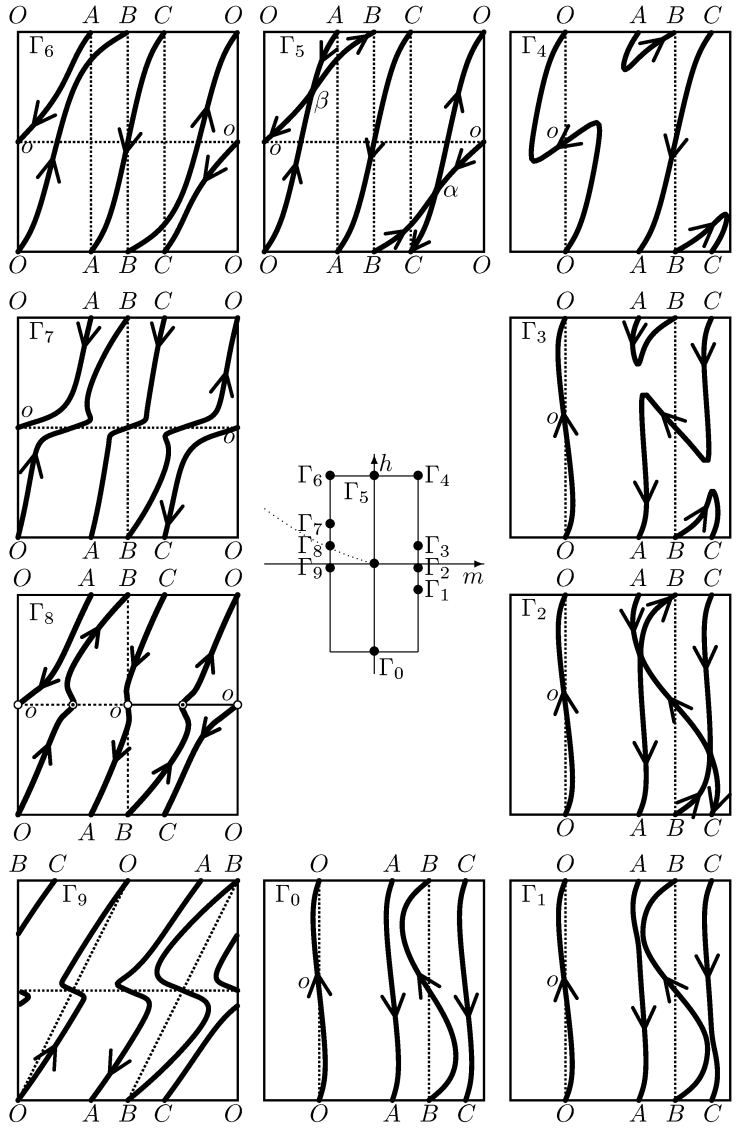

FIGURE 6. Contour Γ in the 1:(−2) case together with evolution of the oriented connected components of intersections $\lambda_{m,h} = \Lambda_{m,h} \cap \sigma$ for $(m, h) \in \Gamma$.

correspondence between the two representations of $\lambda_{m,h}$ for $m = 0$. The following statements provide the description of the nonregular points of $\lambda_{m,h}$.

Lemma 5.2. *For all sufficiently small $|m|$ and $|h|$, the surfaces $\Lambda_{m,h}$ are smooth in all points except points in the plane $\{p_1 = q_1 = 0\}$. All $\Lambda_{m,h}$ intersect the hyperplane σ transversally everywhere except points*

$$\xi^* = (p_1, q_1, p_2, q_2) \in p_1^\sigma \cup p_2^\sigma \cup \theta^\sigma \subset \sigma,$$

where

$$p_1^\sigma = \{p_2 = q_1 = 0\} \cap \sigma \quad \textit{and} \quad p_2^\sigma = \{p_1 = q_1 = 0\} \cap \sigma$$

are coordinate axes on σ, and

$$\theta^\sigma := \left\{ -\tfrac{3}{10} \le p_2 \le 0,\ q_2 = \pm\tfrac{1}{2}\sqrt{-p_2(3+10\,p_2)},\ q_1 = 2\sqrt{2}\,p_2,\ p_1 = \sqrt{2}\,q_2 \right\}$$

has the form of a planar ellipse. The tangent plane $T_{\xi^*}\Lambda_{m,h}$ to $\Lambda_{m,h}$ at any point $\xi^* \in p_1^\sigma \cup \theta^\sigma \setminus \{0 \in \mathbb{R}^4\}$ belongs σ.

This and several auxiliary technical lemmas are proven in Sec. D.1.

Corollary 5.2. *The images of p_1^σ and p_2^σ under the map F (4.3) are*

$$F(p_1^\sigma) = \{m = 0, h > 0\} \quad \textit{and} \quad F(p_2^\sigma) = \{m < 0, h = m^2\} = \mathcal{C},$$

respectively; the image of θ^σ is a curve

$$F(\theta^\sigma)\colon [-\tfrac{3}{10}, 0] \to \mathbb{R}^2, \quad \text{where} \quad s \mapsto \big(3s^2, -\tfrac{1}{4}s^2(9+28s)\big).$$

For sufficiently small $|m|$, $\mathcal{C}$ is the line of the critical values of F (Proposition 3.4), which represent the singular fibers called curled tori (Proposition 3.5).

Proof. Substitute into (4.3) the definitions of p_1^σ, p_2^σ, and θ^σ in Lemma 5.2; cf. Lemma D.6 and Fig. D.2 in Sec. D.1. □

Corollary 5.3. *In the 1:(−2) case, the contour Γ has* three *nonregular points $\Gamma_2 = \Gamma \cap F(\theta^\sigma)$, $\Gamma_5 = \Gamma \cap F(p_1^\sigma)$, and $\Gamma_8 = \Gamma \cap \mathcal{C}$ shown in Fig.* 6. *The first two points are non-critical values of the (F_1, F_2) map; they correspond to regular fibers, whose intersections with σ are nonregular. Γ_8 is the critical value of the (F_1, F_2) map; it lifts to the curled torus Λ_{Γ_8}.*

Evolution of intersections $\lambda_{m,h}$ for $(m,h) \in \Gamma \setminus \Gamma_8$. We now comment on how the oriented components of the intersection $\lambda_{\Gamma_{(t)}}$ shown in Fig. 6 change as $\Gamma_{(t)} = (m,h)$ moves along the contour Γ towards the critical point Γ_8 starting at point Γ_0. The intersection λ_{Γ_0} has *four* connected components, which we denote O, A, B, and C according to the order in which they are traversed by the trajectories $\gamma_{\mathrm{f}} \subset \Lambda_{\Gamma_0}$ of the flow φ_{F_1} (see Lemma D.3 and Fig. 6, bottom). These four components are oriented using the technique explained above in the introductory part of Sec. 5. In particular, any two adjacent components have opposite orientation and the cycle $O + A + B + C$ is homotopic to zero.

While we go from Γ_0 up to Γ_2 via Γ_1, each connected component deforms continuously. Point Γ_2 is nonregular: at this point, the loop $O = OoO$ deforms continuously, but the three other loops (A, B, C) form one connected component with two branching points. Note, that, except at the branching points, the orientation of all regular segments of λ_{Γ_2} remains well defined, and that the cycle

formed by $(A + B + C)$ is homotopic to a simple closed curve, whose orientation is opposite to that of the loop OoO. After we pass Γ_2, the intersection $\lambda_{\Gamma_{(t)}}$ with $\Gamma_{(t)} \in (\Gamma_2, \Gamma_5)$ has *two* connected components OoO and $ABCA$. The orientation of these two closed curves is opposite and the cycle $OoO + ABCA$ is homotopic to zero.

As illustrated at points Γ_3 and Γ_4, the two loops OoO and $ABCA$ deform continuously as we approach the second nonregular point Γ_5, where they merge together at two branching points α and β into a single connected component of λ_{Γ_5}. This nonregular intersection splits into two *new* components OBO and $oACo$ as we pass Γ_5 and move toward Γ_6. (Here note that the origins of the charts of Λ_{Γ_4} and Λ_{Γ_5} in Fig. 6 are chosen differently.) Oriented properly, the loops OBO and $oACo$ form a cycle $OBO + oACo$ on λ_{Γ_6}, which is again homotopic to zero. The deformation $(OoO, ABCA) \to (OBO, oACo)$ for each of the loops involved is, of course, discontinuous. Comparing to the 1:(−1) case (Sec. 5.1 and Fig. 4, top), we observe a definite similarity of points Γ_5 in the 1:(−2) case and Γ_2 in the 1:(−1) case.

Basis elements of H_1. As before, we take the 2π-periodic trajectory γ_{f} of the system with Hamiltonian F_1 to represent the first basis element g_{f} of $H_1(\Lambda_{m,h})$ for all $(m,h) \in \Gamma \setminus \Lambda_{\Gamma_8}$. For (m,h) on the open segment $\Gamma_{\mathrm{I}} = (\Gamma_8, \Gamma_5) \ni \Gamma_0$, we choose the oriented connected component $OoO \subset \lambda_{(m,h)_{\mathrm{I}}}$ as the cycle $\eta_{(m,h)_{\mathrm{I}}}$, which represents the second basis element $e_{(m,h)_{\mathrm{I}}}$ of $H_1(\Lambda_{m,h})$. Note that by choosing the particular component OoO we "bypass" the nonregular point Γ_2, where OoO continues smoothly (Fig. 6, right). We verify that the index of the intersection $OoO \cap \gamma_{\mathrm{f}}$ is 1, and that together with g_{f} such $e_{(m,h)_{\mathrm{I}}}$ forms indeed the basis of $H_1(\Lambda_{(m,h)_{\mathrm{I}}})$, and, in particular, of $H_1(\Lambda_{\Gamma_0})$. At the same time, for (m,h) on the open segment $\Gamma_{\mathrm{II}} = (\Gamma_5\Gamma_6\Gamma_7\Gamma_8)$, the index of the intersection with γ_{f} for each of the two oriented connected components OBO and $oACo$ of $\lambda_{(m,h)_{\mathrm{II}}}$ equals 2. This reflects the change of relation between γ_{f} and connected components of $\lambda_{m,h}$, which occurs when we enter the region Γ_{II} from region Γ_{I}. As illustrated in Fig. 7, right, the cycles γ_{f} coil "once" on the tori $\Lambda_{(m,h)_{\mathrm{I}}}$, such as the "meager" torus Λ_{Γ_9}, and "twice" on the tori $\Lambda_{(m,h)_{\mathrm{II}}}$, such as the "fat" torus Λ_{Γ_7}. As a result, the cycle $\eta_{(m,h)_{\mathrm{II}}}$, which represents the basis element $e_{(m,h)_{\mathrm{II}}}$, cannot be just an oriented component of $\lambda_{(m,h)_{\mathrm{II}}}$. We can, however, choose $\eta_{(m,h)_{\mathrm{II}}}$, which is related explicitly to $\lambda_{(m,h)_{\mathrm{II}}}$ and γ_{f}. The particular choice

$$2\eta_{(m,h)_{\mathrm{II}}} = OBO - \gamma_{\mathrm{f}}$$

is used for the charts of $\Lambda_{(m,h)_{\mathrm{II}}}$ in Figs. 6 and 7, and is also shown on the three-dimensional model of Λ_7 in Fig. 7.

Charts $\Lambda_{\Gamma_8} \to \mathbb{R}^2/\mathbb{Z}^2$ of the curled torus. The curled torus Λ_{Γ_8} is a variety with one singular circle, which corresponds to the special π-periodic orbit γ_{f}^* of φ_{F_1}. (Recall from Proposition 3.3 that γ_{f}^* lies in the plane $\{p_1 = q_1 = 0\}$ and has the isotropy group Z_2.) All other φ_{F_1} orbits $\gamma_{\mathrm{f}} \subset \Lambda_{\Gamma_8}$ are regular and have period 2π. This means that in order to continue using g_{f} for a chart $\mathfrak{m}\colon \Lambda_{\Gamma_8} \to \mathbb{R}^2/\mathbb{Z}^2$ we should follow γ_{f}^* *twice* to time 2π while all other $\gamma_{\mathrm{f}} \subset \Lambda_{\Gamma_8}$ are naturally followed

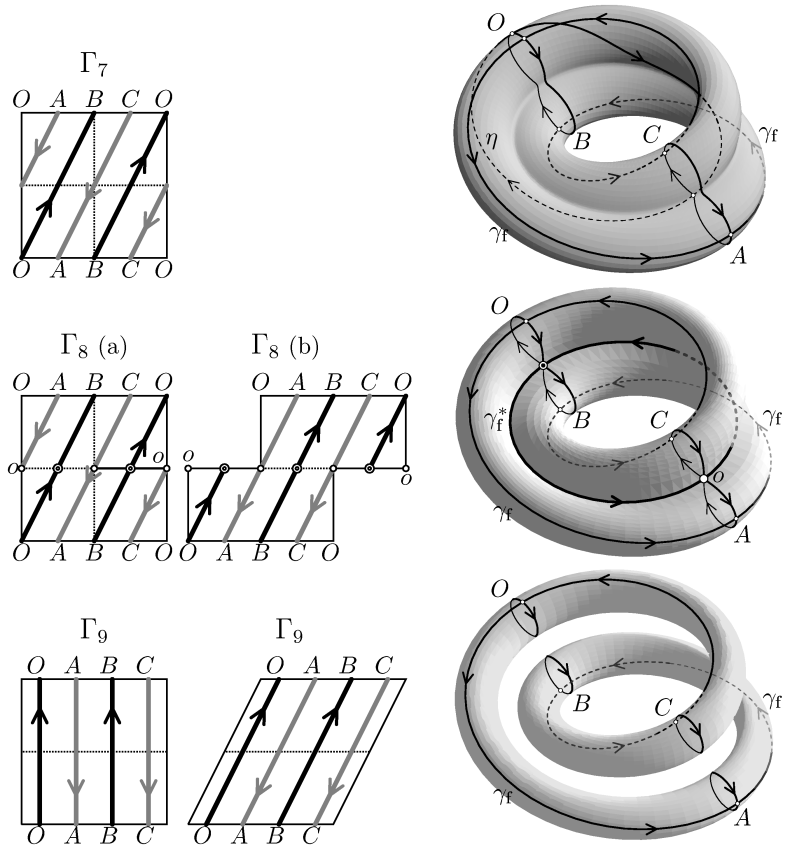

FIGURE 7. Evolution of the fiber $\Lambda_{\Gamma_{(t)}}$ (right column) and the corresponding modification of the image of the intersection $\Lambda_{\Gamma_{(t)}} \cap \sigma$ in the chart $\Lambda_{\Gamma_{(t)}} \to \mathbb{R}^2/\mathbb{Z}^2$ (left column), which occur when $\Gamma_{(t)}$ passes the critical nonregular point Γ_8; cf. Fig. 6, left. (See text for further explanations.)

once. If we do this, however, we should pairwise identify points in $\mathfrak{m}(2\gamma_{\mathrm{f}}^*) \subset \mathbb{R}^2/\mathbb{Z}^2$, which are separated by π. Note also that the open set $\Lambda_{\Gamma_8} \setminus \gamma_{\mathrm{f}}^*$ is simply connected and orientable, and that it can be oriented in the same way as any regular fiber $\Lambda_{\Gamma_{(t)}} \sim \mathbb{T}^2$. Furthermore, the intersection $(\Lambda_{\Gamma_8} \setminus \gamma_{\mathrm{f}}^*) \cap \sigma$ has four open disconnected components, which can be oriented just as any part of any regular intersection $\lambda_{\Gamma_{(t)}}$.

In Fig. 7, we represent λ_{Γ_8} using two equivalent charts $\mathfrak{m}$ of Λ_{Γ_8}, chart (a), which is also used in Fig. 6, and chart (b). On both charts, the horizontal line *oo* in the middle represents (two copies of) γ_{f}^*. On this line, points a and $a + \pi$ are

identical. In particular, the two kinds of identical points in the image $\mathfrak{m}\big(\Lambda_{\Gamma_8} \cap \sigma \cap 2\gamma_{\mathrm{f}}^*\big)$ are marked by empty and filled circles. We can obtain the (b) chart by shifting the upper part of the (a) chart by π along γ_{f}^*. The (a) chart is particularly useful for comparing Γ_8 to Γ_7, while the (b) chart, together with the somewhat unconventional torus chart $\Lambda_{\Gamma_9} \to \mathbb{R}^2/\mathbb{Z}^2$ used in Fig. 7 bottom, helps better understanding the transformation of λ_{Γ_8} as we move towards Γ_9. Namely, we have skewed the fundamental region of the torus covering $\Lambda_{\Gamma_9} \to \mathbb{R}^2/\mathbb{Z}^2$ in such a way that the identical points on the lower and upper boundary are shifted horizontally by π with respect to one another. Such representation corresponds to the (b) chart.

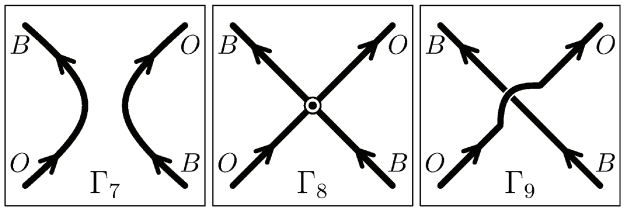

FIGURE 8. Schematic $\mathbb{R}^4$ representation of the rearrangement of the oriented components of the intersection $\Lambda_{\Gamma_{(t)}} \cap \sigma \subset \mathbb{R}^4$, which occurs when $\Gamma_{(t)}$ passes the curled torus point Γ_8. Ends labeled by the same letter are connected.

Crossing the singular line at Γ_8. We now consider the segment $[\Gamma_7, \Gamma_8, \Gamma_9]$, which contains one critical nonregular point Γ_8, and discuss what happens to the oriented components *OBO* and *oACo* of λ_{Γ_7} when $\Gamma_{(t)}$ goes from Γ_7 to Γ_9 and passes Γ_8. As shown in Figs. 6 and 7, *OBO* and *oACo* deform independently and continuously. On Λ_{Γ_8}, each component becomes a figure eight (Fig. 7, center right), whose singular point lies on γ_{f}^*. (Notice that on the charts of Λ_{Γ_8}, each connected component of λ_{Γ_8} has one pair of identified points.) As we depart towards Γ_9, each figure eight separates into two *disconnected* loops. The orientation of all segments of *OBO* and *oACo* is conserved during this continuous transformation: as we further illustrate schematically in Fig. 8, the orientation of the parts of the intersection λ_{Γ_8} agrees continuously with the one defined on the neighboring fibers, such as on the preceding Λ_{Γ_7} and the succeeding Λ_{Γ_9}.

The choice of γ_0. The presence of two qualitatively different regions Γ_{I} and Γ_{II} in the case of the 1:(−2) resonance imposes restrictions on the type of cycles $\gamma_{(t)}$, which can be deformed continuously when $\Gamma_{(t)}$ goes along the contour Γ. Indeed, we observe that section λ_{Γ_0} has *four* "small" disconnected components, while sections $\lambda_{(m,h)_{\mathrm{II}}}$ have only *two* "big" such components. Therefore, a cycle, which contains just one single loop in the direction of the second basis element e_0 of the homology group, cannot pass between Γ_{I} and Γ_{II}. This can be seen most clearly, if we enter Γ_{II} at Γ_8 by coming in reverse from Γ_0 and Γ_9; see Fig. 7. (Notice that the sections λ_{Γ_0} and λ_{Γ_9} are qualitatively the same.) We realize that the only

cycles which can pass this way (cf. Definition 2.4) are the ones, which represent the elements of the homology group which belong to subset $\{2a\,e_0+b\,g_{\rm f},\ a,b\in\mathbb{Z}\}$. In other words, we need to have a double loop in the direction e_0. In particular, the cycle $\gamma_0=2\eta_0=2\,(OoO)$ is passable.

Going back to the statement of the 1:(−2) monodromy Theorem 2, recall that the curled torus $\Lambda_{\Gamma_8}=\Lambda_-$ is part of the internal wall W_0 crossed by the path δ_Γ. Any cycle which can pass through W_0 represents an element of H_1 in the set $\{2a\,e_0+b\,g_{\rm f},\ a,b\in\mathbb{Z}\}$. Consider now the subgroup $\zeta_0\subset H_1(\Lambda_{\Gamma_0})$ generated by the basis elements $(g_{\rm f},g_0)=(g_{\rm f},2e_0)$. Since $\zeta_0=H_1(\Lambda_{\Gamma_0})/Z_2\sim\mathbb{Z}^2$, it is a complete subgroup of $H_1(\Lambda_{\Gamma_0})$. Thus, one of the main requirements for the admissibility of the path δ_Γ in Definition 2.6 is satisfied. Furthermore, ζ_0 is the lowest index subgroup of $H_1(\Lambda_{\Gamma_0})$, for which the map μ_{δ_Γ} in (2.2) can be defined.

Continuous deformation of the cycle $\gamma_0=2\eta_0$. Now we explain the last technical step in the proof of the monodromy Theorem 2. As the point $\Gamma_{(t)}$ starts at $\Gamma_{(t)}\big|_{t=0}=\Gamma_0$ and moves counterclockwise along the contour Γ, we construct and analyze the deformation $\gamma_{(t)}$ of the element $\gamma_0=2\eta_0=2\,OoO$ of H_1 chosen at Γ_0 (see Fig. 6). Compared to the 1:(−1) case, this deformation becomes more complicated in the 1:(−2) case.

When $\Gamma_{(t)}$ passes the interval $[\Gamma_0,\Gamma_5)$, the cycle $\gamma_{(t)}$ follows the cycle $2\eta_{(t)}=2\,OoO$, whose continuous deformation is described above. The cycle OoO cannot be continued past Γ_5, where it gets involved into the rearrangement of the connected components of the intersection $\lambda_{(t)}$. We replace $\gamma_{\Gamma_4}=2\eta_{\Gamma_4}$ by a homotopic cycle $\tilde\gamma_{\Gamma_4}$, which can be deformed smoothly till $\Gamma_{(t)}=\Gamma_6$. A detailed analysis of the intersections $\lambda_{\Gamma_{(t)}}$ and of the homotopically equivalent cycles $\tilde\gamma_{(t)}$ for $\Gamma_{(t)}\in[\Gamma_4,\Gamma_6]$ near Γ_5 is central to the monodromy calculation. (This makes Γ_5 similar to the point Γ_2 of the 1:(−1) case.) Below we explain the construction of $\tilde\gamma_{(t)}$ using the torus charts in Fig. 9. The corresponding analysis on σ is presented in Appendix D. In particular, see Figs. D.7, D.8, and D.9 of Sec. D.2, where the points on σ are denoted by the same letters as the corresponding points on the torus charts.

As shown in Fig. 9, top right, the cycle $\tilde\gamma_{\Gamma_4}=O\beta^1\beta^3B\alpha^3\alpha^1(-\gamma_{\rm f})\alpha^1O$ is built of the following properly oriented fragments:

i. Fragments $O\beta^1$ and α^1O of the initial oriented connected component OoO of the intersection $\lambda_{\Gamma_4}=\Lambda_{\Gamma_4}\cap\sigma$.
ii. Fragment $\beta^3B\alpha^3$ of the other connected component of λ_{Γ_4}.
iii. Fragments $\beta^1\beta^3$ and $\alpha^3\alpha^1$, which belong to the fiber Λ_{Γ_4} but do not lie in σ.
iv. Fragment $\alpha^1(-\gamma_{\rm f})\alpha^1$, which is a φ_{F_1} trajectory taken backward.

The cycle $\tilde\gamma_{\Gamma_4}$ formed by all these fragments is homotopic to the double loop $2(OoO)$. As shown in Fig. 9, top center, the deformation $\tilde\gamma_{(t)}$ of $\tilde\gamma_{\Gamma_4}$ for $\Gamma_{(t)}\in[\Gamma_4,\Gamma_6]$ is smooth, because the two small fragments $\beta^1\beta^3$ and $\alpha^3\alpha^1$ bypass the nonregular points α and β of the intersection λ_{Γ_5} and the discontinuity is avoided. Arriving at point Γ_6, we pull $\beta^1\beta^3$ and $\alpha^3\alpha^1$ back into $\lambda_{\Gamma_6}\subset\sigma$ in order to replace $\tilde\gamma_{\Gamma_6}$ by the homotopically equivalent cycle $\gamma_{\Gamma_6}=O\beta^4B\alpha^4O-\gamma_{\rm f}$. The

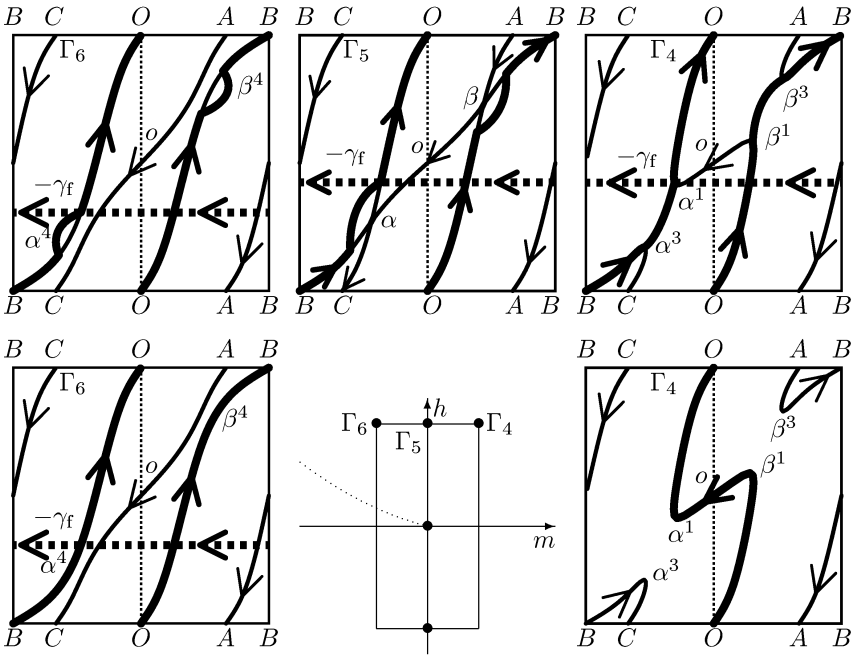

FIGURE 9. Continuous evolution of the cycle $\gamma_{(t)}$ homotopic to $\gamma_0 = 2(OoO)$ as $\Gamma_{(t)} = \Gamma_{m,h}$ goes along the contour Γ from Γ_4 to Γ_6 and passes the nonregular point Γ_5; compare to Figs. D.7, D.8, and D.9 in Appendix D.2 and see text for detailed discussion.

latter cycle is formed by two loops: the reversed φ_{F_1} trajectory $-\gamma_{\rm f}$ and one "big" connected component $OBO = O\beta^4 B\alpha^4 O$ of λ_{Γ_6}.

Further deformation $\gamma_{(t)}$ of γ_{Γ_6} is smooth everywhere except at the critical nonregular point Γ_8, where it is only continuous. But this, of course, is sufficient for our purpose. When we pass Γ_8, the cycle $\gamma_{\Gamma_7} = OBO - \gamma_{\rm f}$ turns into $\gamma_{\Gamma_9} = OO + BB - \gamma_{\rm f}$ formed by two oriented components OO and BB of the intersection λ_{Γ_9} and the loop $-\gamma_{\rm f}$. Then $(OO + BB - \gamma_{\rm f})$ continuous smoothly as we move along the final segment from Γ_9 to $\Gamma_{(t)}\big|_{t=1} = \Gamma_0$. So, after one counterclockwise tour along the contour Γ, the cycle $\gamma_0 = 2(OO)$, which was chosen initially at Γ_0, becomes $\gamma_1 = \gamma_{(t)}\big|_{t=1} = (OO + BB - \gamma_{\rm f})$. Since on the torus Λ_{Γ_0}, the loops OO and BB are homotopically equivalent, γ_1 is homotopic to $\gamma_0 - \gamma_{\rm f}$.

Computing monodromy. The cycle γ_1 represents the element $2e_0 - g_{\rm f}$ of the homology group $H_1(\Lambda_{\Gamma_0})$. Consequently, the basis elements $(g_{\rm f}, 2e_0)$ of the index 2 complete subgroup $\zeta \subset H_1(\Lambda_{\Gamma_0})$ transform as follows

$$\begin{pmatrix} g_{\rm f} \\ 2e_0 \end{pmatrix} = \begin{pmatrix} g_{\rm f} \\ g_0 \end{pmatrix} \to \begin{pmatrix} g_{\rm f} \\ g_1 \end{pmatrix} = \begin{pmatrix} 1 & 0 \\ -1 & 1 \end{pmatrix} \begin{pmatrix} g_{\rm f} \\ g_0 \end{pmatrix} = \begin{pmatrix} g_{\rm f} \\ g_0 - g_{\rm f} \end{pmatrix} = \begin{pmatrix} g_{\rm f} \\ 2e_0 - g_{\rm f} \end{pmatrix}$$

It turns out that in the basis (g_{f}, g_0), the matrix of the automorphism $\mu_{\delta_\Gamma}^{1:(-2)}$: $\zeta \to \zeta$ has the same form as we had for the automorphism $\mu_{\delta_\Gamma}^{1:(-1)}$ of the whole homology group $H_1(\Lambda_{\Gamma_0})$ in the case of the $1{:}(-1)$ resonance. We can formally *extend* $\mu_{\delta_\Gamma}^{1:(-2)}$ from ζ to the whole space $\mathbb{R}^2 \supset H_1(\Lambda) \sim \mathbb{Z}^2$ using the linear transformation of the basis $(g_{\mathrm{f}}, 2\,e_0) \to (g_{\mathrm{f}}, e_0)$. Such extended monodromy map has *fractional* matrix $\left(\begin{smallmatrix} 1 & 0 \\ -\frac{1}{2} & 1 \end{smallmatrix}\right)$. This completes the torus chart explanation of the monodromy theorem for the integrable fibration (4.3). Further details of the proof follow in Appendix D.

6. Quantum manifestation of monodromy

In this section, we consider quantum analogs of the classical integrable systems defined by the integrable mapping (F_1, F_2), which we have studied up to now. We will simplify the general situation (see Sec. 2.2), and imply that, like in our concrete example systems in Sec. 4, each value (f_1, f_2) of (F_1, F_2) corresponds to one fiber Λ_{f_1,f_2}. We construct two quantum commuting differential operators $\hat{F}_1$ and $\hat{F}_2$, which in the classical limit become two classical Hamiltonian functions in involution F_1 and F_2. The operator $\hat{F}_1$ can be regarded as the angular momentum operator, and the operator $\hat{F}_2$ – as the quantum Hamiltonian.

6.1. Lattice representation of the joint quantum spectrum

Solving the above quantum problem means finding a common system of eigenfunctions of $\hat{F}_1$ and $\hat{F}_2$. Since we consider classical systems with compact constant level sets of (F_1, F_2), in other words, since our system is bound and the classical motion is finite, we should have a *discrete* set of eigenfunctions $\{\psi_{\{k\}}(q)\}$ labeled by a finite set $\{k\}$ of integer indexes. The corresponding discrete joint spectrum of eigenvalues $f_{i\{k\}}$, such that $\hat{F}_i\psi_{\{k\}} = f_{i\{k\}}\psi_{\{k\}}$, for $i = 1, 2$, can be represented as a set $\mathcal{L}$ of points in the plane $\mathbb{R}^2$ with coordinates (f_1, f_2) and can be found numerically.

The Einstein–Brillouin–Keller (EBK) quantization scheme of classical integrable systems gives a way of finding the joint quantum spectrum of $(\hat{F}_1, \hat{F}_2)$ in the semiclassical limit. The underlying EBK correspondence principle is well suited to relate our preceding classical study to this spectrum. Recall that in order to find the semiclassical EBK energies, we look for the EBK tori, or such regular tori $\Lambda_{m,h}^{\mathrm{EBK}}$ of our classical system on which the values (i_1, i_2) of the two locally chosen action integrals (I_1, I_2) equal

$$2\pi\hbar(n_1 + \alpha_1) = i_1 = \oint_{\eta_1} p\,dq, \quad 2\pi\hbar(n_2 + \alpha_2) = i_2 = \oint_{\eta_2} p\,dq, \tag{6.1a}$$

where integers $(n_1, n_2) \in \mathbb{Z}$ are called *local quantum numbers*. Near the classical limit, (n_1, n_2) are large and the density of states is high. The quantities (α_1, α_2) in

(6.1) are semiclassical corrections (typically multiples of $\frac{1}{4}$), which are often called Maslov's indexes.

The integrals in (6.1) are taken along any cycle η_k representing the respective element e_k of the local basis (e_1, e_2) of $H_1(\Lambda^{\mathrm{EBK}}_{m,h})$. In our problem the "correcting terms" (α_1, α_2) are the same for all η_k (for all cycles in the same homology class). All operations on elements of H_1 induce operations on actions or, equivalently, on quantum numbers. For each element in $H_1(\Lambda^{\mathrm{EBK}}_{m,h})$ we obtain

$$ae_1 + be_2 \to \oint_{a\eta_1+b\eta_2} pdq = ai_1 + bi_2, \quad a, b \in \mathbb{Z}, \tag{6.1b}$$

thus specifying the explicit isomorphism between the homology group H_1 of the regular 2-torus $\Lambda^{\mathrm{EBK}}_{m,h}$ and the $\mathbb{Z}^2$ lattice of quantum numbers.

In the domain $U \subseteq \mathbb{R}^4_{q,p}$ of their definition, the local actions (I_1, I_2) can be expressed as C^∞ smooth single valued real functions of the first integrals (F_1, F_2). It can be proved [54] that F_1 and F_2 can be expressed locally (on U) as $F_1(I_1, I_2)$ and $F_2(I_1, I_2)$. It can be shown equally that "correcting terms" $\alpha_{1,2}$ in our systems remain the same for all tori $\Lambda \in U$. Then in the corresponding quantum system, the eigenvalues f_1 and f_2 can be represented locally as $f_1(n_1, n_2)$ and $f_2(n_1, n_2)$. These expressions have an unambiguous classical limit, in which they become smooth single-valued real functions $f_1(i_1, i_2)$ and $f_2(i_1, i_2)$. Notice also that due to their S^1 symmetry, our example systems are simpler: the corresponding first integral F_1 is a global action and consequently, $n_1 \in \{k\}$ can serve as a global quantum number of momentum $\hat{F}_1$. At the same time, monodromy makes the global choice of n_2 impossible.

Consider now the range $\tilde{D}$ of the local momentum map

$$I\colon U \subset \mathbb{R}^4 \to \tilde{D} \subset \mathbb{R}^2\colon (q,p) \to \big(I_1(q,p), I_2(q,p)\big) = (i_1, i_2).$$

Under this map, the images of $\Lambda^{\mathrm{EBK}}_{m,h} \subset U$ form a square $\mathbb{Z}^2$ lattice in $\tilde{D} \subset \mathbb{R}^2_{i_1,i_2}$. Using expressions $F_1(I_1, I_2)$ and $F_2(I_1, I_2)$ for the first integrals, we can map $\tilde{D}$ to a domain D in the range of the $\mathcal{EM}$ map in $\mathbb{R}^2_{f_1,f_2}$. Since $\tilde{D} \to D$ is a local diffeomorphism, it maps locally the $\mathbb{Z}^2$ lattice of "integer points" $(i_1, i_2) = \big(2\pi\hbar(n_1+\alpha_1), 2\pi\hbar(n_2+\alpha_2)\big)$ in $\tilde{D}$ to a lattice of points (f_1, f_2) in D, as illustrated below.

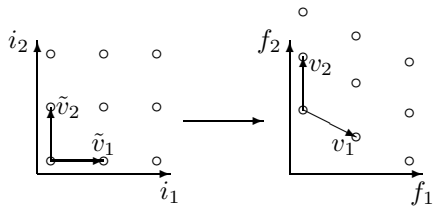

(6.2)

Notice that the thus obtained points $(f_1(n_1, n_2), f_2(n_1, n_2))$ of the semiclassical lattice in D differ from the quantum points $(f_{1\{k\}}, f_{2\{k\}})$ by $o(\hbar)$, i.e., by a small fraction of the typical distance between the vertices of our lattice. It follows that

the joint spectrum of $\hat{F}_1$ and $\hat{F}_2$ has *locally* the structure of the regular $\mathbb{Z}^2$ lattice which is slightly nonlinearly distorted.

Consider now the *elementary cell* of the quantum lattice in $\mathbb{R}^2_{i_1,i_2}$. At a point $\tilde{a} = (i_1, i_2)$, this cell is defined by a pair $(\tilde{v}_1, \tilde{v}_2)$ of 2-vectors. Like the choice of the basis elements of the homology group, the choice of the cell is ambiguous: all that is required from $(\tilde{v}_1, \tilde{v}_2)$ is to begin at (i_1, i_2) and define two translations, which generate the complete $\mathbb{Z}^2$ group. Additionally, we can, of course, require $(\tilde{v}_1, \tilde{v}_2)$ to agree with the choice of the basis (e_1, e_2) for the EBK torus represented by the node (i_1, i_2). Then we obtain a square elementary cell with sides $2\pi\hbar$. As shown schematically in (6.2), this square cell becomes nonlinearly distorted when mapped into $D \subset \mathbb{R}^2_{f_1,f_2}$. The distorted cell at the corresponding node $a = (f_1, f_2)$ in D is a quadrilateral *abcd*

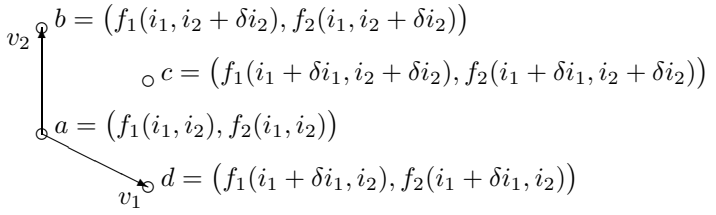

(6.3)

where $\delta i_1 = \delta i_2 = 2\pi\hbar$ are the sides of the cell of the $\mathbb{Z}^2$ lattice in $\tilde{D}$. Near the classical limit $\hbar \to 0$, we obtain

$$
\begin{aligned}
b &= a + 2\pi\hbar \left(\frac{\partial F_1}{\partial I_2}, \frac{\partial F_2}{\partial I_2} \right)_{\tilde{a}} + o(\hbar), \\
d &= a + 2\pi\hbar \left(\frac{\partial F_1}{\partial I_1}, \frac{\partial F_2}{\partial I_1} \right)_{\tilde{a}} + o(\hbar), \\
c &= a + 2\pi\hbar \left(\frac{\partial F_1}{\partial I_1}, \frac{\partial F_2}{\partial I_1} \right)_{\tilde{a}} + 2\pi\hbar \left(\frac{\partial F_1}{\partial I_2}, \frac{\partial F_2}{\partial I_2} \right)_{\tilde{a}} + o(\hbar).
\end{aligned}
$$

Then with an error of $o(\hbar)$, the distorted cell *abcd* can be approximated as a parallelogram defined by the pair (v_1, v_2) of 2-vectors

$$
v_1 = 2\pi\hbar \left. \frac{\partial}{\partial I_1} \right|_{\tilde{a}} \begin{pmatrix} F_1 \\ F_2 \end{pmatrix}, \quad v_2 = 2\pi\hbar \left. \frac{\partial}{\partial I_2} \right|_{\tilde{a}} \begin{pmatrix} F_1 \\ F_2 \end{pmatrix},
$$

or, equivalently, by the matrix

$$
(v_1, v_2) = 2\pi\hbar \begin{pmatrix} \dfrac{\partial F_1}{\partial I_1} & \dfrac{\partial F_1}{\partial I_2} \\ \dfrac{\partial F_2}{\partial I_1} & \dfrac{\partial F_2}{\partial I_2} \end{pmatrix}. \tag{6.4a}
$$

Recall also that in our particular case (Sec. 3), F_1 is a global action and we always use $I_1 = F_1$ with value $f_1 = i_1 = m$. So, consequently,

$$(v_1, v_2) = 2\pi\hbar \begin{pmatrix} 1 & 0 \\ \dfrac{\partial F_2}{\partial I_1} & \dfrac{\partial F_2}{\partial I_2} \end{pmatrix}. \tag{6.4b}$$

Finally notice that (6.4) is a 2×2 matrix whose columns are formed by column-vectors v_1 and v_2. We will denote the transposed matrix as

$$(v_1, v_2)^T = \begin{pmatrix} v_1^T \\ v_2^T \end{pmatrix} := \begin{pmatrix} v_1 \\ v_2 \end{pmatrix}. \tag{6.5}$$

Technically, the rows of this latter matrix are formed by the row-vectors v_1^T and v_2^T, but we drop the transposition symbols in the rightmost shorthand form in (6.5).

6.2. Transformation properties of elementary cells and of bases of homology group

Relation between the basis (e_1, e_2) of the homology group $H_1(\Lambda)$ and the corresponding elementary cell (v_1, v_2) is similar to that of the vector $x \in \mathbb{R}^2$ and the gradient ∇_x. Recall that if we change coordinates in $\mathbb{R}^2$ so that $x = Ay$, where $A \in \mathrm{GL}(2)$, then $\nabla_y = A^T \nabla_x$, i.e., ∇_x transforms as a covector.

To uncover the transformation properties of elementary cells, consider again the regular 2-torus fiber Λ_a represented by the value $a = (f_1, f_2)$ of the integrable map $F = (F_1, F_2)$. Let (e_1, e_2) be a basis of the homology group $H_1(\Lambda_a)$ and consider local actions (I_1, I_2), whose values $\tilde{a} = (i_1, i_2)$ correspond to (e_1, e_2) as in (6.1). Finally, define the corresponding elementary cell (v_1, v_2) using (6.4). Consider next a different basis (e_1', e_2') of $H_1(\Lambda_a)$, such that

$$\begin{pmatrix} e_1' \\ e_2' \end{pmatrix} = A \begin{pmatrix} e_1 \\ e_2 \end{pmatrix}, \quad A \in \mathrm{SL}(2, \mathbb{Z}),$$

and corresponding new actions (J_1, J_2) and elementary cell (u_1, u_2).

Lemma 6.1. *The relation between the new and the old elementary cell is*

$$(u_1, u_2)^T = \left(A^{-1}\right)^T (v_1, v_2)^T.$$

Proof. We can write the transposed cell matrix as

$$(v_1, v_2)^T = \left(\nabla_I F_1, \nabla_I F_2\right), \quad \text{where } \nabla_I = \begin{pmatrix} \dfrac{\partial}{\partial I_1} \\ \dfrac{\partial}{\partial I_2} \end{pmatrix}.$$

Similarly, $(u_1, u_2)^T = \left(\nabla_J F_1, \nabla_J F_2\right)$. As shown in (6.1), actions and cycles transform in the same way. Therefore

$$\begin{pmatrix} J_1 \\ J_2 \end{pmatrix} = A \begin{pmatrix} I_1 \\ I_2 \end{pmatrix}.$$

The lemma follows after a standard calculation of the gradient $\nabla_J = \left(A^{-1}\right)^T \nabla_I$. □

It is useful to extend the above lemma to a larger set $K \subset \mathrm{GL}(2,\mathbb{Q})$ of 2×2 transformation matrices B with integer coefficients and determinant $\det B \geq 1$. Unlike $\mathrm{SL}(2,\mathbb{Z}) \subset K$, the set K is not a group, because $K \not\ni B^{-1}$ for any $B \in K$ with $\det B > 1$. At the same time, $(\det B)B^{-1} \in K$ and $\det\big((\det B)B^{-1}\big) = \det B$.

Corollary 6.1. *Let $e = (e_1, e_2)$ and (v_1, v_2) be the initial basis of H_1 and the respective elementary cell of Lemma* 6.1. *Let matrix $B \in K$ define a pair of elements $g = (g_1, g_2)$ of H_1 as $B\,e$. Then the cell corresponding to g is*

$$(w_1, w_2)^T = \det B \left(B^{-1}\right)^T (v_1, v_2)^T.$$

Definition 6.1. The cell (w_1, w_2) in Corollary 6.1 with $\det B > 1$ is called *multiple cell* defined by matrix B.

Let matrix $B \in K$ with $\det B > 1$ define a basis (g_1, g_2) of some complete subgroup $\zeta \subset H_1(\Lambda_a)$. In the open domain $D \ni a$ of regular values of F in $\mathbb{R}^2_{f_1,f_2}$, where the "quantum" lattice $\mathcal{L}$ can be represented by (mapped to) a regular $\mathbb{Z}^2$ lattice L, the subgroup ζ corresponds to a $\mathbb{Z}^2$ *sublattice* l_ζ of L. The basis cell of l_ζ is a multiple cell. Corollary 6.1 provides the exact relation between multiple and elementary cells. In particular, the volume of (w_1, w_2) is $\det B$ times the volume of (v_1, v_2).

As an example, recall the elements $(g_\mathrm{f}, g_0) = (g_\mathrm{f}, 2e_0)$ of the homology group $H_1(\Lambda_{\Gamma_0})$ and their representatives $(\gamma_\mathrm{f}, \gamma_0)$ introduced in Sec. 5.2. These elements generate an order-two subgroup H_1/Z_2. Let (v_1, v_2) be an elementary cell which corresponds to the basis (g_f, e_0) of $H_1(\Lambda_{\Gamma_0})$. By Corollary 6.1, the multiple cell (w_1, w_2) corresponding to (g_f, g_0) is the double cell $(2v_1, v_2)$.

6.3. Quantum monodromy

Quantum-classical $\mathcal{EM}$ diagram. The global structure of the quantum lattice $\mathcal{L}$ in the quasi-classical limit can be well uncovered if we superimpose the whole joint spectrum, the range of the classical energy–momentum map $\mathcal{EM}$, and the image of the critical values of $\mathcal{EM}$ (the bifurcation diagram of the critical fibers) in the plane $\mathbb{R}^2$ with coordinates (f_1, f_2). Such representation, which we will call *quantum-classical $\mathcal{EM}$ diagram*, is very helpful in the analysis of global qualitative features of the joint quantum spectrum and it will be used throughout this section (cf. Figs. 10 and 12). $\mathcal{EM}$ diagrams have direct applications in attributing physically consistent quantum numbers to quantum states of concrete real systems, e.g., molecules or atoms. Clearly, the attribution becomes a problem if the quantum lattice $\mathcal{L}$ is globally not a regular lattice $\mathbb{Z}^2$. We show that precisely this happens when the classical analogue system has nontrivial monodromy.

Quantum analogue of Γ. We require that the size (area) of the local elementary cells of $\mathcal{L}$ should be much smaller compared to the area encircled by the closed path Γ in Fig. 3. Theoretically this is always achievable by transferring, if necessary, to an equivalent quantum system with higher density of states (closer to the classical limit). Formally we can use a sufficiently small value of $\hbar$; in real systems, we can instead change a combination of physical parameters, such as mass and

size. Working with such equivalent system means introducing additional states, which are fictitious, but which help to uncover monodromy.

Having made sure that the lattice $\mathcal{L}$ in the quantum-classical $\mathcal{EM}$ diagram is sufficiently dense, we construct a small deformation $\Gamma + \delta\Gamma$ of the closed path Γ, which passes through a finite discrete set $\Gamma^{\rm quant} = \{\Gamma^{\rm quant}_{(t)}\}$. To label members of $\Gamma^{\rm quant}$, we use the discrete parameter $t \in [0,1]$, whose values $\{0, t_1, t_2, \ldots, 1\}$ represent nodes of $\mathcal{L}$ with some local quantum numbers (n_1, n_2). The set $\Gamma^{\rm quant}$ can be made large enough for the distances between the neighboring nodes $\Gamma^{\rm quant}_{(t)}$ to be small, i.e., of the order of $\hbar$. Similarly to Sec. 5, we will also use simple indexes $k = 0, 1, 2, \ldots$, for some elements $\{\Gamma^{\rm quant}_k\} \subseteq \Gamma^{\rm quant}$. Again, since the lattice mesh is $2\pi\hbar$-dense, we can make the distances $\|\Gamma_k, \Gamma^{\rm quant}_k\| \le 2\pi\hbar$.

Atlas of local regular $\mathbb{Z}^2$ charts of $\mathcal{L}$ near Γ. To make use of the locally regular $\mathbb{Z}^2$ structure of the quantum lattice $\mathcal{L}$, we construct an *atlas* of $\mathcal{L}$ near Γ, which covers Γ and $\Gamma^{\rm quant}$ by a finite number of overlapping *charts* $\Phi_s\colon D_s \to \tilde{D}_s \supset L_s$, $s = 0, 1, \ldots$. Here $\Phi_s = I_s \circ F^{-1}$ is a map from an open simply connected domain $D_s \subset \mathbb{R}^2_{f_1,f_2}$ to domain $\tilde{D}_s \subset \mathbb{R}^2_{i_1,i_2}$ containing regular $\mathbb{Z}^2$ lattice L_s with basis cell $(\tilde{v_1}, \tilde{v_2})_s$ and $I_s = (I_1, I_2)_s$ are local actions. Each D_s covers part of $\mathcal{L}$ and its linear sizes are large compared to $2\pi\hbar$.

Definition 6.2. When the regular $\mathbb{Z}^2$ lattice L_s represents all nodes of $\mathcal{L}$ covered by D_s, the chart $\Phi_s\colon D_s \to \tilde{D}_s \supset L_s$ is called *full $\mathbb{Z}^2$-lattice chart*; otherwise it is called *$\mathbb{Z}^2$-sublattice chart*.

For clarity, we mark sublattice charts and their basis cells by an asterisk.

Definition 6.3. For full lattice charts we call basis cells $(v_1, v_2)_s$ of $\mathcal{L}_s \subset D_s$ and $(\tilde{v_1}, \tilde{v_2})_s$ of $L_s \subset \tilde{D}_s$ *elementary cells*. For sublattice charts we call basis cells $(u_1, u_2)^*_s$ and $(\tilde{u_1}, \tilde{u_2})^*_s$ *minimal cells*. With respect to elementary cell (v_1, v_2), the minimal cell $(u_1, u_2)^*$ is a multiple cell (see Definition 6.1).

To characterize each chart $\Phi_s\colon D_s \to \tilde{D}_s \supset L_s$ more completely, we can specify a finite set of regular values $G_s \subset \Gamma \cap D_s$ of the integrable map F. If Φ_s is a full lattice chart, then using (6.4) we can choose the elementary cell $(v_1, v_2)_s$ in agreement with the bases of $H_1(\Lambda_{\Gamma_k})$ for *all* Γ_k and the nearby $\Gamma^{\rm quant}_k$ in the set G_s simultaneously. Similarly, the minimal cell of a sublattice chart Φ^*_s can be chosen in agreement with the bases of a given subgroup $\zeta \subset H_1(\Lambda_{\Gamma_k})$ for all $\Gamma_k \subset G_s$.

Any two neighboring charts Φ_a and Φ_b in an atlas overlap on a *common sublattice* $CL(L_a, L_b)$. If both Φ_a and Φ_b are full charts, $CL(L_a, L_b) \sim L_a \sim L_b$; if Φ^*_a is a sublattice chart and Φ_b is a full lattice chart, $CL(L^*_a, L_b) \sim L^*_a$; if both are sublattice charts, their $CL(L^*_a, L^*_b)$ is yet another sublattice corresponding to $\zeta_a \cap \zeta_b$. Elementary cells of the overlapping neighboring full lattice charts are related by a linear map with matrix in $\mathrm{SL}(2,\mathbb{Z})$. In a more general case, when one or both overlapping charts are sublattice charts, we define an $\mathrm{SL}(2,\mathbb{Z})$ map for the minimal cells of their common sublattice.

Definition 6.4. We call the sublattice CL which is common to all charts of atlas $\{\Phi_s\}$ *common sublattice* of this atlas. The basis cell of CL is the *minimal cell* of this atlas.

Notice that for an atlas with no sublattice charts the basis cell is an elementary cell. In other cases, finding a common lattice and its basis cell might be less trivial.

Transporting lattice cells along Γ. Our approach to the semi-global characterization of the quantum lattice $\mathcal{L}$ is similar to the one we used to study classical monodromy in Sec. 5. We choose the initial point $\Gamma_0^{\text{quant}} = \Gamma_{(t)}^{\text{quant}}\big|_{t=0} \in \Gamma^{\text{quant}}$. In the regular open neighborhood D_0 of this point we have the part $\mathcal{L}_0$ of the quantum lattice $\mathcal{L}$ together with a full lattice chart $\Phi_0 \colon D_0 \to \tilde{D}_0 \supset L_0$. We use the elementary cell $(v_1, v_2)_0$ of $\mathcal{L}_0$ which corresponds to the basis (g_{f}, e_0) of $H_1(\Lambda_{\Gamma_0})$.

Next we define the cell $(w_1, w_2)_0$, which corresponds to the basis (g_{f}, g_0) of a subgroup of $H_1(\Lambda_{\Gamma_0})$ chosen in such a way that these elements can pass along the path δ_Γ. In the classical theory (Sec. 5), we construct a continuous deformation $(g_{\text{f}}, g_{(t)})$ of (g_{f}, g_0). In the quantum theory, this corresponds to *transporting* the cell $(w_1, w_2)_{(t)}$ along Γ^{quant}, which can be illustrated in the quantum-classical $\mathcal{EM}$ diagram (see for example Fig. 10) as moving $(w_1, w_2)_{(t)}$ in small steps of order $\hbar$. At each such step, the lower left vertex of the cell moves from the node $\Gamma_{(t_1)}^{\text{quant}}$ to its neighbor $\Gamma_{(t_2)}^{\text{quant}}$ in the counterclockwise direction along Γ^{quant} while the cell undergoes a small deformation.

Transporting $(w_1, w_2)_0$ relies on the atlas. Within each chart $\Phi_s \colon D_s \to \tilde{D}_s \supset L_s$, the cell $(w_1, w_2)_{(t)}$ is transported straightforwardly: we map $D_s \to \tilde{D}_s \subset \mathbb{R}^2_{i_1,i_2}$ and $(w_1, w_2)_0 \to (\tilde{w}_1, \tilde{w}_2)_0$, translate the cell $(\tilde{w}_1, \tilde{w}_2)_0$ in $\tilde{D}_s$ using the generators of the regular $\mathbb{Z}^2$ lattice L_s, and then return to D_s. We transfer the cell between charts using the $\mathrm{SL}(2, \mathbb{Z})$ maps relating them. Notice that in order to pass between a full lattice and a sublattice chart, our cell $(w_1, w_2)_{(t)}$ should be the minimal cell of their common sublattice. Furthermore, in order to pass along the whole contour Γ, our cell should be the minimal cell of the common sublattice of the atlas.

Let now $\mathcal{L}$ be the joint eigenspectrum lattice of quantum analogs $\hat{F}_1$ and $\hat{F}_2$ of the concrete first integrals F_1 and F_2 defined in Sec. 3. Let δ_Γ and Γ be the closed *admissible* path (recall Definition 2.6) and its image under the integrable map F constructed in Sec. 5. Let $\{\Gamma_k\}$ be a finite set of points on Γ, such that all Λ_{Γ_k} are regular 2-torus fibers of F. Some of these points correspond to points in Sec. 5. Let $\{\Gamma_k^{\text{quant}}\}$ be the quantum approximation of $\{\Gamma_k\}$.

Proposition 6.1. *The closed path Γ, the set Γ^{quant}, and their neighborhood can be covered by an atlas $\{\Phi_s \colon D_s \to \tilde{D}_s \supset L_s\}$ of a finite number of charts; each chart is further characterized by a segment $\Gamma \cap D_s$ or just by a set of reference points Γ_k of this segment. This atlas has a nonempty common $\mathbb{Z}^2$ sublattice CL. All charts Φ_s, which cover only regular values of F, are full $\mathbb{Z}^2$ lattice charts. The atlas can include a finite number of $\mathbb{Z}^2$ sublattice charts Φ_s^*, which cover weakly nonregular values c of F near and on Γ. Elementary cells $(v_1, v_2)_s$ of full lattice charts can*

be chosen to agree with the cycle bases of all $H_1(\Lambda_{\Gamma_k})$ *for* $\Gamma_k \in D_s$*; minimal cells* $(v_1, v_2)_s^*$ *of sublattice charts can be chosen to agree with the bases of an appropriate subgroup of* $H_1(\Lambda_{\Gamma_k})$*. The minimal cell* (w_1, w_2) *of the common sublattice* CL *can be transported along the whole contour* Γ *which is approximated by the nearby discrete set* Γ^{quant}*. Starting in the domain* D_0 *with cell* $(w_1, w_2)_{(t)}\big|_{t=0}$ *this cell returns to* D_0 *as* $(w_1, w_2)_{(t)}\big|_{t=1}$*. Any acceptable deformation of* Γ^{quant} *does not affect this final cell.*

The concrete choice of elementary and minimal cells depends, obviously, on the resonance condition. In the subsequent sections, we give more details for each system separately.

Quantum monodromy matrix. Having transported $(w_1, w_2)_0 = (w_1, w_2)_{(t)}\big|_{t=0}$ along Γ, we relate the initial cell $(\tilde{w}_1, \tilde{w}_2)_0$ and the final cell $(\tilde{w}_1, \tilde{w}_2)_1 = (\tilde{w}_1, \tilde{w}_2)_{(t)}\big|_{t=1}$ of the regular $\mathbb{Z}^2$ lattice L_0 in $\tilde{D}_0 \subset \mathbb{R}^2_{i_1,i_2}$ using notation in (6.5)

$$\begin{pmatrix} \tilde{w}_1 \\ \tilde{w}_2 \end{pmatrix}_1 = M^{\text{quant}} \begin{pmatrix} \tilde{w}_1 \\ \tilde{w}_2 \end{pmatrix}_0,$$

where $M^{\text{quant}} \in \mathrm{SL}(2, \mathbb{Z})$ is the *quantum monodromy matrix* defined with respect to the chosen cell $(\tilde{w}_1, \tilde{w}_2)_0$ of L_0. Going to $D_0 \subset \mathbb{R}^2_{f_1,f_2}$ we have

$$\begin{pmatrix} w_1 \\ w_2 \end{pmatrix}_1 = M^{\text{quant}} \begin{pmatrix} w_1 \\ w_2 \end{pmatrix}_0 + o(\hbar).$$

Recall that in our classical study in Sec. 5, we defined in (5.2) the two elements (g_{f}, g_0) of the homology group $H_1(\Lambda_{\Gamma_0})$ and deformed them continuously into two other elements (g_{f}, g_1) of this group. The final transformation (5.3a) was given by the matrix $M \in \mathrm{SL}(2, \mathbb{Z})$. By Lemma 6.1

$$M^{\text{quant}} = \left(M^{-1}\right)^T. \tag{6.6}$$

The classical matrix M represents monodromy of the classical system for the chosen basis (g_{f}, g_0) of $H_1(\Lambda_{\Gamma_0})$, while M^{quant} describes quantum monodromy in terms of the corresponding cell $(w_1, w_2)_0$.

Notice that by our construction, the chart $\Phi_0 \colon D_0 \to \tilde{D}_0 \supset L_0$ near point Γ_0 is a full lattice chart (because D_0 covers only regular values of F). The elementary cell $(v_1, v_2)_0$ corresponds to the basis (g_{f}, e_0) in (5.2), and the cell $(w_1, w_2)_0$, which corresponds to elements (g_{f}, g_0) of H_1, is, in general, a multiple cell. Then, by Corollary 6.1,

$$(w_1, w_2)_k^T = \bar{B}\,(v_1, v_2)_k^T = \det B \left(B^{-1}\right)^T (v_1, v_2)_k^T, \quad \text{where } k = 0, 1,$$

and B is the matrix in (5.2). Similarly to the classical Definition 2.8 in Sec. 2.4.1 and its matrix implementation (5.3b), we can define *extended quantum monodromy matrix*

$$\bar{B}^{-1} M^{\text{quant}} \bar{B} = B^T \left(M^{-1}\right)^T \left(B^{-1}\right)^T = \left(B^{-1}\, M^{-1}\, B\right)^T = \left((B^{-1} M B)^{-1}\right)^T,$$

which extends the transformation formally to the elementary cell (v_1, v_2). Like its classical counterpart $B^{-1}MB$, this matrix belongs to $\mathrm{SL}(2,\mathbb{Q})$. Concrete monodromy matrices for the two example systems studied in our work are given below.

system	M	$B^{-1}MB$	B	M^{quant}	$\bar{B}^{-1}M^{\mathrm{quant}}\bar{B}$	$\bar{B}$
1:(−1)	$\begin{pmatrix} 1 & 0 \\ -1 & 1 \end{pmatrix}$	same	$\begin{pmatrix} 1 & 0 \\ 0 & 1 \end{pmatrix}$	$\begin{pmatrix} 1 & 1 \\ 0 & 1 \end{pmatrix}$	same	$\begin{pmatrix} 1 & 0 \\ 0 & 1 \end{pmatrix}$
1:(−2)	$\begin{pmatrix} 1 & 0 \\ -1 & 1 \end{pmatrix}$	$\begin{pmatrix} 1 & 0 \\ -\frac{1}{2} & 1 \end{pmatrix}$	$\begin{pmatrix} 1 & 0 \\ 0 & 2 \end{pmatrix}$	$\begin{pmatrix} 1 & 1 \\ 0 & 1 \end{pmatrix}$	$\begin{pmatrix} 1 & \frac{1}{2} \\ 0 & 1 \end{pmatrix}$	$\begin{pmatrix} 2 & 0 \\ 0 & 1 \end{pmatrix}$

6.4. Quantum monodromy of the 1:(−1) system

Quantum-classical $\mathcal{EM}$ diagram of the 1:(−1) resonant oscillator system in the neighborhood of the isolated critical value $(F_1, F_2) = (0, 0)$ of the classical $\mathcal{EM}$ map is shown in Fig. 10. We can see that in any simply connected domain D

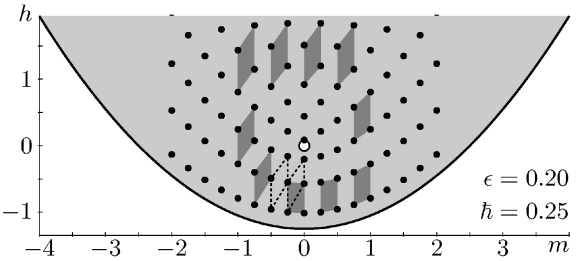

FIGURE 10. Base of the integrable fibration F of the 1:(−1) resonant oscillator system and the corresponding quantum lattice (black dots). Dark gray quadrangles show the evolution of the elementary cell along the closed path Γ which goes around the singular $\mathcal{EM}$ value (large opaque circle) as shown in Fig. 4.

of regular $\mathcal{EM}$ values in this neighborhood, the lattice $\mathcal{L}^{1:(-1)}$ formed by the joint eigenspectrum of the two commuting operators $(\hat{F}_1, \hat{F}_2)$ of this system is isomorphic to a regular $\mathbb{Z}^2$ lattice. For brevity, we will call such lattice $\mathcal{L}$ *locally regular*.

The contour Γ and its possible quantum approximation Γ^{quant} are illustrated in Fig. 11, center. To cover the $\mathcal{L}^{1:(-1)}$ lattice in the neighborhood of Γ we need (a minimum of) two charts shown in Fig. 11, left and right. Both charts cover only regular $\mathcal{EM}$ values and are full lattice charts. The "right" and "left" charts, which we label using Roman indexes I and II, cover the respective segments $[\Gamma_0\Gamma_1\Gamma_2]$ and $[\Gamma_2\Gamma_3\Gamma_0]$ (see Figs. 4 and 11) of Γ.

The elementary cell $(v_1, v_2)_{\mathrm{I}}$ in the domain D_{I} agrees with our choice of basis (g_{f}, e_s) of the homology group H_1 of the regular tori Λ_{Γ_s} which we made in

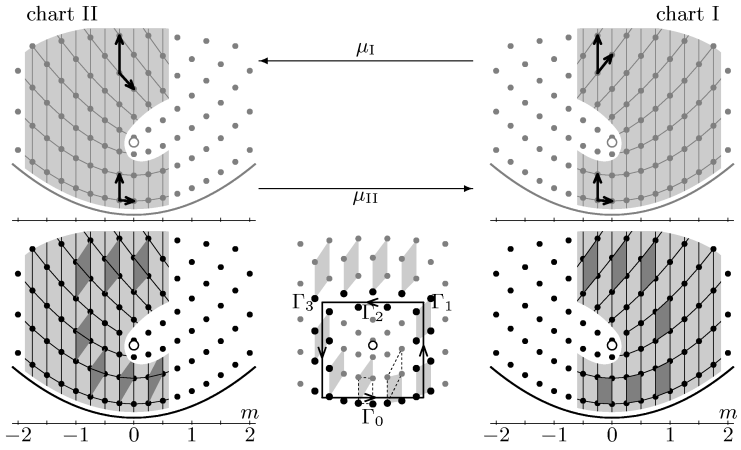

FIGURE 11. Two-chart atlas (left and right panels) of the quantum lattice $\mathcal{L}$ of the 1:(−1) resonant oscillator system. Open simply connected domains $D_{\rm I}$ and $D_{\rm II}$ are shaded grey; solid lines within these domains join nodes of the corresponding full regular lattices $L_{\rm I}$ and $L_{\rm II}$. Top plots show the choice of basis cells $(v_1, v_2)_{\rm I}$ and $(v_1, v_2)_{\rm II}$ and the gluing maps between the charts; bottom plots show the transport of the elementary cell (dark grey quadrangles, compare to Fig. 10) in each chart. Central bottom panel shows contour Γ as a bold solid rectangle and the set $\Gamma^{\rm quant}$ as emphasized black dots, compare to Fig. 4.

Sec. 5.1 for both $s = 0$ and $s = 1$. The local actions $(I_1, I_2)_{\rm I}$ are smooth single-valued real functions of (F_1, F_2) on $D_{\rm I}$ and of (p, q) on $F^{-1}(D_{\rm I}) \subset \mathbb{R}^4_{p,q}$. Similarly, the elementary cell $(v_1, v_2)_{\rm II}$ agrees with the choice of $(g_{\rm f}, e_s)$ for both $s = 0$ and $s = 3$.

As can be seen in Fig. 11, the elementary cells $(v_1, v_2)_{\rm II}$ and $(v_1, v_2)_{\rm I}$ below $(0, 0)$ (near Γ_0) are represented in $\mathbb{R}^2_{f_1,f_2}$ as the same almost rectangular cell $(v_1, v_2)_0$. So below $(0, 0)$, the two charts are glued identically, At the same time, we can also see that in the overlap region above $(0, 0)$, the gluing map $\mu_{\rm I}$: $(v_1, v_2)_{\rm I} \to (v_1, v_2)_{\rm II}$ is defined by the matrix $M_{\rm I} = \left(\begin{smallmatrix} 1 & 1 \\ 0 & 1 \end{smallmatrix}\right)$ plus the usual $o(\hbar)$. Notice that instead of two single-valued charts we can think of a single multi-valued chart.

Since in the classical 1:(−1) system the admissible closed path δ_Γ crosses no walls, any element of $H_1(\Lambda_{\Gamma_0})$ is passable. In the respective quantum system, the passable cell $(w_1, w_2)_0 = (w_1, w_2)_{(t)}\big|_{t=0}$ can be any elementary cell of the local $\mathbb{Z}^2$ lattice near Γ_0. We take $(w_1, w_2)_0 = (v_1, v_2)_0$ and transfer it along Γ in the counterclockwise direction as illustrated in Fig. 10. Due to the sufficiently dense lattice mesh in this figure, the shape of each deformed cell $(w_1, w_2)_{(t)}$ is defined unambiguously by its predecessor as we move in small steps along $\Gamma^{\rm quant}$. More

formally, we transfer $(w_1, w_2)_{(t)}$ within each of the two local $\mathbb{Z}^2$ charts using the basis translations of the chart, which are indicated in Fig. 11 by solid lines joining lattice nodes. As can be seen in the bottom right panel of Fig. 11, the cell $(w_1, w_2)_{(t)}$ coincides with the basis cell $(v_1, v_2)_{\mathrm{I}}$ of chart I when we start at Γ_0 and move in chart I along Γ towards Γ_1. As we switch to chart II in the overlap region above $(0, 0)$ (see bottom left panel in Fig. 11), we find that the cell $(w_1, w_2)_{(t)}$ *differs* from the basis cell $(v_1, v_2)_{\mathrm{II}}$. Notice, that we have deliberately chosen $(v_1, v_2)_{\mathrm{I}}$ and $(v_1, v_2)_{\mathrm{II}}$ so that this process corresponds most directly to our classical study in Sec. 5.2 and Fig. 4.

After returning to the initial point Γ_0, we realize that the defining vectors of the final cell $(w_1, w_2)_1$ are different from those of the initial cell. Specifically,

$$\begin{pmatrix} w_1 \\ w_2 \end{pmatrix}_1 = \begin{pmatrix} 1 & 1 \\ 0 & 1 \end{pmatrix} \begin{pmatrix} w_1 \\ w_2 \end{pmatrix}_0 = \begin{pmatrix} 1 & 1 \\ 0 & 1 \end{pmatrix} \begin{pmatrix} v_1 \\ v_2 \end{pmatrix}. \tag{6.7}$$

The matrix M^{quant}, which relates the two sets of vectors in (6.7), is the inverse transposed monodromy matrix M for basis elements (g_{f}, g_0) of the homology group $H_1(\Lambda_{\Gamma_0})$, which we computed for the corresponding classical system in Sec. 5.1; see (6.6).

6.5. Quantum monodromy of the $1{:}(-2)$ system

Quantum-classical $\mathcal{EM}$ diagram of the $1{:}(-2)$ resonant oscillator system is shown in Fig. 12. We can see that in the neighborhood of the critical value $(F_1, F_2) = (0, 0)$ of the classical $\mathcal{EM}$ map and sufficiently far (several $2\pi\hbar$) away from both $(0, 0)$ and the line $\mathcal{C}$ of weak singular values (4.4), the lattice $\mathcal{L}^{1:(-2)}$ formed by the joint eigenspectrum of the two commuting operators $(\hat{F}_1, \hat{F}_2)$ of this system is a locally regular $\mathbb{Z}^2$ lattice. As in the case of $1{:}(-1)$ discussed in the previous section, we approximate the closed path Γ in Fig. 6 by a set Γ^{quant}. We retain notation in Fig. 6 for points on Γ. In particular, Γ_0 is a regular value of F below $(0, 0)$ with $m = 0$ and $h < 0$.

Any atlas, which covers $\mathcal{L}^{1:(-2)}$ in the neighborhood of Γ, covers also part of $\mathcal{C}$. By Proposition 6.1 such atlas represents a common sublattice of $\mathcal{L}^{1:(-2)}$. Recall that in the classical $1{:}(-2)$ system (Sec. 5.2), the only passable cycles were the ones which represent elements of an index 2 subgroup of $H_1(\Lambda_{\Gamma_0})$ generated by $(g_{\mathrm{f}}, g_0) = (g_{\mathrm{f}}, 2e_0)$. In the respective quantum system, the common sublattice is a sublattice $\mathcal{L}^{1:(-2)}/Z_2$ of index 2. Notice that due to the simplifying presence of the S^1 symmetry and the associated global action F_1 in (4.3a), common sublattice can be easily defined by selecting the subset of quantum states with either even or odd eigenvalue m; we will use odd values.

To cover $\mathcal{L}^{1:(-2)}/Z_2$ in the neighborhood of Γ we need (a minimum of) two charts shown in Fig. 13. The "right" chart Φ_{I} is a full lattice chart. Its domain of definition D_{I} covers only regular $\mathcal{EM}$ values and, in particular, the segment $[\Gamma_0\Gamma_1\Gamma_2\Gamma_3\Gamma_4\Gamma_5]$ of Γ (see Fig. 6). Its elementary cell corresponds to the basis (g_{f}, e_s) chosen in Sec. 5.2 for the homology groups H_1 of the respective regular 2-tori Λ_{Γ_s} with $s = 0, 1, 3, 4$. The "left" chart Φ^*_{II} covers both regular and weakly

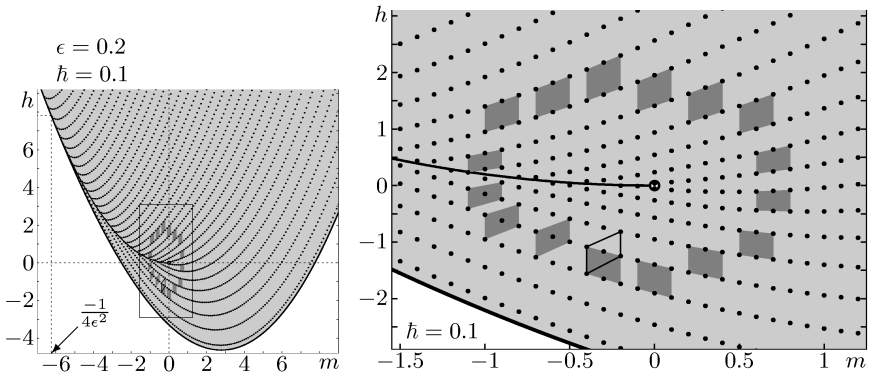

FIGURE 12. Lattice $\mathcal{L}^{1:(-2)}$ of quantum states in the base space (shaded area) of the integrable fibration F in (4.3) of the 1:(−2) resonance oscillator. Bold lines represent critical values of F (see Proposition 3.4): relative equilibria (lower boundary) and weak singular values $\mathcal{C}$ in (4.4); the singular value at $(0, 0)$ is marked by a large opaque circle. Dark gray quadrangles show the evolution of the minimal cell (w_1, w_2) of the index-2 sublattice $\mathcal{L}/Z_2$ along the closed path Γ in Fig. 6 which goes around $(0, 0)$.

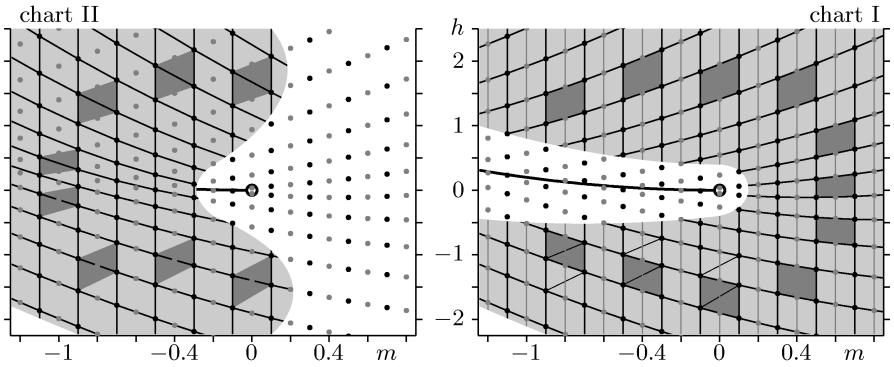

FIGURE 13. Two-chart atlas of the quantum lattice $\mathcal{L}$ of the 1:(−2) resonant oscillator system. Open simply connected domains D_{II} (left) and D_{I} (right) are shaded grey; black dots and lines joining them within these domains correspond to the common sublattice $C\mathcal{L}$ of index 2; faded lines and dots represent the complementary sublattice in the full lattice chart I. Check also Figs. 6 and 13.

singular values of F near and including the segment $[\Gamma_6\Gamma_7\Gamma_8\Gamma_9\Gamma_0]$. This chart is a sublattice chart; its minimal cell corresponds to the elements $(g_{\mathrm{f}}, 2e_s)$ which define the respective index-2 subgroup of $H_1(\Lambda_{\Gamma_s})$ with $s = 0, 9, 7, 6$. Notice that corresponding local actions $(I_1, I_2)^*_{\mathrm{II}}$ are (at least) C^1 smooth on the weak singular points $\mathcal{C} \cap D^*_{\mathrm{II}}$ and are C^∞ smooth elsewhere in D^*_{II}.

At this point, computing quantum monodromy of the common sublattice $C\mathcal{L}^{1:(-2)}$ becomes very similar to the computation in Sec. 6.4 for the full lattice $\mathcal{L}^{1:(-1)}$ of the 1:(−1) system. Below $(0,0)$ the two charts of $C\mathcal{L}^{1:(-2)}$ overlap identically, while above $(0,0)$, i.e., near point Γ_5, the gluing map $\mu_{\mathrm{I}}\colon CL_{\mathrm{I}} \to CL_{\mathrm{II}}$ is given by matrix $M_{\mathrm{I}} = \left(\begin{smallmatrix} 1 & 1 \\ 0 & 1 \end{smallmatrix}\right)$. We choose the initial cell $(w_1, w_2)_0$ as a minimal cell of the sublattice L_0/Z_2 which represents $C\mathcal{L}$ near Γ_0. Note that $(v_1, v_2)_0 = (v_1, v_2)_{\mathrm{I}}$ and that in the full lattice chart Φ_{I}, the cell $(w_1, w_2)_0$ is the *double cell* $(w_1, w_2)_0 = (2v_1, v_2)_0$, which by Corollary 6.1 with $B = \left(\begin{smallmatrix} 1 & 0 \\ 0 & 2 \end{smallmatrix}\right)$ corresponds to the pair of elements $(g_{\mathrm{f}}, 2e_0)$ of $H_1(\Lambda_{\Gamma_0})$.

Transporting $(w_1, w_2)_0$ along Γ in the counterclockwise direction is illustrated in Figs. 12 and 13. We can see in Fig. 12 that a cell doubled in the $f_1 = m$ direction can be transported unambiguously across the singular line $\mathcal{C}$ and the result does not depend on the point of crossing, while the transformation of a single 1×1 cell does depend on the crossing point. Notice also that everywhere outside the small region near $\mathcal{C}$ in Fig. 12, we transport $(w_1, w_2)_{(t)}$ as a multiple cell of the full lattice, while in Fig. 13 we remain – for the sake of clarity – within the same common sublattice. For the final cell $(w_1, w_2)_1 = (w_1, w_2)_{(t)}\big|_{t=1}$ we find

$$\begin{pmatrix} w_1 \\ w_2 \end{pmatrix}_1 = M^{\mathrm{quant}} \begin{pmatrix} w_1 \\ w_2 \end{pmatrix}_0 = \begin{pmatrix} 1 & 1 \\ 0 & 1 \end{pmatrix} \begin{pmatrix} w_1 \\ w_2 \end{pmatrix}_0 = \begin{pmatrix} 1 & 1 \\ 0 & 1 \end{pmatrix} \begin{pmatrix} 2v_1 \\ v_2 \end{pmatrix}_0 . \tag{6.8a}$$

The monodromy matrix M^{quant} in (6.8a) is the same as that of the quantum 1:(−1) system in (6.7). This comes as no surprise once we have uncovered the similarity of the atlases of the two systems. In the chart Φ_0 near Γ_0, transformation (6.8a) can be extended formally to the elementary cell of $L_0 \subset L_{\mathrm{I}}$

$$\begin{pmatrix} v_1 \\ v_2 \end{pmatrix}_1 = \bar{B}^{-1} M^{\mathrm{quant}} \bar{B} \begin{pmatrix} v_1 \\ v_2 \end{pmatrix}_0 = \begin{pmatrix} 1 & \frac{1}{2} \\ 0 & 1 \end{pmatrix} \begin{pmatrix} v_1 \\ v_2 \end{pmatrix}_0 . \tag{6.8b}$$

As indicated in (6.6) and (6.7), the fractional matrix of this latter transformation equals the inverse transposed classical extended monodromy matrix $B^{-1}MB$ for elements (g_{f}, e_0) of the homology group $H_1(\Gamma_0)$, which we computed in Sec. 5.2.

7. Interpretation of quantum monodromy in terms of lattice defects

In this section, we improve our representation of the locally regular joint spectrum lattice $\mathcal{L}$ in order to make this representation a general tool for describing global structure of joint spectrum lattices and underlying singularities of corresponding integrable fibrations. Readers familiar with crystallography will find that our approach is very similar to the approach used in the study of defects of 2-dimensional

crystals. However, the lattice defects, which correspond to integer and fractional monodromy, are not encountered in physical crystal lattices. Following [71, 70], we give a more formal definition of these defects and show that monodromy of lattices $\mathcal{L}^{1:(-1)}$ and $\mathcal{L}^{1:(-2)}$ can be interpreted as a particular point and line defect respectively.

Recall that each chart $\Phi_s\colon D_s \to \tilde{D}_s \supset L_s$, where $\Phi_s = I_s \circ F^{-1}$, defines a map from $D_s \subset \mathbb{R}^2_{f_1,f_2}$ to a domain $\tilde{D}_s \subset \mathbb{R}^2_{(i_1,i_2)_s}$ of its own abstract space. The atlas of charts $\Phi_s, s = 1, 2, \ldots$ covers an open neighborhood $D_\Gamma \subseteq \bigcup D_s$ of the closed path $\Gamma \subset D_\Gamma \subset \mathbb{R}^2_{f_1,f_2}$. This neighborhood contains the part $\mathcal{L}_0$ of the original joint spectrum lattice $\mathcal{L}$.

Central idea. The principally new idea is that we will now consider all $\tilde{D}_s$ as parts of the *same* space $\mathbb{R}^2_{i_1,i_2}$, and all lattices L_s as parts of the *same* regular $\mathbb{Z}^2$ lattice L. More concretely, we suppose that there is a bijective semi-global "patchwork" mapping $\Phi\colon D_\Gamma \to \tilde{D}_\Gamma$, which is constructed on the basis of local diffeomorphisms $\{\Phi_s\}$. The latter may require adjustments in order to fit values of local affine actions $\{(I_1, I_2)_s\}$ together in one space $\mathbb{R}^2_{i_1,i_2}$, and the definition domains D_s may be shrunk to nonoverlapping simply connected subsets $C_s \subseteq D_s$, which may include parts of their boundary $\partial C_s \subset D_s$. The images $\tilde{C}_s \subseteq \tilde{D}_s$ of C_s have similar properties. The ensemble $\{C_s\}$ still covers $D_\Gamma \subseteq \bigcup C_s$, and moreover $\tilde{D}_\Gamma \subseteq \bigcup \tilde{C}_s$. Note that C_s are reminiscent of the lower cells in the cellular decomposition discussed in Sec. 2.2 with the difference that their boundaries ∂C_s are not necessarily related to singularities of the integrable map F.

Lattice model. The nodes of L are labeled by two integer quantum numbers (n_1, n_2), which correspond to points of $\mathbb{R}^2_{i_1,i_2}$ according to (6.1). Using (6.1) to rescale actions (i_1, i_2), we can represent L as a lattice of integer points in $\mathbb{R}^2$ whose elementary cell is a 1×1 square cell defined by orthogonal unit vectors (u_1, u_2). This basis cell is the *same* for all charts L_s. Transporting any cell of L within each L_s is, of course, a simple translation defined by the generators of L. We now explain how all L_s are put together in one lattice.

Definition 7.1. The union $\bigcup L_s \subset L$ is called *locally regular lattice model* if it is equipped with the set of *transport rules*, which have the following properties.

i. each rule connects bidirectionally a pair of lattices $L_{s'} \leftrightarrow L_{s''}$ and corresponds to a nonempty class of homotopically equivalent *direct connection paths*, which connect respective domains $\tilde{C}_{s'} \leftrightarrow \tilde{C}_{s''}$.
ii. each rule applies to minimal cells of a common sublattice $CL(L_{s'}, L_{s''})$.
iii. the transformation rule of transporting a minimal cell between $L_{s'}$ and $L_{s''}$ is given by a matrix in $\mathrm{SL}(2, \mathbb{Z})$.
iv. if $M \in \mathrm{SL}(2, \mathbb{Z})$ gives the rule for $L_{s'} \to L_{s''}$, than M^{-1} defines $L_{s'} \leftarrow L_{s''}$.
v. the set of transport rules is large enough to make all L_s connected: for any two lattices L_a and L_b, there is at least one nonempty class of homotopy equivalent paths, which connect $\tilde{C}_a$ and $\tilde{C}_b$ and define a minimal cell, which can be transported between L_a and L_b.

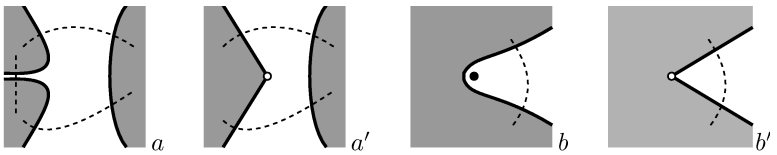

FIGURE 14. Abstract lattice models satisfying conditions in Def. 7.1.

Definition 7.2. If the patchwork mapping $\Phi\colon \mathcal{L} \to \bigcup L_s \subseteq L$ exists then we say that our lattice model gives a *regular representation* of $\mathcal{L}$, Φ is called *deconstruction* or *local regularization* of $\mathcal{L}$, and Φ^{-1} is called *reconstruction*.

Definition 7.1 allows for a wide class of abstract lattice models. Thus, as illustrated in Fig. 14 *a*, we can use several nonoverlapping charts C_s with smooth boundaries. We can use open domains $C_s \setminus \partial C_s$ and avoid using boundaries ∂C because our models represent only lattice nodes covered by $\{D_s\}$ and not all points in $\bigcup D_s$. On the other hand, we can use domains C_s with nonhomogeneous boundaries. In particular, we can allow for two different transport rules between the same lattices $L_{s'} \leftrightarrow L_{s''}$, as shown in Fig. 14 *a*′. Furthermore, Figs. 14 *b* and *b*′ show different ways (an external obstruction or a singular point on the boundary), to obtain nontrivial transport rules for $s' = s''$, i.e., for the same domain. We will see that lattice models with complex boundaries of domains represent more fully the underlying integrable fibration.

To characterize a lattice model in terms of monodromy and defect types, we study transport along closed paths, which we construct as sequences of direct connection paths. It can be seen from Def. 7.1-iv that closed paths, which go from L_a to L_b and then return back to L_a using the same set of transport rules in reverse, result in an identity transformation. Such closed paths can be called trivial or degenerate. If the model allows for nontrivial closed paths Γ, we can expect a nontrivial monodromy transformation.

To find whether a lattice model corresponds to a joint spectrum lattice $\mathcal{L}$ of a dynamical system, we should find (or prove the existence of) map Φ and its inverse Φ^{-1}. The important point to stress is that the correspondence of $\bigcup L_s$ and $\mathcal{L}$ based on Φ assures that these lattices exhibit the same monodromy. On the other hand, different lattice models can have the same monodromy.

A comprehensive study of the regularized representation and the explicit construction of Φ deserve clearly a separate study. At present, we only like to demonstrate the eloquence and universality of the analysis based on lattice models and to suggest the way of how an abstract lattice defect theory can inspire classification of singularities of integrable fibrations. To this end, we construct lattice models $L^{1:(-1)}$ and $L^{1:(-2)}$ with the same monodromy as respective joint spectrum lattices $\mathcal{L}^{1:(-1)}$ and $\mathcal{L}^{1:(-2)}$.

7.1. Cuts of the regular $\mathbb{Z}^2$ lattice, passable cells and admissible cuts

Definition 7.1 gives no concrete way of constructing lattice models $\bigcup L_s$. In this section, we develop special techniques to construct a particular class of lattice models. Following [71, 70], we split the $\mathbb{Z}^2$ lattice L into domains $\tilde{C}_s \supset L_s$ by cutting out parts of L in a special way and by defining simple rules for transporting the cells of L across the cutout regions along one of the basis directions of L. We associate specific defect types with one or several elementary cuts and transport rules.

Consider a regular $\mathbb{Z}^2$ lattice L of points in the plane $\mathbb{R}^2$ spanned by two orthogonal unit vectors u_1 and u_2. The coordinates on $\mathbb{R}^2$ are $x = (x_1, x_2)$ and the nodes L are represented by *integer points* $n_1u_1 + n_2u_2$, with $n_1, n_2 \in \mathbb{Z}$. Take a point $O \in \mathbb{R}^2$ with coordinates x_O and a ray $[Oc)$. Consider an open domain $\mathcal{C}_{Oc}$ and its closure $\overline{\mathcal{C}}_{Oc} \subset \mathbb{R}^2$ such that $\partial\mathcal{C}_{Oc} \ni O$ and $\overline{\mathcal{C}}_{Oc} \supset [Oc)$. Let u_{Oc} define direction of $[Oc)$ and let u_c be one of $\pm u_1$ or $\pm u_2$, such that $u_c.u_{Oc} > 0$. Next introduce quantum number n_c as integer part of the projection of $x - x_O$ on the axis u_c,

$$n_c\colon x \to \big[(x - x_O).u_c\big].$$

Definition 7.3 (terminology used to describe cuts). We call $\overline{\mathcal{C}}_{Oc}$ a *cut* with *vertex* or *defect point* at O, *reference axis* $[Oc)$, and *cutout region* or *interior* $\mathcal{C}_{Oc}$. A node of L in $\mathcal{C}_{Oc}$ is called *empty*; empty nodes represent no nodes of the model lattice. We associate each cut $\overline{\mathcal{C}}_{Oc}$ with a fixed choice of *coordinate axis vector* u_c; the respective quantum number n_c is called *axis number* of $\overline{\mathcal{C}}_{Oc}$.

Consider now a path Γ, which crosses transversally a cut $\overline{\mathcal{C}}_{Oc}$, and use the value of $n = n_c(x)$ to characterize the *crossing point* $x = \Gamma \cap [Oc)$. Let the unit vector u_Γ define the direction of Γ at x. We say that Γ crosses $\overline{\mathcal{C}}_{Oc}$ in the positive or negative direction if $\varkappa = (u_c \wedge u_\Gamma).(u_1 \wedge u_2)$ equals $+1$ or -1, respectively. Let $(w_1, w_2)_0$ be an arbitrary cell of the regular $\mathbb{Z}^2$ lattice L. Suppose that after being transported across $\overline{\mathcal{C}}_{Oc}$ along Γ this cell becomes $(w_1, w_2)_1$. In general, the transformation

$$\mu_c(n)\colon \begin{pmatrix} w_1 \\ w_2 \end{pmatrix}_0 \to \begin{pmatrix} w_1 \\ w_2 \end{pmatrix}_1 = M_c(n) \begin{pmatrix} w_1 \\ w_2 \end{pmatrix}_0 .$$

depends on the point of crossing n and, of course, on the particular cell taken.

Definition 7.4. A cell of L is called *passable* across a cut $\overline{\mathcal{C}}_{Oc}$, if its transformation $\mu_c(n)$ does not depend on the crossing point n. A cut $\overline{\mathcal{C}}_{Oc}$ for which such cells exist is called *admissible*, cf. Def. 2.5. The transformation $\mu_c(n) = \mu_c$ of passable cells is called *cell transformation associated with* $\overline{\mathcal{C}}_{Oc}$. If a particular passable cell $(w_1, w_2)_0$ is carried across $\overline{\mathcal{C}}_{Oc}$ in the positive direction, we call the corresponding matrix M_c *transformation matrix of* $\overline{\mathcal{C}}_{Oc}$ in the basis of $(w_1, w_2)_0$. The *common sublattice* CL_c *of the cut* $\overline{\mathcal{C}}_{Oc}$ is such maximal sublattice of L, whose basis cell (= minimal cell) is passable across $\overline{\mathcal{C}}_{Oc}$.

7.2. Parallel transport across simple cuts

We continue detailing our cut construction. Consider straight lines $l(d) = \{x | x.u_c = d\}$ with $d > x_O.u_c$ a constant. These lines are orthogonal to u_c and intersect $[Oc)$ transversely. Finally define the unit vector u_l such that $u_c.u_l = 0$ and $\varkappa = (u_c \wedge u_l).(u_1 \wedge u_2) = 1$. In other words, let the base (u_c, u_l) be a proper rotation of (u_1, u_2). Note that $\varkappa$ is the oriented volume spanned by unit vectors u_c and u_l and computed as $\det(u_c, u_l)$.

Definition 7.5. The lines $l(d)$ are called *lines of parallel transport* and u_l points to *positive transport direction*. Points x' and x'' of the boundary $\partial\mathcal{C}_{Oc}$ are called *opposite* if they lie on the same parallel transport line, i.e., if $x'.u_c = x''.u_c$. The number of empty nodes with the same value of $n_c > 0$, i.e., of empty nodes, which lie on the same transport line $\{x | x.u_c = n_c\}$, is given by function $\Delta(n_c)$; the *defect function* $\delta_c(n_c)$ of $\overline{\mathcal{C}}_{Oc}$ is defined as $\Delta(n_c + 1) - \Delta(n_c) \geq 0$.

As their name implies, we intend to use the lines $l(d)$ to define particular rules of transporting cells of L across cuts. Consider a path Γ which crosses transversally a cut $\overline{\mathcal{C}}_{Oc}$, deform Γ homotopically so that $\Gamma \cap \overline{\mathcal{C}}_{Oc}$ as well as adjacent parts of Γ lie on one parallel transport line $\{x.u_c = n\}$, where integer n is the value of the axis number n_c which specifies the point of crossing $\Gamma \cap \overline{\mathcal{C}}_{Oc}$. Notice that $u_\Gamma = u_l$ when we cross $\overline{\mathcal{C}}_{Oc}$ in the positive direction and otherwise $u_\Gamma = -u_l$.

Parallel transport. Let (w_1, w_2) be an arbitrary cell of the regular $\mathbb{Z}^2$ lattice L; position of (w_1, w_2) can be specified using coordinates x, x', and x'' of three of its four vertices. Translating (w_1, w_2) within L outside $\overline{\mathcal{C}}_{Oc}$, we place vertex x so that $x.u_c = n$, while two other vertices settle on neighbor transport lines: $x'.u_c = n'$ and $x''.u_c = n''$. Of course, this does not change the shape of (w_1, w_2), which we will denote as the "old" cell $(w_1, w_2)_0$. We now step each vertex along its transport line in the same direction and by the same number of nonempty nodes of L, so that the whole cell gets across $\overline{\mathcal{C}}_{Oc}$ and becomes the "new" cell $(w_1, w_2)_1$. Since for a valid cell $(w_1, w_2)_0$ at least two of the numbers (n, n', n'') differ and unless the defect function $\delta(n)$ of the cut is trivially 0, the transformation $\mu_c(n)$ is nontrivial.

Definition 7.6. We call $\overline{\mathcal{C}}_{Oc}$ a *simple cut* if it has the following properties.

i. $\partial\mathcal{C}_{Oc}$ is transversal to the lines of parallel transport $l(n)$.
ii. cells of L are taken across $\overline{\mathcal{C}}_{Oc}$ using parallel transport along $l(n)$, $n \in \mathbb{Z}_+$.
iii. $\Delta(n_c)$ is a linear quasipolynomial in the sense of [62]; the period t_c of $\Delta(n_c)$ and its amplitude $a_c = \Delta(n_c + t_c) - \Delta(n_c)$ are called *period* and *amplitude* of the cut.
iv. opposite points x' and x'', which are nodes of L (= integer points), represent the same node of the model lattice, i.e., they are identified (glued).

In many cases, a simple cut can be constructed as a solid angle bounded by rays $[Oa)$ and $[Ob)$. Various complex cuts can be constructed by combining elementary cuts. For other possible extensions of Def. 7.6 see [71]; generalization to three-dimensional lattices is discussed in [30].

Lemma 7.1. *Simple cuts are admissible.*

The proof of Lemma 7.1 exploits quasi-linearity of $\Delta(n_c)$.

Let $(w_1, w_2)_0$ be the minimal cell which can pass simple cut $\overline{\mathcal{C}}_{Oc}$. Recall that according to Definition 7.4 the cell transformation matrix M_c of $\overline{\mathcal{C}}_{Oc}$ describes the transformation of this cell carried across $\overline{\mathcal{C}}_{Oc}$ in the *positive* direction.

Lemma 7.2. *In the basis of* $(w_1, w_2)_0$ *the cell transformation matrix* M_c *is a matrix in* $\mathrm{SL}(2,\mathbb{Z})$ *which is conjugate to* $\begin{pmatrix} 1 & k \\ 0 & 1 \end{pmatrix}$ *with* $k \in \mathbb{Z}_+$.

In Secs. 7.3 and 7.4 below we show that simple cuts fall into two classes: integer and rational, and that cuts of both kinds are admissible. After classifying all possible simple cuts, Lemma 7.1 and 7.2 follow from direct construction of passable cells.

Corollary 7.1. *A lattice model constructed using simple cuts conforms Definition* 7.1*.*

In particular, one simple cut produces a model of kind b' in Fig. 14.

We can see that crossing admissible simple cuts is equivalent to switching charts of the atlas described in Sec. 6.3. Furthermore, let us consider a closed path $\Gamma \in \mathbb{R}^2_{i_1,i_2}$, which crosses transversally a finite number K of admissible simple cuts. Label the cuts so that starting at point $\Gamma_0 \in \Gamma$ and going in the direction defined on Γ, we cross sequentially the cuts of indexes $s = 1, \ldots, K$ and then come back to Γ_0; the direction of each crossing is given by $\varkappa_s = \pm 1$. Let $(w_1, w_2)_0$ be a cell of L near Γ_0, which can pass sequentially (i.e., in the order defined by Γ) across the cuts $s = 1, \ldots, K$, and denote respective cell transformation matrices of these cuts in the basis of $(w_1, w_2)_0$ as M_s with $s = 1, \ldots, K$.

Lemma 7.3. *The monodromy matrix for the transport of* $(w_1, w_2)_0$ *along closed path* Γ *is*

$$M^{\mathrm{quant}} = (M_K)^{\varkappa_K} \cdots (M_2)^{\varkappa_2} (M_1)^{\varkappa_1}.$$

In particular consider a model lattice with just one admissible simple cut $\overline{\mathcal{C}}_{Oc}$. Then monodromy is nontrivial only for closed paths which encircle the vertex O.

7.3. The $1{:}(-1)$ lattice: integer cut, point defect, and integer monodromy

To construct a model lattice $\bigcup L_s = L^{1:(-1)}$, whose defect has the same monodromy as the $\mathcal{L}^{1:(-1)}$ lattice in Fig. 10, we make one simple cut with axis vector $u_c = (-1, 0)$ and defect function $\delta(n_c) \equiv 1$; the parallel transport lines are vertical lines. A particular realization of such cut is shown in Fig. 15, left, where vertex O is placed at the lattice node $(0, 0)$ and the boundaries are formed by rays $[Oa)$ and $[Ob)$ which go symmetrically with respect to the reference axis of the cut. It can be seen that $\Delta(n_c) = n_c = -n_1$ is a *linear* function of n_c. Also note that following Def. 7.6-iv, nodes $(n_c, \pm\frac{1}{2}n_c)$ of L with $n_c = 2, 4, \ldots$, which lie on the two boundaries of the cut in Fig. 15, should be identified and thus represent one node of $L^{1:(-1)}$.

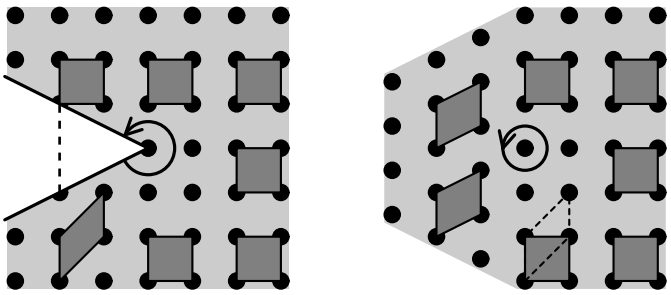

FIGURE 15. Construction of the 1:(−1) lattice defect starting from the regular $\mathbb{Z}^2$ lattice L: regular lattice with removed solid angle or "cut" (left), "reconstructed" lattice with a point defect (right). Dark grey quadrangles show the evolution of an elementary lattice cell along a closed path around the defect point, compare to Fig. 10.

Using the parallel transport procedure in Sec. 7.1, we can take a 1×1 square elementary cell $(w_1, w_2)_0 = (u_1, u_2)$ of L across the described cut (downwards in Fig. 15, left). It is easy to see that for any crossing point this results in the new cell

$$\begin{pmatrix} w_1 \\ w_2 \end{pmatrix}_1 = \begin{pmatrix} 1 & 1 \\ 0 & 1 \end{pmatrix} \begin{pmatrix} w_1 \\ w_2 \end{pmatrix}_0 .$$

In other words, (u_1, u_2) is passable and our cut is admissible. Furthermore, any other cell of L is also passable. In the basis (u_1, u_2), the cell transformation matrix of this cut is $\left(\begin{smallmatrix} 1 & 1 \\ 0 & 1 \end{smallmatrix}\right)$.

We can now define any closed path Γ which goes once about O in the counterclockwise direction. The monodromy matrix for Γ is, of course, the cell transformation matrix $\left(\begin{smallmatrix} 1 & 1 \\ 0 & 1 \end{smallmatrix}\right)$ of the simple cut we crossed.

Definition 7.7 (integer cuts). We call simple cut with defect function $\delta(n_c) = k \in \mathbb{Z}^+$ *an integer cut of amplitude* k. When $k = 0$ the cut is *trivial*.

We summarize properties of integer cuts.

Lemma 7.4 (properties of integer cuts). *An integer cut* $\overline{\mathcal{C}}_{Oc}$ *of amplitude* k *is admissible; any cell of* L *is passable across it. The cell transformation matrix* M_c *of* $\overline{\mathcal{C}}_{Oc}$ *in the basis of* (u_1, u_2) *equals* $\begin{pmatrix} 1 & k \\ 0 & 1 \end{pmatrix}$ *when* $u_c.u_2 = 0$, *and* $\begin{pmatrix} 1 & 0 \\ -k & 1 \end{pmatrix}$ *when* $u_c.u_1 = 0$.

Remark 7.1. The concept of simple cuts is further generalized in [71] where "insert cuts" are introduced to complement the ones we use here. Instead of leaving empty nodes, insert cuts *add extra nodes* to the regular lattice L. Thus an *integer insert cut of amplitude* k can be defined very similarly to the integer cut in Definitions 7.6 and 7.7, albeit its defect function $\delta(n_c)$ equals a *negative* integer $-k \in \mathbb{Z}_-$. In the

case $u_c.u_2 = 0$, such cut leads to a point defect with monodromy matrix $\left(\begin{smallmatrix} 1 & -k \\ 0 & 1 \end{smallmatrix}\right)$. Even though the latter is simply the inverse of $\left(\begin{smallmatrix} 1 & k \\ 0 & 1 \end{smallmatrix}\right)$ in Lemma 7.4, it represents, in fact, a different kind of singularity of integrable fibrations of systems with two degrees of freedom, which appears in non-Hamiltonian systems [17]. The two kinds of singularities can be distinguished using the *sign of monodromy* [70], whose precise dynamical meaning was uncovered in [19]. For the above matrices, it corresponds to the sign of the upper right element $\pm k$. We fix this sign unambiguously in Definition 7.4, when we choose the direction $\varkappa = 1$ of crossing the admissible simple cut before associating the cell transformation matrix M_c with it. Mathematically, the sign of monodromy distinguishes the monodromy matrices as members of two different classes of conjugate elements of $\mathrm{SL}(2, \mathbb{Z})$.

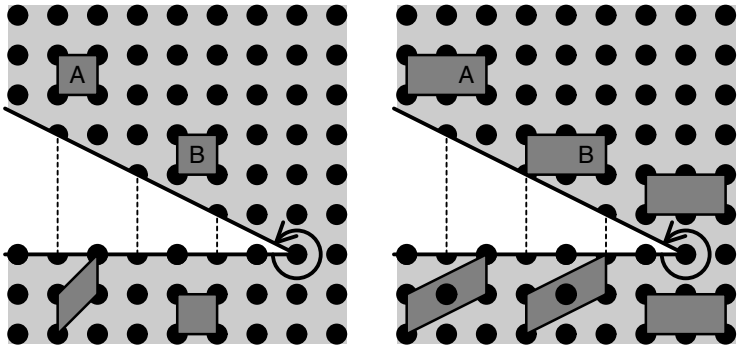

FIGURE 16. Construction of the 1:(−2) rational lattice defect starting from the regular square lattice: 1×1 cells cannot pass unambiguously through the cut (cf. cells A and B, left) while all double cells transfer in the same way (right).

7.4. The 1:(−2) lattice: rational cut, line defect, and fractional monodromy

In this section, we consider more general simple cuts of the regular square lattice L. We construct the regularized lattice $\bigcup L_s = L^{1:(-2)}$, which has the monodromy of the $\mathcal{L}^{1:(-2)}$ lattice in Fig. 12, using one simple cut. Since $I_1 = F_1$ corresponds again to a global action (momentum), the axis of the cut is horizontal and the parallel transport lines are vertical. The main difference from the integer cuts in Sec. 7.3 is that now $\Delta(n_c)$ is a quasi-polynomial. The respective defect function $\delta(n_c)$ equals a constant term plus an oscillatory part of period 2 and takes values 0 and 1. Such $\delta(n_c)$ can be expressed as $\frac{1}{2}\big(1 + (-1)^{n_c+k}\big)$ with $k = 1$ or 0. A particular realization of such cut with vertex in $O = (0, 0)$ and axis vector $u_c = (-1, 0)$ is shown in Fig. 16. Note that $n_c = -n_1 = 0$ at point O, and that defect function $\delta(n_c)$ equals $\frac{1}{2}\big(1 + (-1)^{n_c+1}\big)$. Comparing to Fig. 15, left, we see that our new cut is built by removing half the cutout region of the simple integer cut in Fig. 15.

We now use the parallel transport procedure in Sec. 7.1 to take a cell of L across the cut in the positive direction, which for the cut in Fig. 16 is downwards. We see in Fig. 16, left, that the result for the square 1×1 elementary cell $(v_1, v_2)_0 = (u_1, u_2)$ depends on the crossing point: such cell either passes unchanged (cell B) or ends up skewed (cell A) depending on whether its left side transports along the odd-n_c or the even-n_c line.

This ambiguity can be avoided if instead of the 1×1 cell we use a cell $(w_1, w_2)_0 = (2u_1, u_2)$, which is doubled horizontally, i.e., in the direction of the axis u_c of the cut. As shown in Fig. 16, right, transformation of such double cell after passing across the cut does not depend on the crossing point. For the new cell (below the cut in Fig. 16) we have

$$\begin{pmatrix} w_1 \\ w_2 \end{pmatrix}_1 = M_c \begin{pmatrix} w_1 \\ w_2 \end{pmatrix}_0 = M_c \begin{pmatrix} 2u_1 \\ u_2 \end{pmatrix} = M_c \bar{B} \begin{pmatrix} u_1 \\ u_2 \end{pmatrix}, \quad \text{where } M_c = \begin{pmatrix} 1 & 1 \\ 0 & 1 \end{pmatrix}.$$

We conclude that our simple cut is admissible and that $(w_1, w_2)_0$ is the minimal passable cell for this cut. Notice that the structure of this cell changes: in the crystallographic terminology, the "face centered" $(w_1, w_2)_0$ becomes the "body centered" $(w_1, w_2)_1$. This change is also independent on the crossing point. It can be seen that the main reason of such uniformity with respect to all effects on the scale smaller than the period of $\delta(n_c)$ is making the dimension of (w_1, w_2) an integer multiple of this period.

We can now define the monodromy transformation μ_Γ of the lattice cell $(w_1, w_2)_0$ transported along a closed path Γ, which goes around the defect point O in the counterclockwise direction (as indicated in Fig. 16) and crosses our cut once. By Lemma 7.3 the matrix of this μ_Γ equals M_c. As before in (6.8b) of Sec. 6.5, we can formally extend μ_Γ to the "single" cell $(v_1, v_2)_0$ using matrix

$$\bar{B}^{-1} M_c \bar{B} = \begin{pmatrix} 1 & \frac{1}{2} \\ 0 & 1 \end{pmatrix},$$

where $\bar{B} = \begin{pmatrix} 2 & 0 \\ 0 & 1 \end{pmatrix}$ is the same as in (6.8b). This extended matrix is the quantum monodromy matrix of the joint spectrum lattice $\mathcal{L}^{1:(-2)}$ and is the inverse transposed of the monodromy matrix of the corresponding classical $1:(-2)$ system, cf. (6.7) and (6.8b).

Our construction in Sec. 6.5 of the $\mathcal{L}^{1:(-2)}$ atlas in terms of a common Z_2-sublattice suggests a complimentary way of describing the lattice model $L^{1:(-2)}$. Separating nodes with odd and even values of momentum F_1, we can represent both $\mathcal{L}^{1:(-2)}$ and $L^{1:(-2)}$ as a union of two Z_2-sublattices. Furtermore, as illustrated in Fig. 17, each sublattice $L^{1:(-2)}/Z_2$ individually can be modeled as a regular lattice with one integer cut of amplitude 1.

We can now provide a general description of cuts which leads to construction of lattice models with arbitrary fractional monodromy.

Definition 7.8. A simple cut of period $1 < t_c \in \mathbb{Z}_+$ and amplitude $a_c \in \mathbb{Z}_+$ is called *rational*.

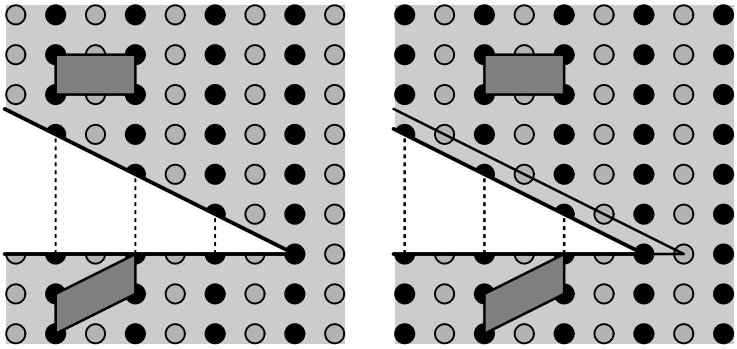

FIGURE 17. The 1:(−2) lattice model as a union of two sublattices with even m (left) and odd m (right). In each case, the nodes of the sublattice are shown by filled black circles.

Note that integer cuts in Def. 7.7 can be formally considered as rational cuts of period 1.

Lemma 7.5 (properties of rational cuts). *Let $\overline{\mathcal{C}}_{Oc}$ be a rational cut with direction $u_c = \pm u_1$, amplitude $a_c \geq 1$, and period $t_c > 1$.*

i. *$\overline{\mathcal{C}}_{Oc}$ is admissible, its common sublattice CL_c is an index-t_c sublattice L/Z_{t_c}.*

ii. *the minimal cell of CL_c is defined by matrix $\bar{B} = \begin{pmatrix} t_c & 0 \\ 0 & 1 \end{pmatrix}$.*

iii. *the cell transformation matrix (c.t.m.) and the extended c.t.m. of $\overline{\mathcal{C}}_{Oc}$ are*

$$M_c = \begin{pmatrix} 1 & a_c \\ 0 & 1 \end{pmatrix} \quad \text{and} \quad \bar{B}^{-1} M_c \bar{B} = \begin{pmatrix} 1 & a_c/t_c \\ 0 & 1 \end{pmatrix}.$$

7.5. Further examples

Formal construction of lattices with more general and more complicated defects is not difficult. In fact it can be shown that any two-dimensional lattice defect which can be characterized by an $\mathrm{SL}(2,\mathbb{Z})$ monodromy matrix can be reproduced as a combination of simple cuts [71, 70]. We give some examples below. Correspondence between lattice defects and singularities of toric fibrations may be established in a number of concrete systems. At the same time, despite considerable progress [32], a comprehensive theory remains yet to be developed. So we avoid making statements as to whether and how the classical systems, which inspired the lattice models we present below, can be related to these models.

Lattice model with two rational cuts. As a concrete example, consider the locally regular lattice model in Fig. 18 with two rational cuts. The cuts share the same vertex O and go "leftward" ($F_1 < 0$) and "rightward" ($F_1 > 0$) with corresponding axis vectors $-u_1$ and u_1; the transport lines are parallel to axis F_2. The leftward cut has period 2 while the period of the rightward cut is 3, the amplitude of both cuts is 1.

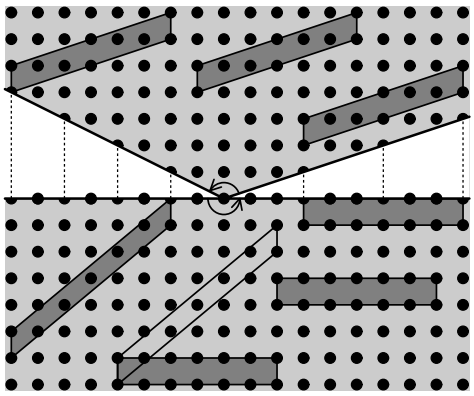

FIGURE 18. Lattice model with rational cuts of period 2 (directed leftward) and 3 (rightward) and common vertex O. The minimal cell, which is passable across both cuts, is a horizontally stretched 6×1 cell.

It is easy to see that the usual 1×1 square basis cell (u_1, u_2) of the regular $\mathbb{Z}^2$ lattice L should be doubled in the F_1 direction in order to pass the leftward cut and should be tripled in the same direction in order to pass the rightward cut. Consequently, the minimal cell passable across *both* cuts is the 6×1 cell

$$\begin{pmatrix} w_1 \\ w_2 \end{pmatrix} = \bar{B} \begin{pmatrix} u_1 \\ u_2 \end{pmatrix} = \begin{pmatrix} 6 & 0 \\ 0 & 1 \end{pmatrix} \begin{pmatrix} u_1 \\ u_2 \end{pmatrix}.$$

The 6×1 cell (w_1, w_2) can be transported along a closed path Γ, which goes around O and crosses necessarily both cuts. Figure 18 illustrates the associated monodromy transformation μ_Γ. Starting below the cuts and transporting (w_1, w_2) along Γ in the counterclockwise direction, we cross the right cut first and then cross the left cut; in both cases the crossing direction is positive. To find the transformation of (w_1, w_2), we begin by finding the cell transformation matrices M_2 and M_3 of the left and right cuts, respectively, in the basis of (w_1, w_2). Turning to Lemma 7.5 we obtain

$$M_2 = \bar{B} \begin{pmatrix} 1 & \frac{1}{2} \\ 0 & 1 \end{pmatrix} \bar{B}^{-1} = \begin{pmatrix} 1 & 3 \\ 0 & 1 \end{pmatrix} \quad \text{and} \quad M_3 = \bar{B} \begin{pmatrix} 1 & \frac{1}{3} \\ 0 & 1 \end{pmatrix} \bar{B}^{-1} = \begin{pmatrix} 1 & 2 \\ 0 & 1 \end{pmatrix}.$$

By Lemma 7.3, transformation μ_Γ of the 6×1 cell is given by monodromy matrix

$$M = M_2 M_3 = \bar{B} \begin{pmatrix} 1 & \frac{1}{2} \\ 0 & 1 \end{pmatrix} \begin{pmatrix} 1 & \frac{1}{3} \\ 0 & 1 \end{pmatrix} \bar{B}^{-1} = \bar{B} \begin{pmatrix} 1 & \frac{5}{6} \\ 0 & 1 \end{pmatrix} \bar{B}^{-1} = \begin{pmatrix} 1 & 5 \\ 0 & 1 \end{pmatrix}.$$

The same result can be obtained graphically from Fig. 18.

Integrable oscillator systems with 1:1 **resonance.** Up to now we have not discussed the boundary of the range of the $\mathcal{EM}$ map because we studied specific critical $\mathcal{EM}$ values, which lied inside a domain of regular $\mathcal{EM}$ values. Here we like to consider toric fibrations in Hamiltonian systems with two degrees of freedom and

first integrals (F_1, F_2) which have just one simply connected lower cell C without internal boundaries. We suppose that C can have an external boundary ∂C where one or both cycles of the first homology group H_1 of the regular 2-torus fibers vanish. Note that such ∂C can be considered as the most basic boundary and that its points represent either relative equilibria (when only one cycle vanishes) or equilibria (when both cycles vanish) of the system. Furthermore, the latter are, typically, isolated singular points of ∂C.

It can be shown that in the described situation we can introduce global action variables (I_1, I_2) and global momentum map J. The image of J in $\mathbb{R}^2_{i_1,i_2}$ is a *convex polygon* [3, 4, 35]. Such systems have been the subject of considerable interest and work [23, 36, 65, 40]. Many statements, such as the Duistermaat–Heckman theorem, have been rigorously proven in this particular context. So it may be instructive to consider how lattice models can be used to describe singularities in this case.

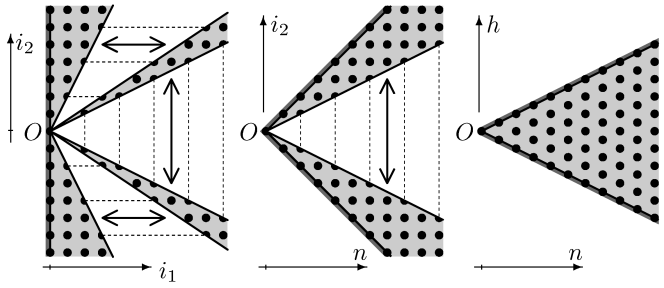

FIGURE 19. Possible three-cut lattice model (left) for the 1:1 resonance oscillator system and its reconstruction (center and right). The upward, central, and downward simple cuts of the model have axes i_2 (vertical), $+i_1$ (horizontal), and $-i_2$, respectively. Shaded areas represent (the deconstructed and reconstructed image of) the range of the $\mathcal{EM}$ map; bold dark shaded line indicates the boundary of this range. Dashed lines connect identified nodes; arrows indicate parallel transport direction for each cut.

Arguably, one of the simplest and most frequently studied 2-toric fibrations is the one which occurs in the 2-oscillator system with 1:1 resonance, see for example [15]. As one of the first integrals of this system we can take the momentum[3] $F_1 = \frac{1}{2}(q_1^2+p_1^2)+\frac{1}{2}(q_2^2+p_2^2)$, which is typically used as the linearized Hamiltonian. The other integral F_2 can be the whole nonlinear Hamiltonian (= energy). The image of the $\mathcal{EM}$ map defined by these integrals is qualitatively equivalent to that shown in Fig. 19, right. This image has the form of a solid angle whose vertex O

[3]In molecular applications F_1 is called *polyad integral*, and the corresponding quantum number n is called *polyad number*. The 1:1 system has the Poisson algebra so(3), and the analogy with the Euler top system, where the role of n is played by the value of the total angular momentum j, is often exploited.

represents the equilibrium of the oscillator. The joint spectrum lattice $\mathcal{L}_{1:1}$ of the 1:1 system has $n+1$ nodes for $F_1 = n = 0, 1, 2, \ldots$.

To reproduce the above lattice and the singular point O of its boundary, consider the plane $\mathbb{R}^2_{i_1,i_2}$ and take the regular lattice L_+, which lies in the half-plane $\{i_1 \geq 0\}$ and has smooth boundary $\{i_1 = 0\}$. Further, we need to make several simple integer cuts. Specifically, as shown in Fig. 19, left, we use three cuts of amplitude 1 which share the same vertex $O \in \{i_1 = 0\}$ and whose transport lines go in either the i_1 or the i_2 direction. To characterize the ensemble of these cuts (and thus the singularity at O), consider a "semicircle" path Γ_+ which starts near the boundary below O and passes in the counterclockwise direction to the point near the boundary above O. Note that Γ_+ crosses each of the three cuts once in the positive direction. Recalling our Lemma 7.4, we can easily see that the corresponding transformation is given by

$$\begin{pmatrix} 1 & 0 \\ -1 & 1 \end{pmatrix} \begin{pmatrix} 1 & 1 \\ 0 & 1 \end{pmatrix} \begin{pmatrix} 1 & 0 \\ -1 & 1 \end{pmatrix} = \begin{pmatrix} 0 & 1 \\ -1 & 0 \end{pmatrix}.$$

A possible reconstruction of our three-cut model which leads to the $\mathcal{L}_{1:1}$ lattice is illustrated in Fig. 19, center and right. In this figure, dashed lines, which follow the parallel transport lines, show how the opposite (in the sense of Def. 7.5) nodes of L_+ should be identified. Since the points which we glue together are regular and identical, gluing leaves no trace, i.e., there is no one-dimensional stratum left inside the reconstructed model.

The above computation of the cell transformation near O suggests that the same boundary defect at O can be reproduced alternatively by just *one* cut of a special kind [71] shown in Fig. 20, left. The transport rule for this cut involves a 90° rotation of the cells defined by matrix $\left(\begin{smallmatrix} 0 & 1 \\ -1 & 0 \end{smallmatrix}\right)$ and the transport lines are arcs

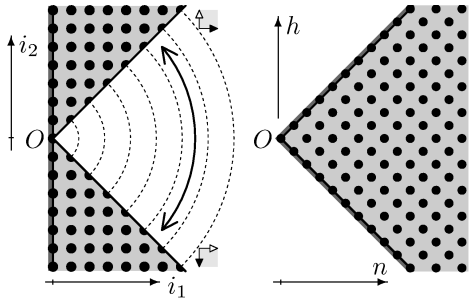

FIGURE 20. Rotational disclination cut (left) and its reconstruction (right), which is equivalent to the model of the 1:1 resonance oscillator system with three simple cuts shown in Fig. 19, left. Bold shaded line represents the boundary of the $\mathcal{EM}$ range. Dashed lines join identical nodes; arrows indicate transport across the cut as rotation about the defect point.

centered at O. The opposite points are again identical, and in order to reconstruct the model, the two "halves" of what is left of L_+ should be rotated towards each other about O and glued together seamlessly. Interestingly, the described construction is the most common crystallographic defect type called *rotational disclination* [39, 42, 71, 70].

Integrable oscillator systems with 1:2 **resonance.** A two-dimensional 1:2 resonant oscillator is yet another popular model of a large number of important physical systems, notably the Fermi resonance of molecular vibrational modes. It is interesting to compare this oscillator to the 1:(−2) system in Sec. 3 and to discuss briefly possible models of its joint spectrum lattice. The two first integrals are

$$F_1 = (p_1^2 + q_1^2) + \tfrac{1}{2}(p_2^2 + q_2^2), \quad F_2 = \tfrac{1}{2} z_1 \bar{z}_2^2 + \bar{z}_1 z_2^2 = q_1(q_2^2 - p_2^2) + 2p_1 q_2 p_2.$$

Here again F_1 represents a momentum of an S^1 action and is often taken in applications as a linearized Hamiltonian, while F_2 describes the lowest (principal) order resonance of the two oscillations. The energy is, generally, a smooth function $H(F_1, F_2)$, but for the purposes of the present brief discussion it suffices to simply take $H = F_2$. The values of F_1 and H are denoted as n and h, respectively. Note that the 1:2 system has been analyzed in detail by Vũ Ngọc and Colin de Verdière [13], and that the classical analysis based on the S^1 reduction is described briefly in [15, Appendix B.4, Example 3].

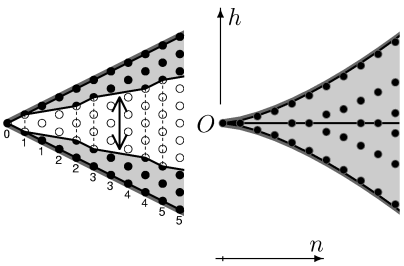

FIGURE 21. Lattice model (left) and numerical computation (right) of the joint energy–momentum spectrum lattice of the 1:2 resonance oscillator system. The model is obtained by introducing an additional rational cut in the reconstructed 1:1 lattice model in Fig. 19, right. This extra cut has axis $+i_1$, amplitude 1, and period 2; the number of empty (= removed) lattice nodes $\Delta(n_c)$ on each parallel transport line is indicated below the lower boundary.

The image of the $\mathcal{EM}$ map of the 1:2 oscillator system with $H = F_2$ is shown in Fig. 21, right. Like that of the 1:1 system in Fig. 19, right, this image is a wedge-like domain in a half-plane $\{(n, h) : n \geq 0\}$ whose $n = h = 0$ vertex corresponds to the equilibrium of the oscillator. This image is, however, formed by *two* lower cells. For the model system in Fig. 21, right, the boundary separating the two cells

is a ray $\mathcal{C}^{1:2} = \{(n,h) : n > 0, h = 0\}$ of critical values. This ray is similar to the line $\mathcal{C}_-$ of the critical $\mathcal{EM}$ values of the 1:(-2) system (see Proposition 3.4): like the points of $\mathcal{C}_-$, each point on $\mathcal{C}^{1:2}$ lifts to a curled torus. Furthermore, the preimage of $\mathcal{C}^{1:2}$ is a passable wall, which in this case separates two different upper cells.

The joint spectrum lattice $\mathcal{L}^{1:2}$ of the 1:2 system is shown in Fig. 21, right. For each fixed value n of momentum F_1 (i.e., on each transport line), the number of nodes of this lattice is given by a quasipolynomial in n

$$\tfrac{1}{2}(n+1) + \tfrac{1}{4}\big(1 - (-1)^{n+1}\big),$$

whose oscillatory part has period 2. The oscillation of the number of nodes for $F_1 > 0$ is the quantum manifestation of the presence of the line of singular values $\mathcal{C}^{1:2}$. Note also that $\mathcal{L}^{1:2}$ can be considered as a union of two sublattices with momentum indices $n = 2k$ and $n = 2k+1$, where $k = 0, 1, 2, \ldots$, and that the number-of-nodes function for each sublattice equals $k + 1$, just like in the 1:1 case. Of course, this composition of sublattices is entirely similar to the one we observed in the 1:(-2) case in Sec. 6.5 and 7.4. Furthermore, just like in the 1:(-2) case we can pass a double cell across the critical line $\mathcal{C}^{1:2}$.

In Fig. 21, left, we show the construction of the $\mathcal{L}^{1:2}$ lattice model starting from the assembled $\mathcal{L}^{1:1}$ lattice model in Fig. 19, right. This construction requires one rational cut of amplitude 1, period 2, and axis n. Comparing to Fig. 16, note that in the particular realization of this cut shown in Fig. 21, left, its boundaries are quasilinear. The "wiggling" of the boundaries goes to zero in the classical limit and they become straight rays. However, reconstruction of such cut by gluing the two boundaries together leaves the singular line $\mathcal{C}^{1:2}$.

8. Conclusion

In this paper, we developed the new concept of fractional monodromy and demonstrated its utility on the concrete examples of classical and quantum mechanical systems. Initially, the principal motivation of our analysis was the qualitative characterization of highly excited quantum (mainly atomic and molecular) systems. However, it quickly became apparent that fractional monodromy should play a more general role and have wider applications both in mathematics and physics. Yet up to now the phenomenon of fractional monodromy has remained practically unnoticed even in purely classical systems.

Our approach to monodromy is based on a direct study of the deformation of cycles γ representing basis elements g of first homology groups $H_1(\mathbb{T}^n)$ of the regular fibers of toric fibrations. In this work we have restricted ourselves to the detailed analysis of one nontrivial example, the case of the 1:(-2) resonance. Nevertheless, our method is sufficiently general and useful for the study of classical systems with other resonances and of corresponding quantum systems.

Many qualitative properties of purely quantum systems can be analyzed on the basis of a much more simpler study of purely classical limiting problems. Simultaneous analysis of classical and corresponding quantum systems gives ample

evidence to support this general idea. At the same time, the study of the quantum joint spectrum lattice can give important indications to the nature of singularities of the underlying classical dynamical system. Thus fractional monodromy itself was initially conjectured for quantum lattices and only after that it inspired the mathematical formulation of the corresponding phenomenon in classical mechanics.

Further generalization of monodromy and in particular of its lattice defect representation is both naturally possible and very appealing. In this paper we have only discussed those energy–momentum maps F which define integrable fibrations with fibers $F^{-1}(f)$ consisted of one connected component. Extending our definitions of monodromy in Sec. 2 to classical limit systems with several connected components in the inverse image of F and to quantum analogs of such systems should be especially interesting when the number of components differs for different values f of F. Many questions concerning examples of dynamical systems with multiple singularities and with more complex singularities remain unclear even in the case of systems with two degrees of freedom. Many physically relevant examples of multi-dimensional systems with nontrivial resonances (which are quite typical in molecular physics in particular) are potential candidates for the study of further obstructions to the existence of global action-angle variables and for the classification of typical patterns in quantum joint energy–momentum spectra.

A great number of questions, for example the possibility of "irrational" monodromy, remain completely open. Our study demonstrated most convincingly the power of the lattice based approach. However, a general theory of lattice defects and their relation to singularities of classical toric foliations and joint spectra of fully and partially integrable quantum systems has yet to be developed. In a more global context, relation to real physical crystal lattices and, probably, to some other areas should also be uncovered systematically.

This work is the result of a joint effort in an interdisciplinary field, which required substantial expertise in modern mathematics, physics, and theoretical chemistry. We hope that it will stimulate further research in this direction and encourage better mutual understanding of scientists, who work on seemingly distant but intrinsically close subjects.

Appendix A. Singular fibers of integrable map in systems with monodromy

The *pinched torus* is the most typical singular fiber in two degrees of freedom Hamiltonian systems with monodromy. It can be represented as a 2D-surface of revolution obtained by rotating a cusped loop around its cusp point. This terminology and representation is due to Cushman, see [15]. Figure A.1 illustrates two possible reconstructions of the pinched torus in $\mathbb{R}^3$ and respective two alternative 3D-space representations. In both cases, the cusp point O stays fixed in $\mathbb{R}^3$, while the opposite middle point x of the cusped loop C goes along circle A or circle B.

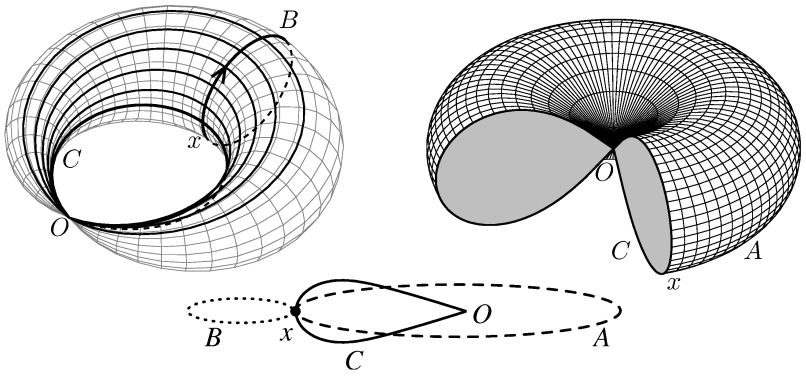

FIGURE A.1. Pinched torus is the $\Lambda_0 = F^{-1}(0,0)$ fiber of the 1:(−1) fibration. Two alternative representations (top left and right) of the same torus in the 3D space are obtained by continuous deformation of the cusped loop C (bottom figure): the cusp point O is fixed while point x moves either along circle A or along circle B.

In spite of their different 3D images, this produces two singular varieties in $\mathbb{R}^4$ which are topologically equivalent.

Pinched torus appears as an isolated singular fiber of $\mathcal{EM}$ in the case of integrable fibration F introduced in Sec. 3 in the case $m_1 = m_2 = 1$. The cusp point O is the critical point of $\mathcal{EM}$ of rank 0, all other points of the pinched torus are regular. In our case O is at $0 \in \mathbb{R}^4_{q,p}$ and A or B circles represent trajectories γ of the phase flow $\{g^t_{F_1^{(0)}}, t \in R\}$ of the system with Hamiltonian $F_1^{(0)}$ whose action on $\mathbb{R}^4$ is isomorphic to a circle.

The *k-curled torus* can be represented in $\mathbb{R}^4$ as a singular surface of translation and revolution of a Z_k-symmetric "k-petal-flower planar curve". The latter is a union of k cusped loops (= petals) with common self-intersection cusp point O. A rotation of the plane of the flower about O by $2\pi/k$ permutes the petals cyclically while leaving the flower as a whole invariant. To obtain the *k-curled torus*, we take a circle trajectory γ_c, which intersects the plane of the flower transversally at O, and move the plane so that O remains on γ_c. As O makes one tour on γ_c, we rotate the flower about O so that the petals become cyclically permuted. Alternatively, we can start with just one cusped loop (= one petal) whose cusp point O makes k tours on γ_c, while the spiral traced out by the opposite point x has k tours along γ_c and one tour in the transversal direction about γ_c.

Note that in the case of the 1:(−2) resonance, k equals 2 and γ_c is the special short trajectory of the system with Hamiltonian $F_1^{(0)}$ in (3.1a) with $m_1 = 1$ and $m_2 = 2$. In our particular example system (4.3), the 2-curled (or simply curled) torus is the "weak" singular fiber $F^{-1}(m,h)$ with $-\frac{1}{4} < m < 0$ and $h = m^2$. All

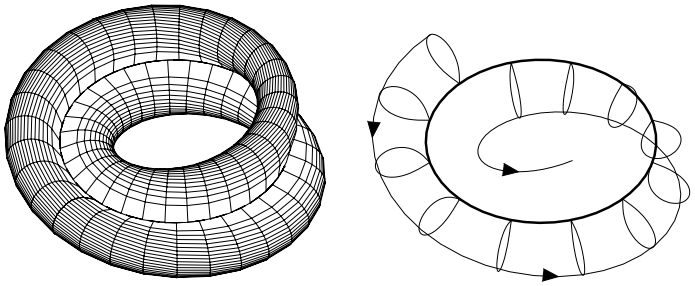

FIGURE A.2. Curled torus (left) and its possible reconstruction (right).

points on γ_c are critical points of map F of rank 1, all other points of the curled torus are regular. As shown in Fig. A.2, such singular fiber can be constructed by moving a figure eight curve so that its self-intersection point O goes around a circle γ_c, while the rest of the curve rotates about O. After O comes back in time $t = \pi$ the two loops of the curve are interchanged.

The 2-*curled pinched torus* (or simply pinched curled torus) is the singular fiber Λ_0 which corresponds to the critical value $(F_1, F_2) = (0, 0)$ of the integrable fibration F introduced in Sec. 3 in the case of $m_1 = 1$ and $m_2 = 2$. It can be obtained as a deformation of the 2-curled torus, whose critical circle γ_c is contracted to a point. This fiber has one critical point of rank 0; in the $\mathbb{R}^3$ space, it can be represented as a self-intersecting surface shown in Fig. A.3.

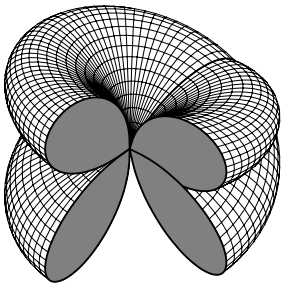

FIGURE A.3. Pinched curled torus.

Appendix B. Dynamical symmetry and space of orbits

In this appendix we describe integrable fibrations (3.1a) and (3.1b) using their underlying dynamical symmetry. Assuming $R_1(q, p) = 0$, the phase flow generated by Hamiltonian F_1 in (3.1a) can be identified with the action of one-dimensional compact Lie symmetry group $\mathbb{S}^1_t$. Action of $\mathbb{S}^1_t$ on the four-dimensional symplectic

space $\mathbb{R}^4_{p,q}$ has a particularly simple form in terms of complex variables

$$z_s = q_s - \mathrm{i}p_s, \quad \bar{z}_s = q_s + \mathrm{i}p_s, \quad \text{where } s = 1, 2. \tag{B.1}$$

The Poisson bracket becomes $\{z, \overline{z}\} = 2i$ and the action $\mathbb{S}^1_t \colon (z, \bar{z}) \mapsto U_t(z, \bar{z})$ is given by the diagonal 4×4 matrix

$$U_t = \operatorname{diag}\bigl(\mathrm{e}^{\mathrm{i}m_1 t}, \mathrm{e}^{-\mathrm{i}m_2 t}, \mathrm{e}^{-\mathrm{i}m_1 t}, \mathrm{e}^{\mathrm{i}m_2 t}\bigr). \tag{B.2}$$

The 3D space of orbits of the $\mathbb{S}^1_t$ action (B.2) on $\mathbb{R}^4_{p,q}$ can be geometrically represented in terms of invariant polynomials (for an invariant theory survey which is close in spirit to this application, see [49] and references therein). All $\mathbb{S}^1_t$ invariant polynomials form a module, whose structure is described by the Molien generating function

$$g_{m_1:m_2}(\lambda) = \frac{1 + \lambda^{m_1+m_2}}{(1-\lambda^2)^2(1-\lambda^{m_1+m_2})}, \tag{B.3}$$

where the formal variable λ represents any of variables $z, \bar{z}$. According to (B.3) there exist three algebraically independent polynomials of degrees 2, 2, and $m_1 + m_2$, and one linearly independent but algebraically dependent invariant polynomial of degree $m_1 + m_2$. We can choose them as

$$\eta = \tfrac{1}{4}(m_1 z_1 \bar{z}_1 - m_2 z_2 \bar{z}_2)(m_1 m_2)^{-1}, \tag{B.4a}$$

$$\pi_1 = \tfrac{1}{4}(m_1 z_1 \bar{z}_1 + m_2 z_2 \bar{z}_2)(m_1 m_2)^{-1}, \tag{B.4b}$$

$$\pi_2 = \tfrac{1}{4}\bigl(z_1^{m_2} z_2^{m_1} + \bar{z}_1^{m_2} \bar{z}_2^{m_1}\bigr)\bigl(2^{m_1+m_2-2} m_1^{m_1} m_2^{m_2}\bigr)^{-1/2}, \tag{B.4c}$$

$$\pi_3 = \tfrac{\mathrm{i}}{4}\bigl(z_1^{m_2} z_2^{m_1} - \bar{z}_1^{m_2} \bar{z}_2^{m_1}\bigr)\bigl(2^{m_1+m_2-2} m_1^{m_1} m_2^{m_2}\bigr)^{-1/2}. \tag{B.4d}$$

The only one algebraic relation between these polynomials is

$$2\Phi_\eta^{m_1:-m_2}(\pi_1, \pi_2, \pi_3) = \pi_2^2 + \pi_3^2 - (\pi_1 - \eta)^{m_1}(\pi_1 + \eta)^{m_2} = 0. \tag{B.5}$$

Notice that our two initial integrals (F_1, F_2) are easily expressed in terms of (B.4)

$$F_1 = 2m_1 m_2\, \eta, \tag{B.6a}$$

$$F_2 = \bigl(2^{m_1+m_2} m_1^{m_1} m_2^{m_2}\bigr)^{1/2} \pi_3 + (2m_1 m_2 \pi_1)^s. \tag{B.6b}$$

Applying standard invariant theory [49] to our case gives

Proposition B.1. *All orbits of the* $\mathbb{S}^1_t$ *group action* (B.2) *can be labeled by the values of three algebraically independent* principal (*denominator*) *invariant polynomials and the sign of one* auxiliary (*numerator*) *invariant polynomial.*

As principal and auxiliary invariants we can take, for example, (η, π_1, π_3) and π_2 respectively. We can also replace η and π_1 by their linear combinations

$$r_1 = (\pi_1 + \eta)m_2 = \tfrac{1}{2}(q_1^2 + p_1^2), \quad r_2 = (\pi_1 - \eta)m_1 = \tfrac{1}{2}(q_2^2 + p_2^2),$$

which represent one-dimensional harmonic oscillators. On the other hand, invariants (B.4) are particularly suitable in view of the following property.

Lemma B.1. *Polynomials* (π_1, π_2, π_3) *generate a Poisson algebra with Poisson bracket*

$$\{\pi_a, \pi_b\} = \varepsilon_{abc} \frac{\partial}{\partial \pi_c} \Phi_\eta^{m_1:-m_2}, \tag{B.7}$$

and Casimir η*. Here* ε_{abc} *is the Levi-Civita symbol.*

Remark B.1. We can define a meaningful reversing symmetry operation

$$(\eta, \pi_1, \pi_2, \pi_3) \mapsto (\eta, \pi_1, -\pi_2, \pi_3) \tag{B.8}$$

for systems with first integrals (B.6). This operation leaves both the Hamiltonian and relation (B.5) invariant but reverses some signs in the Poisson structure (B.7). In view of this extra symmetry, using π_2 as an auxiliary invariant is particularly convenient.

B.1. Orbit space of the $\mathbb{S}^1$ action

Proposition B.1 and relation (B.5) give the way to describe explicitely the space $\mathcal{O}^{m_1:(-m_2)}$ of orbits of the $\mathbb{S}^1$ action (B.2). It can be seen that $\mathcal{O}^{m_1:(-m_2)}$ is a 3D body which can be decomposed into two parts, one for $\pi_2 \leq 0$ and another for $\pi_2 \geq 0$, and that points $\{\pi_2 = 0\}$ constitute the intersection of these parts. In order to visualize $\mathcal{O}^{m_1:(-m_2)}$ and to study sections of this space with constant values of integrals F_1 and F_2, we can represent each part of $\mathcal{O}^{m_1:(-m_2)}$ in the space $\mathbb{R}^3$ with coordinates (η, π_1, π_3). To this end, we solve (B.5) with $\pi_2 = 0$ with respect to $\pi_1 \geq 0$. It can be shown that solution $\pi_1^0(\eta, \pi_3)$ is a single valued continuous function on $\mathbb{R}^2$ and that each part of $\mathcal{O}^{m_1:(-m_2)}$ is an algebraic variety given by the

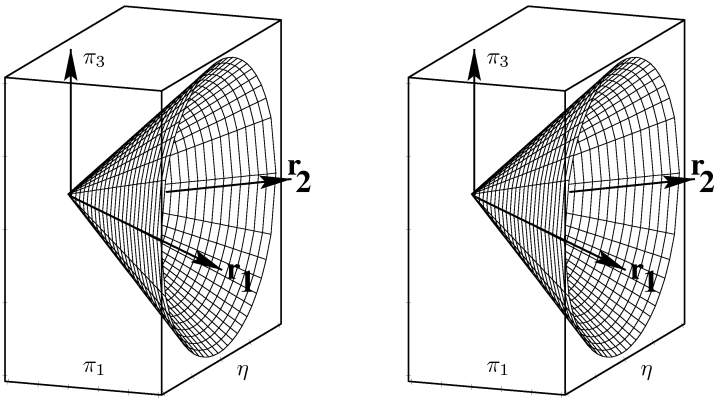

FIGURE B.1. Space of orbits of the $\mathbb{S}^1_t$ action on the phase space $\mathbb{R}^4$ of the 1:(−1) resonant oscillator system. All points inside and on the surface of each cone except the vertex represent generic circular orbits γ; the vertex represents the equilibrium. Surface points of the cones with the same (η, π_3) should be identified.

inequality $\pi_1 \geq \pi_1^0(\eta, \pi_3)$. For each (η, π_3) we should identify (glue together) the points on the surfaces $\pi_1 = \pi_1^0$ of the two parts. In the simplest case of the space $\mathcal{O}^{1:(-1)}$, the surface $\{\pi_1 = \pi_1^0(\eta, \pi_3)\}$ is a straight cone shown in Fig. B.1. The whole space $\mathcal{O}^{1:(-1)}$ can be therefore represented as two filled cones glued together on their surface $\{\pi_1 = \pi_1^0(\eta, \pi_3)\}$. Specifically, points inside each cone represent different $\mathbb{S}^1$ orbits, while boundary points with the same η and π_3 represent the same orbit with $\pi_2 = 0$ and should be identified. The space $\mathcal{O}^{1:(-1)}$ contains two strata: the identified vertices of the cones represent one exceptional one-point orbit which is the unstable equilibrium of the system with Hamiltonian F_1; all other points represent generic circular orbits γ in $\mathbb{R}^4$.

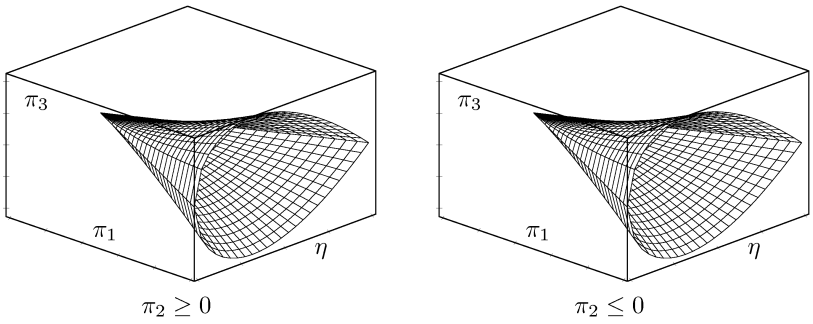

FIGURE B.2. Space of orbits of the $\mathbb{S}^1_t$ action for the $1:(-2)$ resonant oscillator system. Surface points of the two bodies with the same (η, π_3) should be identified.

The orbit space $\mathcal{O}^{1:(-2)}$ is shown in Fig. B.2. In addition to generic circular orbits γ of period 2π and one exceptional equilibrium orbit, which is represented by the vertex of the deformed conical surface, there is also a 1D set of orbits γ_c represented by points in $\{r_1 = 0, r_2 > 0\}$. These orbits have period π and possess a nontrivial stabilizer Z_2. Similar stratification occurs in the case of $m_1 = 1$ and any integer $m_2 > 1$ but the stabilizer of orbits belonging to the 1D-stratum is different.

In the most general situation, when integers $m_1 > 1$, $m_2 > 1$ and $\mathrm{lcd}(m_1, m_2) = 1$, the space of orbits includes four different strata. Points of the generic stratum lift to generic circular orbits γ of period 2π. The 0-dimensional stratum is formed by the vertex point which represents one exceptional one point orbit (equilibrium point). The two 1-dimensional strata $\{r_1 = 0, r_2 > 0\}$ and $\{r_2 = 0, r_1 > 0\}$ include points which lift to special "short" circular orbits in $\mathbb{R}^4$ whose stabilizers are two different finite groups.

Our geometric representation $\Pi\colon \mathbb{R}^4_{q,p} \to \mathcal{O} \subset \mathbb{R}^4_{\pi_1,\pi_3,\eta;\pi_2}$ of the space of orbits $\mathcal{O}$ of the $\mathbb{S}^1$ action can be used to analyze the topology of isoenergetic surfaces of any Hamiltonian system with such $\mathbb{S}^1$ symmetry. We can also classify mutual constant level sets of two commuting Hamiltonians whose flow is invariant with respect to the $\mathbb{S}^1_t$ action. Thus we will obtain an explicit reduced geometric repre-

sentation $s_{m,h} = \Pi(\{F_1 = m\} \cap \{F_2 = h\})$ of the fibers of the integrable fibration defined by (F_1, F_2) in Sec. 3, find all different possible $s_{m,h}$, and reconstruct their preimages $\Pi^{-1}(s_{m,h})$. To this end it will be most convenient to slice the orbit space $\mathcal{O}$ first by the constant m-level sets of $\mathcal{F}_1 = F_1 \circ \Pi^{-1}$.

B.2. Reduction in the case of the $\mathbb{S}^1$ symmetry

Our concrete example systems in Sec. 3 have two first integrals (F_1, F_2). We will consider F_1 as a *momentum* because the flow φ_{F_1} of the system with Hamiltonian F_1 generates $\mathbb{S}^1$ symmetry (B.2). We can reduce this symmetry for each given value m of F_1. Each point on the reduced phase space P_m lifts to an orbit of φ_{F_1}. Since the action (B.2) is not free, some of the spaces P_m have singularities. For a general discussion of singular reduction, see [15]. We only mention that P_m can be equipped with the Poisson structure using Lemma B.1.

In order to construct P_m we slice the space of orbits $\mathcal{O}$ by constant m-level sets of $\mathcal{F}_1 = F_1 \circ \Pi^{-1}$. We thus have $P_m = \Pi(\{F_1 = m\}) = \{\mathcal{F}_1 = m\} \cap \mathcal{O}$. It can be easily seen from (B.6a), (B.5) and Figs. B.1 and B.2 that we should simply intersect orbit spaces $\mathcal{O}$ by planes $\{\eta = \text{const}\}$ which are parallel to the coordinate plane (π_1, π_3). This gives two sections, one for $\pi_2 \geq 0$ and the other for $\pi_2 \leq 0$, which should be glued together along their boundaries, i.e., at the points with the same (π_1, π_3) and $\pi_2 = 0$. In most cases when the boundary points belong to the generic stratum this gluing is smooth.

Proposition B.2 (reduced phase spaces P_m). *Each space P_m can be embedded explicitly in $\mathbb{R}^3$ with coordinates (π_1, π_2, π_3) where P_m is represented as a surface of revolution about axis π_1. This surface is bounded by $\pi_1(m) \geq 0$ and can be projected bijectively on the 2-plane $\{\pi_1 = 0\}$ with coordinates (π_2, π_3). The point of P_m with the lowest value of π_1 lies on axis π_1, i.e., $\pi_2 = \pi_3 = 0$; for some m this point is singular.*

The proof can be obtained analytically by fixing the value of η in (B.5). The singular point of P_m will be called *vertex*.

In particular, $P_m^{1:(-1)}$ is smooth for all $m \neq 0$; all points of such spaces are regular and lift to generic $\mathbb{S}^1$ orbits. $P_0^{1:(-1)}$ is a straight cone whose vertex represents the exceptional one-point equilibrium orbit. The spaces $P_m^{1:(-2)}$ are smooth (regular) for $m > 0$ and have one conical cusp vertex otherwise. The singularity can be characterized explicitely using (B.5). The singular point lifts to the equilibrium when $m = 0$ and to a non-generic "short" $\mathbb{S}^1$ orbit γ_c with stabilizer Z_2 when $m < 0$.

B.3. Energy-momentum map, critical points and critical values

We can now easily construct the energy–momentum map $\mathcal{EM}$ for our concrete systems in Sec. 3 and Fig. 2. To obtain a geometric representation of the fibers of $\mathcal{EM}$ we study intersections $\{\mathcal{F}_2 = h\} \cap P_m$ where $\mathcal{F}_2 = F_2 \circ \Pi^{-1}$ assumes the role of "energy". This study can be further simplified if we account for symmetry property (B.8). This symmetry allows using just one part V_m of P_m which can be

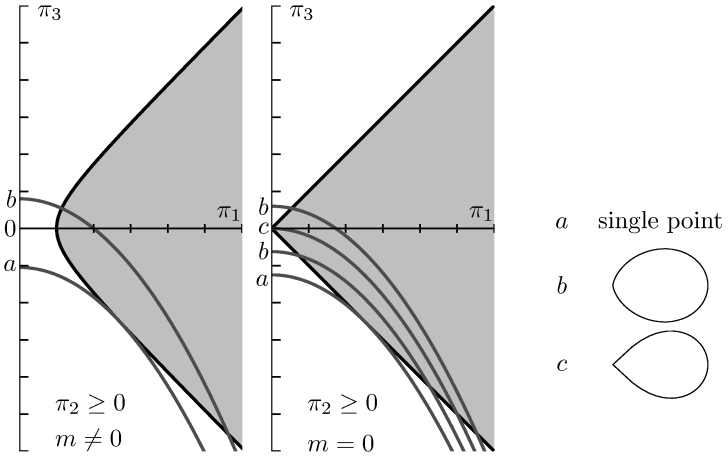

FIGURE B.3. Projection of P_m on the $\{\pi_2 = 0\}$ plane in the case of 1:(−1) resonance, sliced by the constant h-level sets of $\mathcal{F}_2 = F_2 \circ \Pi^{-1}$ with F_2 in (4.1b); only one part V_m of each P_m for $\pi_2 \geq 0$ is shown.

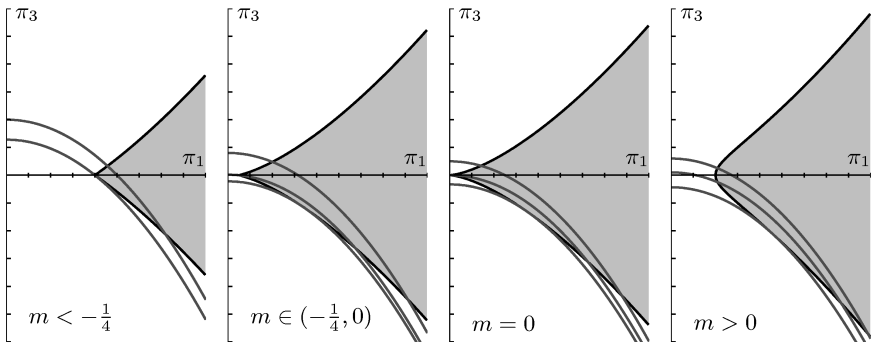

FIGURE B.4. Projections of P_m on the $\{\pi_2 = 0\}$ plane in the case of 1:(−2) resonance, sliced by the constant h-level sets of $\mathcal{F}_2$ (bold lines). Only one part V_m of each P_m for $\pi_2 \geq 0$ is shown.

obtained as $\{\mathcal{F}_1 = m\}$ for $\pi_2 \geq 0$, or, equally, as a projection of P_m on the 2-plane with coordinates (π_1, π_3).

Figures B.3 and B.4 show constant h-level sets of $\mathcal{F}_2$ on V_m for the cases 1:(−1) and 1:(−2) respectively. Since we are interested in fibers $\Lambda_{m,h}$ which lie close to the singular fiber Λ_0, the value of $|m|$ is taken close to 0. Qualitative description of such fibers follows from that of the intersections $\{\mathcal{F}_2 = h\} \cap V_m$. In particular we obtain

Proposition B.3. *Nonempty intersections, $v_{m,h} = \{\mathcal{F}_2 = h\} \cap V_m$ for $\mathcal{F}_2 = F_2 \circ \Pi^{-1}$ with F_2 in* (4.1b) *or* (4.3b)*, are compact, and are either a single point or a closed segment. The set of h values, for which $v_{m,h} \neq \emptyset$ is limited from below; the value $h_{\min}(m)$ corresponds to a single point intersection $v_{m,h_{\min}(m)}$, which can be a regular point of the boundary ∂V_m where $\{F_2 = h_{\min}\}$ and ∂V_m touch, or a singular point, i.e., vertex of ∂V_m. When $v_{m,h}$ is a closed segment, both its end points are typically regular points of ∂V_m. However, if P_m (and therefore V_m and ∂V_m) with $m \neq 0$ has a vertex, there exist a critical segment $v_{m,h_c(m)}$ with $h_{\min}(m) < h_c(m) < \infty$ which has the vertex as one of its endpoints.*

Compactness of $v_{m,h}$ follows from the analysis of the intersections of the level sets of F_2 in (B.6a) and ∂V_m defined by (B.5) with $\pi_2 = 0$ and fixed $\eta(m)$. We can show easily that the proper choice of s in (3.2b) and (B.6a) assures compactness of $v_{m,h}$. This justifies the specific choice of the compactifier (3.2). Lifting $v_{m,h}$ to $P_m \subset \mathcal{O}$ and then to the original space $\mathbb{R}^4$ using the inverse reduction map leads to

Proposition B.4 (fibers of the $\mathcal{EM}$ map in the 1:(−1) case). *Nonempty intersections $s_{m,h} = \{\mathcal{F}_2 = h\} \cap P_m^{1:(-1)}$ for $\mathcal{F}_2 = F_2 \circ \Pi^{-1}$ and F_2 in* (4.1b) *are connected and compact, and are either a single regular point of P_m, a smooth closed loop, or a closed loop with one singular point* (*see Fig.* B.3)*. The respective fibers $\Pi^{-1}(s_{m,h})$ of the integrable fibration defined by (F_1, F_2) are a circular orbit* (*relative equilibrium*)*, a regular 2-torus* (*generic fiber*)*, and a* pinched torus *when $m = 0$ and $h = 0$.*

Proposition B.5 (fibers of the $\mathcal{EM}$ map in the 1:(−2) case). *Nonempty intersections $s_{m,h} = \{\mathcal{F}_2 = h\} \cap P_m^{1:(-2)}$ for $\mathcal{F}_2 = F_2 \circ \Pi^{-1}$ and F_2 in* (4.3b) *are connected and compact, and are either a regular single point of P_m, a vertex of P_m, a smooth closed loop* (*generic intersection*)*, or a closed loop with one singular point. The respective fibers $\Pi^{-1}(s_{m,h})$ of the integrable fibration defined by (F_1, F_2) are a generic circular orbit γ (relative equilibrium) of the flow of X_{F_1}, a special short orbit γ_c (relative equilibrium with stabilizer Z_2), a regular 2-torus (generic fiber), and a singular 2-torus. The latter is a* pinched curled torus *when $m = 0$ or a* curled torus *when $m \neq 0$.*

Finally, in order to describe the images of the $\mathcal{EM}$ map in Figs. 2, 10, and 12, we can derive explicit expressions for $h_c(m)$ and $h_{\min}(m)$ from a more detailed analytic study of the intersections $v_{m,h}$. We do not provide this analysis here because these expressions are found in Appendices C and D on the basis of a direct computation of critical values of the map (F_1, F_2).

Appendix C. Proofs in the case $m_1 = m_2 = 1$

In this section, we collect analytical proofs of some auxiliary statements required for the proof of the monodromy Theorem 1 (the case of the 1:(−1) resonance). We begin with proving Lemma 5.1. We then consider cycles, which represent basis

elements of $H_1(\mathbb{T}^2_{m,h})$, and describe their deformation which occurs when the point (m,h) moves along the contour Γ. This description is given directly in the hyperplane σ. The central issue is the detailed analysis of small modifications which occur near the fibers with $m=0$. This analysis completes the analytical proof of the monodromy Theorem 1.

C.1. Technical lemmas. Case of the $1{:}(-1)$ resonance

We start with simple auxiliary technical lemmas. Recall that the hyperspace σ is defined in (5.4) as $\{F_3=0\}$ where $F_3 := p_1 - q_2$.

Lemma C.1. *The phase flow of the system with Hamiltonian F_1*

$$\{g^t_{F_1},\ t\in\mathbb{R}\}\colon \mathbb{R}^4_{q,p}\times\mathbb{R}\to\mathbb{R}^4_{q,p}\colon (\xi,t)\mapsto M(t)\,\xi,\quad \xi=(q_1,p_1,q_2,p_2),$$

is given by the block-diagonal matrix $M(t)=\operatorname{diag}\big(M_1(t),M_2(t)\big)$, where

$$M_k(t)=\begin{pmatrix}\cos\omega_k t & -(-1)^k\sin\omega_k t\\ (-1)^k\sin\omega_k t & \cos\omega_k t\end{pmatrix},\quad k=1,2 \text{ and } \omega_1=\omega_2=1. \tag{C.1}$$

The action of $\{g^t_{F_1},\ t\in R\}$ is equivalent to an $\mathbb{S}^1$ circle action. Moreover,

$$g^{\pi}_{F_1}\colon (p,q)\mapsto(-p,-q),$$

i.e., after a time $t=\pi$ each point goes into a central symmetric point. The two coordinate planes $\{p_k=q_k=0\}$, $k=1,2$, are $g^t_{F_1}$ invariant. In each of these planes, $g^t_{F_1}$ acts as a rotation by angle t in opposite directions with respect to the ordered basis axes $(p_{k'},q_{k'})$.

There is another pair of invariant and mutually orthogonal with respect to the Euclidian structure planes $\{p_1-q_2=p_2-q_1=0\}$ and $\{p_1+q_2=p_2+q_1=0\}$ where $g^t_{F_1}$ also acts as a rotation. The former plane lies in σ. Each trajectory γ of the phase flow $\{g^t_{F_1}, t\in R\}$ either belongs to this plane and thus lies in σ or intersects σ in exactly two points, which are symmetric with respect to $0\in R^4$.

Proof. Consider the vector field

$$X_{F_1}(q,p)=\left(\frac{dp_1}{dt},\frac{dq_1}{dt},\frac{dp_2}{dt},\frac{dq_2}{dt}\right)=(-q_1,p_1,q_2,-p_2)$$

generated by the system with Hamiltonian F_1. The condition $dF_3(X_{F_1})=0$, where F_3 is given by (5.4), for the phase flow $\{g^t_{F_1}, t\in R\}$ to be tangent to σ defines the 2-plane $\{-q_1+p_2=p_1-q_2=0\}\subset\sigma$. One can easily verify that the restricted vector field $X_{F_1}|_\sigma=(-q_1,p_1,p_1,-p_2)$ is also tangent to the plane $\{-q_1+p_2=0\}$. This means that the whole trajectory γ belongs to the 2-plane $\{-q_1+p_2=p_1-q_2=0\}\subset\sigma$. The proofs of all other statements of Lemma C.1 are either analogous or evident. □

Lemma C.2. *Restrictions of coordinate functions p_1,q_1,p_2 on σ define coordinates on σ which we denote by the same letters. In these coordinates restrictions of functions F_1 and F_2 on σ have the form*

$$\mathcal{F}_1=\tfrac12(q_1^2-p_2^2),\quad \mathcal{F}_2=p_1^2+p_2q_1+\tfrac14(2p_1^2+q_1^2+p_2^2)^2. \tag{C.2}$$

In order to simplify $\mathcal{F}_1$ we change the coordinates (p_2, q_1) as

$$x = (q_1 - p_2)/\sqrt{2}, \quad y = (q_1 + p_2)/\sqrt{2}.$$

Then functions $\mathcal{F}_1$ and $\mathcal{F}_2$ take the form

$$\mathcal{F}_1 = xy, \quad \mathcal{F}_2 = -\tfrac{1}{2}x^2 + \tfrac{1}{2}y^2 + p_1^2 + R(x, y, p_1).$$

The plane $\{x = 0\} \subset \sigma$ coincides with the mentioned above plane $\{p_1 - q_2 = p_2 - q_1 = 0\} \subset R^4$ which is invariant with respect to the flow $\{g^t_{F_1}, t \in R\}$.

The proof consists of straightforward computations.

Lemma C.3. *Consider $U_\epsilon := \cup_{|m|+|h|<\epsilon}\Lambda_{m,h}$ and its intersection $U_\epsilon \cap \sigma$ with σ. For sufficiently small $\epsilon > 0$ the condition*

$$\operatorname{rank} \frac{\partial(F_1, F_2, F_3)}{\partial(p, q)} \leq 2$$

for the "extended" Jacobian matrix on $U_\epsilon \cap \sigma$ is satisfied at all points of the axis p_1 on σ and only in these points. The values of the map F at points of the axis p_1 in σ (i.e., on the line $p_1^\sigma := \{q_1 = p_2 = p_1 - q_2 = 0\}$) are $(F_1, F_2) = (0, p_1^2 + p_1^4)$.

Proof. The Jacobian matrix in Lemma C.3 has the form

$$\begin{pmatrix} p_1 & q_1 & -p_2 & -q_2 \\ q_2 + 2p_1\chi & p_2 + 2q_1\chi & q_1 + 2p_2\chi & p_1 + 2q_2\chi \\ 1 & 0 & 0 & -1 \end{pmatrix}, \tag{C.3}$$

where

$$\chi = p_1^2 + q_1^2 + p_2^2 + q_2^2.$$

After adding the first column of (C.3) to its fourth column and eliminating the first column and the last row from the resulting matrix, we obtain the 2×3 matrix

$$\begin{pmatrix} q_1 & -p_2 & -q_2 + p_1 \\ p_2 + 2q_1\chi & q_1 + 2p_2\chi & (p_1 + q_2)(1 + 2\chi) \end{pmatrix}, \tag{C.4}$$

whose rank is smaller than that of the initial matrix (C.3) exactly by 1. Consequently, we should analyze further the 2×3 matrix (C.4). It is clear that at all points of axis p_1 in σ the rank of (C.4) is not maximal. Direct substitution of $\{q_2 = p_1, p_2 = q_1 = 0\}$ gives the values (m, h) of the map F on p_1^σ. It can be seen that F maps p_1^σ to the halfline $\{m = 0, h = p_1^2 + p_1^4\}$.

Let us show that at all other points of $U_\epsilon \cap \sigma$ the rank of (C.4) is maximal. Taking into account that the coefficient in the right upper corner of matrix (C.4) becomes equal to zero on σ, one can easily verify that the non-maximal rank condition reduces either to equations $\{p_1 - q_2 = p_2 = q_1 = 0\}$, which specify axis p_1 on σ, or to the system

$$p_1 = q_2 = 0, \quad (q_1^2 + p_2^2)(1 + 4q_1p_2) = 0. \tag{C.5}$$

It is easy to see that in a sufficiently small neighborhood of $0 \in \mathbb{R}^4$ the only solution this system has is $p_1 = q_2 = p_2 = q_1 = 0 \in \mathbb{R}^4$. An explicit solution of (C.5), which is far from zero, can also be found. Supposing that $q_1^2 + p_2^2 > 0$ the

second equation in (C.5) becomes $1 + 4q_1p_2 = 0$. The image of the corresponding solution $\{p_1 = q_2 = 0, q_1 = -(4p_2)^{-1}\}$ of the complete system under the map F

$$\left\{ m = \tfrac{1}{2}\left(\frac{1}{16p_2^2} - p_2^2\right), \quad h = -\tfrac{1}{4} + \tfrac{1}{4}\left(\frac{1}{16p_2^2} + p_2^2\right)^2 \right\}$$

is obtained by direct substitution into F_1 and F_2. From this we get the relation $h = m^2 - \frac{3}{16}$ which defines the boundary of the range of F. Of course, critical points of F represented by this boundary lie outside U_ϵ, i.e., far from $0 \in \mathbb{R}^4$. □

Figure C.1 shows the image of the $\{F_1, F_2\}$ map together with image of the points where the intersection $\Lambda_{m,h} \cap \sigma$ is non-regular.

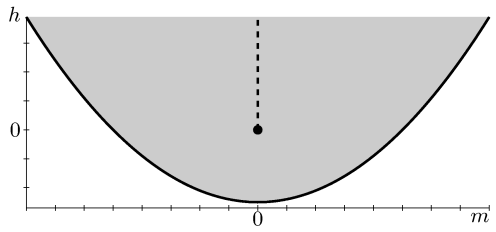

FIGURE C.1. Critical values of the (F_1, F_2) map (solid line and black dot) and the image of nonregular intersections $\sigma \cap \Lambda_{m,h}$ (dashed line) in the 1:(−1) case.

We are now ready to prove Lemma 5.1.

Proof. It follows from Lemma C.3 that condition $\left(\operatorname{rank} \frac{\partial(F_1,F_2)}{\partial(p,q)}\right) < 2$ can be only met on axis p_1 in σ and only in a sufficiently small neighborhood of $0 \in \mathbb{R}^4$. A straightforward analysis of the "shortened" in comparison to (C.3) 2×4 matrix

$$\begin{pmatrix} p_1 & q_1 & -p_2 & -q_2 \\ q_2 + 2p_1\chi & p_2 + 2q_1\chi & q_1 + 2p_2\chi & p_1 + 2q_2\chi \end{pmatrix},$$

shows that on σ its rank can be non-maximal only at points satisfying the system of equations

$$p_1^2 + 4p_1q_2\chi + q_2^2 = q_1^2 + 4q_1p_2\chi + p_2^2 = 0.$$

It is easy to see that the only solution of this system which belongs to a small neighborhood of point $0 \in \mathbb{R}^4$ is that point itself. Consequently, surfaces $\Lambda_{m,h} = F^{-1}(m,h)$ for all $|m| + |h| < \epsilon$ are smooth at all points of σ except the point $0 \in \Lambda_{0,0}$. Smoothness of the $\Lambda_{m,h}$ surfaces outside σ follows from two simple facts: (i) $\Lambda_{m,h}$ are invariant with respect to phase flow $\{g^t_{F_1},\ t \in \mathbb{R}\}$ and (ii) each trajectory γ of this flow intersects σ.

It follows from the above argument and from Lemma C.3 that the non-transversality of the intersection $\sigma \cap \Lambda_{m,h}$ can occur only at points on axis p_1^σ.

The differential dF_1 at any point of axis p_1^σ has the form $dF_1 = p_1(dp_1 - dq_2)$, see upper line in (C.3). Consequently, σ is tangent to surfaces $\Lambda_{m,h}$ at all points of p_1^σ except point $0 \in \mathbb{R}^4$. Lemma 5.1 is proven. □

C.2. Intersections $\Lambda_{m,h} \cap \sigma$ in the case $m_1 = m_2 = 1$

We describe intersection curves $\lambda_{m,h} := \Lambda_{m,h} \cap \sigma$ directly in the three-dimensional hyperplane σ. We will use coordinates (p_1, x, y) defined in Lemma C.2. Recall that the alternative representation of $\lambda_{m,h}$ on the torus chart of $\Lambda_{m,h}$ was used in Sec. 5 in order to explain the idea of the proof. The especially simple intersection $\lambda_{0,h}$ will be called *skeleton*.

Lemma C.4. *The skeleton $\lambda_{0,h<0}$ is regular and consists of two closed skeleton curves, which lie in the same 2-plane $\{y = 0\} \subset \sigma$, see Fig.* C.2. *The skeleton $\lambda_{0,h=0}$ consists of two closed curves which lie in the same 2-plane and have one common point 0 (a figure eight). $\lambda_{0,h>0}$ is a union of two skeleton curves which lie in 2-planes $\{y = 0\}$ and $\{x = 0\}$ on σ and connect in two points, see Figs.* C.3, C.4. *The orientation of these curves, which corresponds to the orientation introduced in Sec.* 5, *is shown in Figs.* C.2, C.3, C.4.

Proof. The entire skeleton curve $\lambda_{0,h} \subset \big(\{y = 0\} \cup \{x = 0\}\big)$ is the union of two curves $\lambda^x_{0,h} := \lambda_{0,h} \cap \{y = 0\}$ and $\lambda^y_{0,h} := \lambda_{0,h} \cap \{x = 0\}$. In the coordinates (p_1, x) on $\{y = 0\} \subset \sigma$ the skeleton curve $\lambda^x_{0,h} \subset \{y = 0\} \subset \sigma$ is defined by the equation

$$p_1^2 - \tfrac{1}{2}x^2 + (p_1^2 + \tfrac{1}{2}x^2)^2 = h. \tag{C.6}$$

By changing to variables $z := p_1^2$, $u := x^2/2$ in equation (C.6) we transform it into

$$z^2 + bz + c = 0, \quad \text{with} \quad b = 2u + 1, \quad \text{and} \quad c = u^2 - u - h. \tag{C.7}$$

Let us set $h = 0$ and analyze roots $z_{1,2}(u)$ of this equation for $u \geq 0$. We have:
i) if $u = 0$, then $b = 1, c = 0$, $z_1 = 0, z_2 = -1$;
ii) if $u \in (0, 1)$, then $b > 0, c < 0$, $z_1 > 0 > z_2$;
iii) if u=1, then $b = 3, c = 0$, $z_1 = 0$, $z_2 = -3$;
iv) if $u \in (1, +\infty)$, then $b > 0, c > 0$, there is no real non-negative roots.

It follows from Lemma C.3 that the curve $\lambda^x_{0,h}$ for $h = 0$ is smooth everywhere except points of its intersection with axis p_1, i.e., except point $p_1 = x = 0$. In a small neighborhood of this point we can take equation $p_1^2 - x^2/2 = 0$ as the leading part of (C.6). Now it follows that the curve $\lambda^x_{0,h}$ near the origin is the union of graphics of two smooth functions of the form $p_1 = p_1(x) = \pm x/\sqrt{2} + \dots$ Taking into account the fact that $z = p_1^2$ we get the form of the curve $\lambda^x_{0,h}$ for $h = 0$. More specifically, we can see that this curve has the form of a figure eight which is symmetric with respect to coordinate axes p_1 and x and is aligned along axis x. From the solution of the biquadratic equation (C.6) with respect to p_1 it follows immediately that the curve $\lambda^x_{0,h}$ for small $|h|$ is obtained from $\lambda^x_{0,0}$ by "deflation" for $h < 0$ (see Fig. C.2) or by "inflation" for $h > 0$ (see Fig. C.3).

As soon as the derivative of the left-hand side of (C.7) at small $z \neq 0$ is different from zero, the curve $\lambda^x_{0,h}$ at $h \neq 0$ is smooth everywhere, and in particular it is smooth in points of its intersection with coordinate axis p_1 on σ.

The intersection $\lambda^y_{0,h} := \lambda_{0,h} \cap \{x = 0\}$ is given by equation

$$p_1^2 + \tfrac{1}{2}y^2 + (p_1^2 + \tfrac{1}{2}y^2)^2 = h, \tag{C.8}$$

which has a solution only for $h \geq 0$. For $h = 0$ the solution is the single point $p_1 = y = 0$. The curve $\lambda^y_{0,h}$ is also symmetric with respect to both coordinate axes p_1 and y for all $h \geq 0$. It is clear that the leading part of (C.8) is the "short" equation $p_1^2 + \frac{1}{2}y^2 = 0$. Thus, the curve $\lambda^y_{0,h}$ at small $h > 0$ has the form of slightly deformed ellipse $p_1^2 + y^2/2 = h$ with axes length of order $\sqrt{h}$ when $h \to 0$. Notice that the "diameter" of the curve $\lambda^x_{0,h}$ is of the order of 1 at $h \to 0$.

For $h < 0$ the intersection $\lambda^x_{0,h}$ consists of two components shown in Fig. C.2. The orientation of these components which is also indicated in Fig. C.2 follows from the definition of the orientation given in Sec. 5.

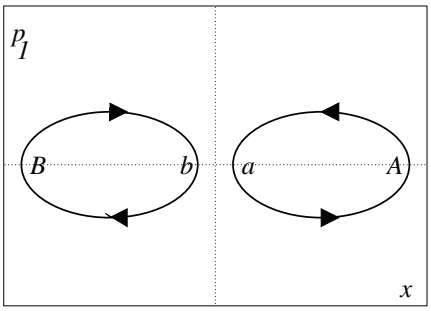

FIGURE C.2. Skeleton curves $\lambda_{0,h}$ for $h < 0$. The orientation shown by arrows is chosen for both components in accordance with the orientation of the intersection $\Lambda_{0,h} \cap \sigma$.

The two planar components of skeleton curves $\lambda_{0,h>0} \subset \sigma$ are shown in Fig. C.3. These components have two common points which lie on axis p_1. If we exclude these two points we obtain four open fragments. Orientation on each fragment is defined by the intersection $\Lambda_{0,h} \cap \sigma$. The 3D-view of the entire skeleton curve $\lambda_{0,h}$ is given in Fig. C.4. □

Let us now study intersection $\lambda_{m,h}$ with $m \neq 0$. It consists of two components lying on two sheets of the cylindrical hyperboloid $\{xy = m\}$. In the case of $m > 0$ these sheets belong to the first and third quadrants ($xy > 0$), and in the case of $m < 0$ they belong to second and forth quadrants ($xy < 0$).

The exact statement about the correspondence between $\lambda_{0,h}$ and $\lambda_{m,h}$ can be formulated as follows. Without loss of generality it is sufficient to consider the case $m \geq 0$, because the case $m \leq 0$ is absolutely similar. Using the same arguments

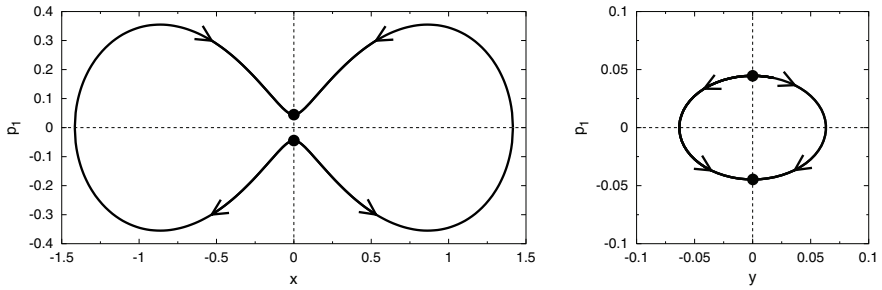

FIGURE C.3. Planar components of skeleton curves $\lambda_{0,h}$ for $h > 0$. The figure in the plane $\{x = 0\}$ is zoomed in. Black points are common for both curves. Orientation of each fragment is imposed by intersection $\Lambda_{0,h} \cap \sigma$ and is indicated by arrows.

we restrict ourselves to the case of the first "quadrant" $K^1 := \{x \geq 0, y \geq 0\} \subset \sigma$. The case of the third "quadrant" $K^3 := \{x \leq 0, y \leq 0\} \subset \sigma$ is analogous. Let us denote $s_{m,h} := \lambda_{m,h} \cap K^1$ and let $\mathcal{V}_\eta := \{x^2 + y^2 < \eta\} \subset \sigma$ be the cylinder of radius $\sqrt{\eta}$ with axis p_1 as the cylinder axis.

Lemma C.5. *There exists such $h_0 > 0$ that for all arbitrarily small $\epsilon > 0$ and $\eta > 0$ there is $\delta = \delta(h_0, \epsilon, \eta) > 0$ with the following property. For m and h such that $|h| < h_0$ and $|m| < \delta$,*

i. *Curves $s_{m,h}$ and $s_{0,h}$ are homeomorphic to each other. The curve $s_{m,h}$ for $m \neq 0$ and the curve $s_{0,h} \setminus \{x = y = 0\}$ are smooth.*
ii. *The distance between these curves does not exceed ϵ: $\rho_0(s_{m,h}, s_{0,h}) < \epsilon$. Here the distance $\rho_0(A, B)$ between subset A and subset B is defined in a standard way: $\rho_0(A, B) = \max_{\xi \in A} \rho_0(\xi, B)$, where ρ_0 is the distance induced by the coordinates (p, q) in $\mathbb{R}^4$.*
iii. *$\rho_1(s_{m,h} \setminus \mathcal{V}_\eta,\ s_{0,h} \setminus \mathcal{V}_\eta) < \epsilon$, where ρ_1 is the distance defined similarly to ρ_0, but with the C^1 norm, rather than C^0, i.e., the norm takes into account both the distance between points and between directions of lines tangent at these points to curves $s_{m,h} \setminus \mathcal{V}_\eta$, and $s_{0,h} \setminus \mathcal{V}_\eta$. In other words, curves $s_{m,h}$ and $s_{0,h}$ are almost parallel each other outside the cylinder $\mathcal{V}_\eta$.*
iv. *The mapping ϕ between the curve $s_{m,h} \setminus \mathcal{V}_\eta$ and the part of the curve $s_{0,h}$ which sends each point from $s_{m,h} \setminus \mathcal{V}_\eta$ to the nearest point of the curve $s_{0,h}$ is a diffeomorphism.*

The proof of this lemma follows from Lemma 5.1 and the analysis of equations defining skeleton curves $\lambda_{0,h}$ [see eqs. (C.6, C.7)] and is based on the implicit function theorem. The proof is standard and we omit it here.

It is clear that the orientation of each component of the intersection curves is well defined for all $\lambda_{m,h}$ except when $m = 0$, $h \geq 0$. In the latter case the orientation is well defined on each of four open fragments of the intersection line

$\lambda_{0,h}\backslash\{x=y=0\}$. In what follows we will always consider curves or their fragments with orientation defined in this way.

Curves $s_{m,h}$ belong to the first quadrant and we denote them as $s^1_{m,h}$. In a similar way we define curves $s^k_{m,h}$, lying in quadrants $k=2,3,4$. Examples of curves $s^k_{m,h}$ are shown in Fig. C.5.

Notice that a curve $\lambda_{m,h}$ with sufficiently small $|m|$ lies close to some part of the skeleton curve $\lambda_{0,h}$ with the same h and inherits the geometrical form of that part of the skeleton curve and its orientation. Let us describe the mentioned part of the skeleton curve in the more complicated case of positive h. Axis p_1 splits each planar component $\lambda^x_{0,h}$ and $\lambda^y_{0,h}$ into two symmetric parts which we take closed. The described above part of the skeleton curve $\lambda_{0,h}$ consists of two such half-curves, lying in planes $\{x=0\}$ and $\{y=0\}$ (see Fig. C.3). Note that the $x=0$ component of the skeleton curve consists of a single trajectory of the F_1 flow.

C.2.1. Curve fragments used for the construction of the deformation of cycle γ_0. We take the curve $\gamma_0 = s^1_{0,-h_{\max}}$ as a cycle $\gamma_0 \subset \Lambda_{0,h}$ corresponding to the basis element e_0 forming together with g_f the basis of homology group $H_1(\Lambda_{0,h})$ for

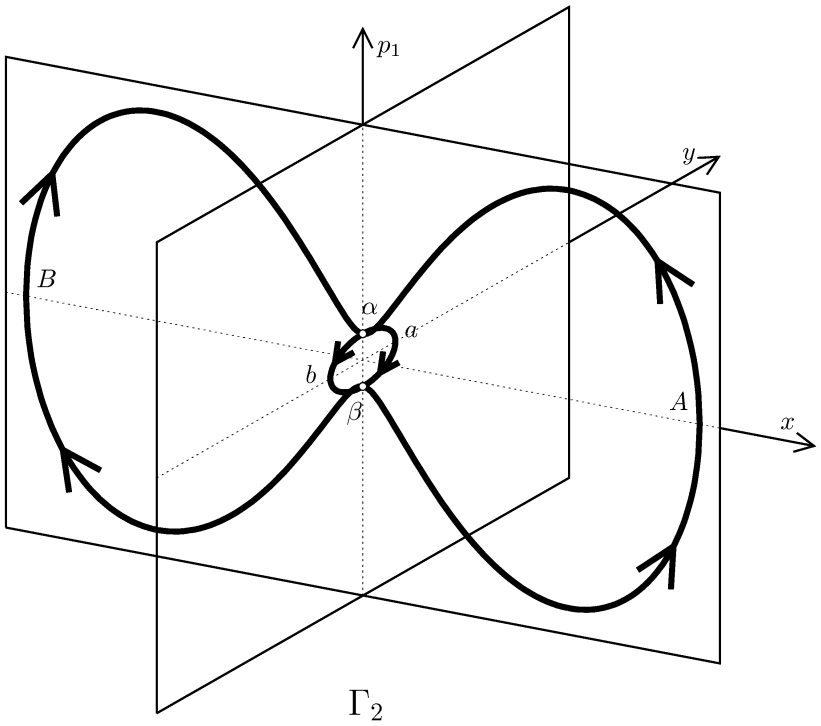

FIGURE C.4. Skeleton curves $\lambda_{0,h}$, $h>0$ in σ.

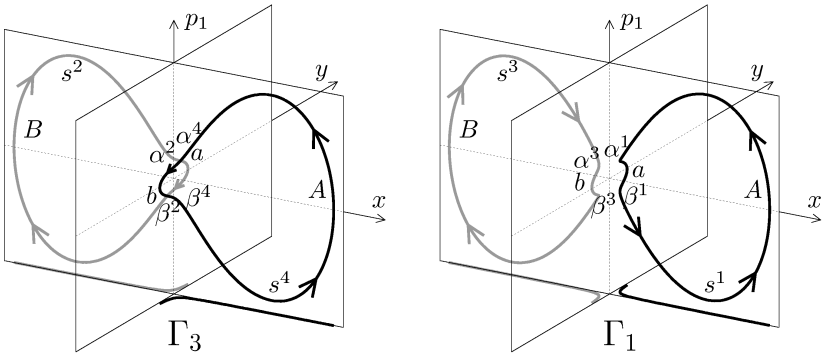

FIGURE C.5. Evolution of intersection lines of $\Lambda_{m,h} \cap \sigma$ along the contour δ_Γ on σ near the Γ_2 point. Projections of intersections on the plane (x, y) are shown at the bottom of each plot.

$h < 0$. During the deformation of this cycle we use fragments of curves $s^k_{m,h}$. In order to describe these fragments for $h > 0$ we denote points A, B and a, b corresponding to the intersection of the curve $\lambda_{0,h}$ with the plane $\{p_1 = 0\} \subset \sigma$, and points α, β of the intersection of this curve with axis p_1^σ. For the fragment of the curve $s^1_{0,h}$ connecting points A and β and passing through α and a we use the notation $s^1_{0,h}[A\alpha a\beta]$ or simply $A\alpha a\beta$. Similar notation will be used for other fragments of curves $s^k_{0,h}$. According to Lemma C.5 we can unambiguously associate points A and a of $s^1_{0,h}$ with points lying on curve $s^1_{m,h}$ for sufficiently small $m > 0$. With points α and β we associate the closest points of $s^1_{m,h}$. It is clear that these points exist, are unique, and continuously depend on the parameters (m, h). Accordingly, we will denote the fragment of the curve $s^1_{m,h}$ which is close to $s^1_{0,h}[A\alpha a\beta]$ by $s^1_{m,h}[A\alpha a\beta]$ or simply by $A\alpha^1 a\beta^1$. Notice that on the torus chart in Fig. 5 we use the similar α^1 and β^1 notation for points situated on curve $s^1_{m,h}$.

Definition of the shadow fragment $\mathcal{I}_{m,h}[\xi_1\xi_2]$**.** We will also use as fragments trajectories γ_f of the system with Hamiltonian F_1. For example, by $\gamma^f_{m,h}[A, B]$ we mean the fragment of the curve γ_f lying on torus $\Lambda_{m,h}$ and connecting points on $\Lambda_{m,h} \cap \sigma$, which correspond (in the sense of Lemma C.5) to points A and B of the skeleton curve $\lambda_{0,h}$. We take this fragment with positive orientation if it corresponds to increasing time when moving from A to B according to the phase flow $g^t_{F_1}$.

We will equally use small fragments $\mathcal{I}_{m,h}[\xi_1\xi_2]$, which belong to surfaces $\Lambda_{m,h}$. We will name them as "shadow fragments". Each such fragment belongs to small neighborhood $U \subset \mathbb{R}^4$ of a nonzero point on the axis p_1^σ and connects some points ξ_1 and ξ_2, which belong to $\Lambda_{m,h} \cap \sigma \cap U$.

From Lemma C.2 and C.3 it follows that surfaces $\Lambda_{m,h}$ in the neighborhood of each nonzero point in $\mathbb{R}^4$ regularly foliate this neighborhood into smooth two-

dimensional local surfaces. The tangent space to $\Lambda_{m,h}$ at a nonzero point κ on axis p_1^σ belongs to σ. Note that surfaces $\Lambda_{m,h}$ intersect axis p_1^σ in nonzero point only for $m = 0$ and $h > 0$.

Let ξ_1 and ξ_2 be any two points which belong to intersection $\lambda_{m,h} \cap U$ for small $|m|$ and $h > 0$, where $U = U(\kappa)$ is a small neighborhood in $\mathbb{R}^4$ of a point $\kappa \in \lambda_{0,h} \cap p_1^\sigma$. The tori $\Lambda_{m,h}$ have an affine structure defined on them by two commuting vector fields X_{F_1} and X_{F_2} which are in turn defined by the systems with Hamiltonians F_1 and F_2 respectively. It is clear that this structure depends smoothly on the position of point κ in U. Let us connect points ξ_1 and ξ_2 by a segment which is part of the geodesic on torus $\Lambda_{m,h}$ with respect to this structure. We take this segment as $\mathcal{I}_{m,h}[\xi_1\xi_2]$. From the above mentioned facts about the structure of surfaces $\Lambda_{m,h}$ near axis p_1^σ it follows that this segment is close (with respect to norm C^1) to small segment $[\xi_1\xi_2]$ in the hyperspace σ with the same ends ξ_1 and ξ_2: $\mathcal{I}_{m,h}[\xi_1\xi_2] \overset{C^1}{\sim} [\xi_1\xi_2]$.

C.2.2. Deformation of cycle γ_0 along contour Γ. We now repeat the analysis of the deformation of γ_0 along contour Γ described in Sec. 5.1 by using more detailed analytical arguments.

Deformation of cycle γ_0 along Γ in positive direction starting from the point Γ_0 consists in four steps. In the initial point $\Gamma_0 = (0, -h_{\max})$ we have $\gamma_0 = s^1_{\Gamma_0}$. At the first step we use deformation $\left\{s^1_{m,h},\ (m,h) \in [\Gamma_0, \Gamma_1]\right\}$, where $[\Gamma_0, \Gamma_1]$ is the part of contour Γ going from Γ_0 to Γ_1 in counterclockwise direction.

At the second step we replace the cycle $s^1_{\Gamma_1}$ by another curve which belongs to torus Λ_{Γ_1}, remains homotopic to $s^1_{\Gamma_1}$ but does not belong completely to σ. This new curve is constructed in the following way. Using two shadow segments the curve $s^1_{\Gamma_1}$ is transformed into the closed curve which mostly belongs to λ_{Γ_1}, but at the same time is close to curve $s^4_{\Gamma_3}$. We add to this curve the whole trajectory $\gamma_f \subset \Lambda_{\Gamma_1}$ of the system with Hamiltonian F_1. The curve γ_f will not be further transformed except for its deformation as (m, h) and hence the torus $\Lambda_{m,h}$ vary.

The third step consists of the "transfer" of the constructed curve (which is homotopic to γ_0) along the contour Γ from point Γ_1 to point Γ_3 overcoming the point Γ_2 of the non-regular intersection of $\Lambda_{m,h}$ with σ. As a result, the part of this curve which was close to $s^4_{\Gamma_3}$, becomes exactly $s^4_{\Gamma_3}$.

The fourth step is similar to the first one and consists in deformation $\left\{s^4_{m,h} \cup \gamma_f,\ (m,h) \in [\Gamma_3, \Gamma_0]\right\}$.

Let us now describe each step in more details. According to Lemma 5.1 and Lemma C.3 the singularities of the intersection of subspace σ with tori $\Lambda_{m,h}$ appear only on coordinate axis p_1^σ. But the intersection $\lambda_{m,h} = \Lambda_{m,h} \cap \sigma$ has common points with this axis only in the case $m = 0$ and $h \geq 0$. From this it follows that the first step is correct in the sense that the closed curve $s^1_{m,h}$, which belongs to torus $\Lambda_{m,h}$, depends continuously on the deformation parameter $(m, h) \in [\Gamma_0, \Gamma_1] \subset \Gamma$. The same is true for the last (fourth) step.

At the second step, the curve $s^1_{\Gamma_1}$ is replaced by the closed curve

$$r := s^1_{m,h}[A\alpha] \cup \mathcal{I}_{m,h}[\alpha^1\alpha^3] \cup s^3_{m,h}[\alpha b\beta] \cup \mathcal{I}_{m,h}[\beta^3\beta^1] \cup s^1_{m,h}[\beta A] \cup \gamma^f_{m,h}[\beta^1\beta^1],$$

which lies on the same torus Λ_{Γ_1}. Here α^1 and α^3 are, respectively, the end points of fragments $s^1_{m,h}[A\alpha]$ and $s^3_{m,h}[\alpha B\beta]$ which lie near the point $\alpha \in \lambda_{0,h}$. The points β^3 and β^1 are, respectively, the end points of fragments $s^3_{m,h}[\alpha B\beta]$ and $s^1_{m,h}[\beta A]$ which lie near the $\beta \in \lambda_{0,h}$. The curve $\gamma^f_{m,h}[\beta^1\beta^1] = \beta^1(-\gamma_f)\beta^1$ is a complete trajectory of the system with Hamiltonian F_1 passing through the point β_1. Its orientation is opposite to the flow of X_{F_1}.

It is easy to see that the curve r can be obtained from $s^1_{\Gamma_1}$ by cutting $s^1_{\Gamma_1}$ at point β_1 and by incorporating the closed curve

$$r_0 := s^1_{m,h}[\beta a\alpha] \cup \mathcal{I}_{m,h}[\alpha^1\alpha^3] \cup s^3_{m,h}[\alpha b\beta] \cup \mathcal{I}_{m,h}[\beta^3\beta^1] \cup \gamma^f_{m,h}[\beta^1\beta^1]$$

which results in

$$r = s^1_{m,h}[A\alpha] \cup s^1_{m,h}[\alpha a\beta] \cup r_0 \cup s^1_{m,h}[\beta A].$$

Consequently, in order to prove that $s^1_{m,h}$ and r are homotopic it is sufficient to prove that the closed curve r_0 is homotopic to a point on the covering of the torus $\Lambda_{m,h}$ with $(m,h) = \Gamma_1$. Since $\Gamma_1 = (m_{\max}, h_{\max})$ and $m_{\max} \ll h_{\max}$, this curve belongs to a small neighborhood of the trajectory $\gamma_f[\beta\beta] \subset \lambda_{0,h} = \Lambda_{0,h} \cap \sigma$. It follows that by shifting points of the curve r_0 along the trajectories of the system with Hamiltonian F_1, this curve can be transformed homotopically so that it lies entirely in a small neighborhood of the point $\beta \in \lambda_{0,h}$, where $h = h_{\max} > 0$. From this and Lemma 5.1 it follows that the transformed curve and consequently r_0 are homotopic to a point.

The third step consists in deformation $\{r_{m,h},\ (m,h) \in [\Gamma_1, \Gamma_3]\}$ of the curve $r = r_{\Gamma_1}$. This deformation is realized as follows. For all six fragments forming r only the lower index (m,h) varies. In addition, when passing through $m = 0$ the upper index changes from 1 and 3 to 4, so that s^1, s^3, α^1, α^3, β^1, β^3 are transformed into s^4, s^4, α^4, α^4, β^4, β^4. Using Lemma C.5 we obtain the continuity of this transformation. It is clear that fragments $\mathcal{I}_{m,h}[\alpha^4\alpha^4]$ and $\mathcal{I}_{m,h}[\beta^4\beta^4]$ are points. Consequently the curve obtained after such a deformation becomes

$$s^4_{m,h}[A\alpha] \cup s^4_{m,h}[\alpha b\beta] \cup s^4_{m,h}[\beta A] \cup \gamma^f_{m,h}[\beta^4\beta^4],$$

where $\gamma^f_{m,h}[\beta^4\beta^4] = \beta^4(-\gamma_f)\beta^4$, and it coincides with $s^4_{m,h} \cup (-\gamma_f)$. This concludes the description of the third step. The fourth step was described earlier together with the first step.

In this way, the continuous deformation of closed curves γ_f and γ_0 which lie on tori $\Lambda_{m,h}$, with $(m,h) \in \Gamma$ going along contour Γ is constructed. As a result of this deformation, curves γ_f and γ_0 are transformed into γ_f and $\gamma_0 - \gamma_f$, respectively:

$$(\gamma_f, \gamma_0) \mapsto (\gamma_f, \gamma_0 - \gamma_f). \tag{C.9}$$

It is easy to see that the mapping (C.9) can be linearly extended to the whole lattice $H_1(\Lambda_{\Gamma_0})$ and the resulting map is represented by matrix (4.2). This concludes the analytical proof of the Theorem 1.

Appendix D. Proofs in the case $m_1 = 1$, $m_2 = 2$

We begin this section with analytical proofs of some auxiliary statements used in the proof of the monodromy theorem in the 1:(−2) case. In particular, we prove Lemma 5.2 formulated in Sec. 5.2.

Subsequently, we represent the intersections $\lambda_{m,h} = \Lambda_{m,h} \cap \sigma$ for $(m,h) \in \Gamma$ directly in the hyperspace σ and prove Lemma D.9, which establishes the exact correspondence between the representation of $\lambda_{0,h}$ in σ and that on the torus chart $\Lambda_{0,h} \to \mathbb{R}^2/\mathbb{Z}^2$ in Sec. 5.2.

Further in Sec. D.2.2, we use this correspondence in order to reproduce in σ the homotopy transformation of cycles $\gamma_{m,h}$ constructed earlier on the torus charts and the diffeomorphism which occurs near the $m = 0$ fibers between deformed cycles as described in Lemma D.8. This completes the proof of the monodromy theorem in the case of the 1:(−2) resonance.

D.1. Technical lemmas. Case of the 1:(−2) resonance

Some technical statements in the 1:(−2) case are quite similar to those in the $m_1 = m_2 = 1$ case. At the same time, in this case we need to characterize the phase flow in more detail. We do that in Lemmas D.2, D.3, D.4.

Lemma D.1. *The phase flow $\{g^t_{F_1},\ t \in \mathbb{R}\}$ of the system with Hamiltonian F_1 in* (4.3a) *is given in coordinates (p,q) in $\mathbb{R}^4$ by a block-diagonal matrix whose two blocks are given by equation* (C.1) *with $\omega_1 = 1$ and $\omega_2 = 2$. The action of this phase flow is equivalent to the action of a circle $\mathbb{S}^1$. All trajectories γ_f of this flow are passed in time $t = 2\pi$, except trajectories lying on the plane $\{p_1 = q_1 = 0\}$, which are passed in time $t = \pi$ and except the point $0 \in \mathbb{R}^4$ which is the only fixed point of the flow. Trajectories γ_f intersect transversally the section σ defined as $\sigma := \{p_1 - \sqrt{2}q_2 = 0\}$ everywhere except points of two-dimensional plane $\{p_1 - \sqrt{2}q_2 = q_1 - 2\sqrt{2}p_2 = 0\}$. In all points of this plane trajectories γ_f are tangent to hyperspace σ but they are not tangent to the plane itself except at the line $\{p_1 = q_2 = q_1 - 2\sqrt{2}p_2 = 0\}$. In all points of this line trajectories are not tangent to the line itself except at the point $\gamma_f = \{0\}$, which is the only trajectory of the system with Hamiltonian F_1 which lies completely in σ.*

Proof. Let us denote by $X_{F_1} = (-q_1, p_1, 2q_2, -2p_2)$ the vector field generated by the system with Hamiltonian F_1. This vector field is tangent to γ_f. The condition on X_{F_1} to be tangent to σ has the form $dF_3(X_{F_1}) = 0$, $F_3 = 0$, where $F_3 = p_1 - \sqrt{2}q_2$. Former condition can be rewritten as $q_1 - 2\sqrt{2}p_2 = 0$. If now $\zeta := \{p_1 - \sqrt{2}q_2 = q_1 - 2\sqrt{2}p_2 = 0\}$, we have $X_{F_1}|_\zeta = \left(-2\sqrt{2}p_2, p_1, \sqrt{2}p_1, -2p_2\right)$ and consequently $\left(d(q_1 - 2\sqrt{2}p_2)\right)(X_{F_1}) = -3p_1$ on ζ, where $X_{F_1}|_\zeta$ is the restriction of

the field X_{F_1} on ζ. This means that trajectories γ_f intersect plane ζ transversally everywhere except at the line $l : \{p_1 = q_2 = q_1 - 2\sqrt{2}p_2 = 0\}$. Finally, at points of this line the vector field $X_{F_1}|_l = (-2\sqrt{2}p_2, 0, 0, -2p_2)$ is not tangent to the line except at $p_2 = 0$, which corresponds to the only trajectory $\gamma_f = \{0\}$ of the system with Hamiltonian F_1 which completely lies in σ. This concludes the proof of the lemma. □

The next three lemmas give a more detailed description of the vector field X_{F_1} in $\mathbb{R}^4$ and the phase flow of system with Hamiltonian F_1.

Lemma D.2. *Each orbit γ_f of the vector field X_{F_1} in $\mathbb{R}^4$ except point $0 \in \mathbb{R}^4$ is a closed curve which intersects $\sigma \subset \mathbb{R}^4$ in no more than four points.*

Proof. The system of the differential equations with Hamiltonian F_1 is linear and its general solution has the form:

$$p_1 = -c_1 \sin t + c_2 \cos t, \tag{D.1}$$

$$q_1 = c_1 \cos t + c_2 \sin t, \tag{D.2}$$

$$p_2 = c_3 \sin 2t + c_4 \cos 2t, \tag{D.3}$$

$$q_2 = c_3 \cos 2t - c_4 \sin 2t. \tag{D.4}$$

Consider function $\psi_c(t) = p_1(t) - \sqrt{2}q_2(t)$. For any values of constants c_1, c_2, c_3, and c_4, this function is a trigonometric polynomial of the second order. It is known that such polynomial either has no more than four roots or is equal identically to zero. In our case the last possibility means that the whole trajectory belongs to σ. According to Lemma D.1 this can happen only if the trajectory coincides with the point 0. Lemma is proven. □

Restriction of coordinate functions p_1, q_1, p_2 on σ defines the coordinates on σ which we denote by the same letters. For further use, it is convenient to replace coordinates q_1 and p_2 for x and y:

$$x = (q_1 - \sqrt{2}p_2)/\sqrt{2}, \quad y = (q_1 + \sqrt{2}p_2)/\sqrt{2}. \tag{D.5}$$

Lemma D.3. *The orbit of the point O [given on σ in coordinates $(x, y, p_1) = (\mu, 0, 0)$] generated by action of the phase flow of the system with Hamiltonian F_1 intersects hyperplane σ in exactly 4 points for any $\mu \neq 0$. In coordinates (x, y, p_1) these points are*

$$(\mu, 0, 0), \quad (-\mu/2, 0, -\mu\sqrt{3}/2\sqrt{2}), \quad (0, -\mu, 0), \quad (-\mu/2, 0, \mu\sqrt{3}/2\sqrt{2}).$$

As t increases, these points are passed by the flow $g^t_{F_1}$ in the order they are listed.

Proof. In $\mathbb{R}^4$ the coordinates (p_1, q_1, p_2, q_2) of point O are $(0, \mu/\sqrt{2}, -\mu/2, 0)$. Constants c_i in expressions (D.1)–(D.4) corresponding at $t = 0$ to the initial condition at this point are $c_1 = \mu/\sqrt{2}$; $c_2 = c_3 = 0$; $c_4 = -\mu/2$. Function $\psi_c(t) = p_1(t) - \sqrt{2}q_2(t)$ at these values of constants c_i has the form $\psi_c(t) = -(\mu/\sqrt{2})(\sin t + \sin 2t)$. Zero values of $\psi_c(t)$ correspond to points of intersection of σ by trajectory $(p(t), q(t))$ defined in (D.1)–(D.4). For the constructed trajectories

(with $\mu \neq 0$) function $\psi_c(t)$ equals zero in four points $t = 0, 2\pi/3, \pi, 4\pi/3$. In coordinates (p, q) these points have, respectively, the form

$$\left(0, \tfrac{\mu}{\sqrt{2}}, -\tfrac{\mu}{2}, 0\right), \quad \left(-\tfrac{\mu\sqrt{3}}{2\sqrt{2}}, -\tfrac{\mu}{2\sqrt{2}}, \tfrac{\mu}{4}, -\tfrac{\mu\sqrt{3}}{4}\right),$$
$$\left(0, -\tfrac{\mu}{\sqrt{2}}, -\tfrac{\mu}{2}, 0\right), \quad \left(\tfrac{\mu\sqrt{3}}{2\sqrt{2}}, -\tfrac{\mu}{2\sqrt{2}}, \tfrac{\mu}{4}, \tfrac{\mu\sqrt{3}}{4}\right).$$

Rewriting these points in terms of the coordinates (x, y, p_1) on σ we obtain the statement of the lemma. □

Lemma D.4. *Curves $\lambda_{m,h} := \Lambda_{m,h} \cap \sigma$ outside singular points of torus $\Lambda_{m,h}$ and singular points of intersection of $\Lambda_{m,h}$ with σ are tangent to trajectories of the field X_{F_1} in points of the plane $\{q_1 = 2\sqrt{2}p_2\}$ given in coordinates (p_1, q_1, p_2) and only in these points.*

Vector field X_{F_1} is tangent to σ on the coordinate axis p_1^σ on σ. On this axis we have

$$\dot{p}_1 = 0, \quad \dot{q}_1 = p_1, \quad \dot{p}_2 = \sqrt{2}p_1, \quad \dot{q}_2 = 0. \tag{D.6}$$

Here p_1 is a natural parameter on axis p_1^σ. Projections (parallel to the axis p_1^σ) of the vectors X_{F_1} on the plane $p_1^\sigma = 0$ in coordinates (x, y) are parallel to vector $(-1, 3)$. For some $p_1 > 0$ this vector is shown in Fig. D.1. *At $p_1 < 0$ its direction is opposite to that for $p_1 > 0$.*

Under the above described projection map the plane $\{q_1 = 2\sqrt{2}p_2\}$ projects on the line $\{y - 3x = 0\}$.

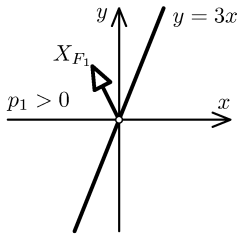

FIGURE D.1. Projection of vectors $X_{F_1}(\xi)$ on the plane $p_1^\sigma = 0$. Points ξ lie on axis p_1^σ which belongs to the plane $\{q_1 = 2\sqrt{2}p_2\} \subset \sigma$ where curves $\lambda_{m,h}$ are tangent to trajectories of the vector field X_{F_1}.

Proof. Except at the points mentioned in the statement of the lemma, curves $\lambda_{m,h}$ are smooth. Let ξ be a non-exceptional (in the same sense as mentioned above) point on σ at which the vector field X_{F_1} is tangent to the curve $\lambda_{m,h}$. Then $X_{F_1}(\xi)$ is tangent to σ as well. According to Lemma D.1, all points where vector field X_{F_1} is tangent to σ belong to the plane $\{q_1 = 2\sqrt{2}p_2\}$. Hence, ξ belongs to that plane. Inversely, if point ξ is non-exceptional and belongs to that plane, the vector $X_{F_1}(\xi)$ is tangent to $\Lambda_{m,h}$ and, according to Lemma D.1, is tangent to σ. Consequently, this vector is tangent to $\lambda_{m,h} = \Lambda_{m,h} \cap \sigma$. The form (D.6) of vectors

X_{F_1} at points of axis p_1^σ follows from the equations of motion for Hamiltonian $F_1 = (p_1^2 + q_1^2)/2 - p_2^2 - q_2^2$. The form of the projection of this vector on the plane $\{q_1 = 2\sqrt{2}p_2\}$ follows from the coordinate transformation $(q_1, p_2) \to (x, y)$ in (D.5). □

Lemma D.5. *Restrictions of the coordinate functions p_1, q_1, p_2 on σ define the coordinates on σ which we denote by the same letters. In these coordinates the restrictions $\mathcal{F}_i := F_i\big|_\sigma$ of functions F_i, $(i = 1, 2)$, on σ have the form*

$$\mathcal{F}_1 = \tfrac{1}{2}(q_1^2 - 2p_2^2), \quad \mathcal{F}_2 = \sqrt{2}p_1^2 q_1 + q_1^2 p_2 - p_1^2 p_2 + \tfrac{1}{4}(2p_1^2 + q_1^2 + 2p_2^2)^2. \quad \text{(D.7)}$$

In coordinates (x, y, p_1) defined by equation (D.5) *functions $\mathcal{F}_1$ and $\mathcal{F}_2$ take the form*

$$\mathcal{F}_1 = xy, \quad \mathcal{F}_2 = \tfrac{1}{2}p_1^2(y + 3x) + \tfrac{1}{4}(y - x)(x + y)^2 + \tfrac{1}{4}(2p_1^2 + y^2 + x^2)^2. \quad \text{(D.8)}$$

Proof. The statement is evident. □

Lemma D.6. *Consider $U_\epsilon := \cup_{|m|+|h|<\epsilon}\Lambda_{m,h} \in \mathbb{R}^4$ and its intersection $U_\epsilon \cap \sigma$ with σ. For sufficiently small $\epsilon > 0$ condition*

$$\operatorname{rank} \frac{\partial(F_1, F_2)}{\partial(p, q)} \le 1$$

on the Jacobian matrix of the map F is satisfied on $U_\epsilon \cap \sigma$ at all points of the coordinate axis $p_2^\sigma := \{p_1 = \sqrt{2}q_2 = p_1 = q_1 = 0\}$ on σ and only at those points. The value (m, h) of F on p_2^σ equals $(-p_2^2, p_2^4)$, i.e., $h = m^2$ while $m \le 0$. Furthermore, for sufficiently small $\epsilon > 0$ condition

$$\operatorname{rank} \frac{\partial(F_1, F_2, F_3)}{\partial(p, q)} \le 2$$

on the "extended" Jacobian matrix where $F_3 := p_1 - \sqrt{2}q_2$ is satisfied on $U_\epsilon \cap \sigma$ at all points of the straight lines

$$p_2^\sigma = \{p_1 = q_1 = q_2 = 0\}, \quad p_1^\sigma = \{q_1 = p_2 = p_1 - \sqrt{2}q_2 = 0\},$$

and of the curve θ defined in the following parametric form:

$$\big\{p_1 = \pm\sqrt{-\tfrac{1}{2}p_2(3 + 10p_2)}, \quad q_1 = 2\sqrt{2}p_2, \quad q_2 = p_1/\sqrt{2}, \quad -\tfrac{3}{10} \le p_2 \le 0\big\}.$$

The image of p_1^σ under F is $\{m = 0, h = p_1^4\}$; the image of θ is $\big\{m = 3p_2^2, h = -\frac{1}{4}p_2^2(9 + 28p_2)\big\}$, i.e., $\{h = -\frac{3}{4}m + \frac{7}{9}\sqrt{3}m^{3/2}, m \ge 0\}$.

Proof. To prove Lemma D.6 we should analyze the Jacobian matrix

$$M_3 := \begin{pmatrix} p_1 & q_1 & -2p_2 & -2q_2 \\ 2q_1q_2 - 2p_1p_2 + p_1\chi & 2q_2p_1 + 2q_1p_2 + q_1\chi & q_1^2 - p_1^2 + 2p_2\chi & 2q_1p_1 + 2q_2\chi \\ 1 & 0 & 0 & -\sqrt{2} \end{pmatrix}$$

where

$$\chi = (p_1^2 + q_1^2 + 2p_2^2 + 2q_2^2).$$

We begin with the statement for the "shortened" 2×4 matrix

$$M_2 := \begin{pmatrix} p_1 & q_1 & -2p_2 & -2q_2 \\ 2q_1q_2 - 2p_1p_2 + p_1\chi & 2q_2p_1 + 2q_1p_2 + q_1\chi & q_1^2 - p_1^2 + 2p_2\chi & 2q_1p_1 + 2q_2\chi \end{pmatrix},$$

which is obtained from M_3 by omitting its bottom row. If $p_1 = q_1 = q_2 = 0$, we have $\operatorname{rank} M_2 = 1$ in all points except $0 \in \mathbb{R}^4$, where $\operatorname{rank} M_2 = 0$. Thus on the coordinate axis $p_2^\sigma \subset \sigma$, which coincides with the coordinate axis p_2 in $\mathbb{R}^4_{p,q}$, the rank of M_2 is not maximal. Substituting $p_1 = q_1 = q_2 = 0$, we find the set of critical values

$$\{F_1(p_1^\sigma), F_2(p_2^\sigma)\} = \{m = -p_2^2, h = p_2^4\} = \{h = m^2, m \le 0\} \tag{D.9}$$

of map $F = (F_1, F_2)$.

Let us now show that $\operatorname{rank} M_2 = 2$ (maximal) at all other points in U_ϵ. First we prove the absence of critical points in the neighborhood of $0 \in \sigma \subset \mathbb{R}^4$ in σ. If $\operatorname{rank} M_2$ is not maximal, all 2-minors should be zero. Let us consider the three minors which include the second column. This gives the system of equations

$$q_2(2q_2^2 + 2\sqrt{2}q_1p_2 - q_1^2) = 0, \tag{D.10a}$$

$$q_1^3 - 2q_1q_2^2 + 4\sqrt{2}p_2q_2^2 + 4q_1p_2^2 + 4q_1p_2\chi = 0, \tag{D.10b}$$

$$q_2^2(\sqrt{2}q_1 - p_2 + \chi) = 0, \tag{D.10c}$$

$$p_1 - \sqrt{2}q_2 = 0, \tag{D.10d}$$

where $\chi = (q_1^2 + 2p_2^2 + 4q_2^2)$. Notice that (D.10d) defines σ and is added because the rank condition is studied at points on σ and (D.10d) should be taken into account when solving the three initial equations. Equation (D.10d) was used to obtain (D.10a)–(D.10c).

When $q_2 = 0$ equation (D.10b) becomes

$$q_1(q_1^2 + 4p_2^2 + p_2(q_1^2 + 2p_2^2)) = 0.$$

It follows from this equation that $q_1 = 0$ for small $|(p, q)|$. Consequently, $p_1 = q_1 = q_2 = 0$ and this system specifies axis p_2^σ. If $q_2 \neq 0$, then we get from (D.10a) and (D.10c)

$$2q_2^2 + 3q_1^2 + 2\sqrt{2}q_1\chi = 0,$$

and for $|(p, q)| \ll 1$, it follows again that $q_1 = q_2 = 0$, and consequently $p_1 = 0$.

Let us now show that $\operatorname{rank} M_2 = 2$ at all points from $U_\epsilon \cap \sigma$ outside a small neighborhood of axis p_1^σ and except points of axis p_2^σ. From (D.9) it follows that the intersection $U_\epsilon \cap \sigma$ with a small neighborhood of axis p_1^σ is a small neighborhood of $0 \in \sigma$. Consequently, this region is complementary in $U_\epsilon \cap \sigma$ to a small neighborhood of $0 \in \mathbb{R}^3$, and therefore the entire region $U_\epsilon \cap \sigma$ is studied.

From the explicit form $\mathcal{F}_1 = (q_1^2 - 2p_2^2)/2$ of function $\mathcal{F} = F_1|_\sigma$ for sufficiently small $\epsilon > 0$ we obtain the following. Outside a small fixed neighborhood of axis p_1^σ in σ, intersections $\Lambda_{m,h} \cap \sigma$ for $|m| + |h| < \epsilon$ belong to arbitrarily small neighborhood

of planes $\{q_1 - \sqrt{2}p_2 = 0\}$ and $\{q_1 + \sqrt{2} = 0\}$. Thus, it is sufficient to find the rank of matrix M_2 in $U_\epsilon \cap \sigma$ exactly on these two planes.

Let us replace (D.10c) from the system (D.10) for $q_1^2 - 2p_2^2 = 0$ and $F_2(p,q) = h$. Taking into account that $q_1 = \pm\sqrt{2}p_2$ we obtain the system with parameter h

$$q_2(2q_2^2 + (-2 \pm 4)p_2^2) = 0, \tag{D.11a}$$

$$p_2[\pm 3p_2^2 + (2 \mp 1)q_2^2 \pm 8p_2(p_2^2 + q_2^2)] = 0, \tag{D.11b}$$

$$p_1 - \sqrt{2}q_2 = 0, \tag{D.11c}$$

$$q_1 = \pm\sqrt{2}p_2, \tag{D.11d}$$

$$\pm 4p_2q_2^2 + 2p_2^3 - 2p_2q_2^2 + 4(p_2^2 + q_2^2)^2 = h, \tag{D.11e}$$

where $|h| < \mu$ and $\mu > 0$ can be taken arbitrary small.

Equation (D.11a) has three solutions:

Case $q_2 = 0$**.** In this case, (D.11b) has the form $p_2^3(3 + 8p_2) = 0$ with solutions $p_2 = 0$, and $p_2 = -\frac{3}{8}$. At the same time eq. (D.11e) for $q_2 = 0$ becomes $2p_2^3(1 + 2p_2) = h$ and consequently, $p_2 \approx (h/2)^{1/3}$ or $p_2 \approx -\frac{1}{2}$. Therefore $p_2 = 0$ and $h = 0$, and the only solution of system (D.11) in this case is $0 \in \mathbb{R}^4$.

Case $q_2 = p_2 = 0$**.** This case reduces to the previous case $q_2 = 0$.

Case $q_1 = -\sqrt{2}p_2, q_2 = \pm\sqrt{3}p_2$**.** In this case (D.11b) and (D.11e) become

$$p_2^3(6 - 32p_2) = 0, \quad -16p_2^3 + 64p_2^4 = h.$$

The first of these equations has roots $p_2 = 0$ and $p_2 = \frac{3}{16}$, while the second gives $p_2 \approx (-h/16)^{1/3}$ and $p_2 \approx \frac{1}{4}$. Thus the only solution of the whole system (D.11) for sufficiently small h is $0 \in \mathbb{R}^4$ where $h = 0$.

The statement of Lemma D.6 about the subset in $U_\epsilon \cap \sigma$ associated with the non-maximal rank of matrix M_2 is completely proven.

Let us now turn to the study of the condition $\operatorname{rank} M_3 \le 2$. Adding to the last column of M_3 its first column multiplied by $\sqrt{2}$ and eliminating the first column and the last row, we get the 2×3 matrix

$$M_2^r = \begin{pmatrix} q_1 & -2p_2 & \sqrt{2}p_1 - 2q_2 \\ 2q_2p_1 + 2q_1p_2 + q_1\chi & q_1^2 - p_1^2 + 2p_2\chi & X \end{pmatrix}, \tag{D.12}$$

$$X = 2q_1p_1 + 2\sqrt{2}q_1q_2 - 2\sqrt{2}p_1p_2 + 2q_2\chi + \sqrt{2}p_1\chi,$$

$$\chi = p_1^2 + q_1^2 + 2p_2^2 + 2q_2^2.$$

Since the rank of M_2^r is smaller than the rank of M_3 exactly by one, we should check the condition

$$\operatorname{rank} M_2^r \le 1$$

to be satisfied on $\sigma = \{p_1 - \sqrt{2}q_2 = 0\}$. Taking into account that the upper right element of M_2^r on σ is zero, we get the system of three equations (three minors of

M_2^r should be zero).

$$q_1 p_1(\sqrt{2}q_1 - p_2 + 2p_1^2 + q_1^2 + 2p_2^2) = 0, \tag{D.13a}$$

$$p_1 p_2(\sqrt{2}q_1 - p_2 + 2p_1^2 + q_1^2 + 2p_2^2) = 0, \tag{D.13b}$$

$$q_1^3 - q_1 p_1^2 + 2\sqrt{2}p_2 p_1^2 + 4q_1 p_2^2 + 8q_1 p_2 p_1^2 + 4p_2 q_1^3 + 8q_1 p_2^3 = 0. \tag{D.13c}$$

The first equation (D.13a) is satisfied if: (i) $p_1 = 0$, or (ii) $q_1 = 0$, or (iii) $p_1^2 = (p_2 - \sqrt{2}q_1 - q_1^2 - 2p_2^2)/2$. Let us analyze these cases consecutively.

Solution $p_1 = 0$**.** In this case the system (D.13) on σ reduces to the single equation $q_1(q_1^2 + 4p_2 q_1^2 + 8p_2^3 + 4p_2^2) = 0$. It has one obvious solution $\{q_1 = p_1 = q_2 = 0\}$ on σ which corresponds to axis p_2^σ and to critical points of the map F. Another solution is $q_1^2 = -4p_2^2(2p_2 + 1)/(1 + 4p_2)$. Since $q_1^2 \geq 0$, this solution is meaningful only for $-1/2 \leq p_2 \leq -1/4$. This solution does not belong to $U_\epsilon \cap \sigma$. In fact, the image of the map F for this solution is given as

$$F_1 = -\frac{p_2^2(3 + 8p_2)}{1 + 4p_2}, \quad F_2 = -\frac{p_2^3(23p_2 + 32p_2^2 + 4)}{(1 + 4p_2)^2}.$$

It corresponds to the part of the boundary of the range of map F.

Solution $q_1 = 0$**.** In this case equations (D.13b) and (D.13c) become

$$p_1 p_2(2p_1^2 - p_2 + 2p_2^2) = 0, \quad p_1^2 p_2 = 0.$$

They have two solutions. One $\{q_1 = p_1 = q_2 = 0\}$ has been already found in the previous case. The other solution $q_1 = p_2 = p_1 - \sqrt{2}q_2 = 0$ satisfies the system (D.13) and defines axis p_1^σ. The value of the map F at points on p_1^σ is $\{m = 0, h = p_1^4\}$, i.e., $\{m = 0, h \geq 0\}$.

Solution $p_1^2 = \frac{1}{2}(p_2 - \sqrt{2}q_1 - q_1^2 - 2p_2^2)$**.** In this case eqns. (D.13a) and (D.13b) are satisfied and eq. (D.13c) becomes

$$(-3q_1^2 - \sqrt{2}q_1 + 4\sqrt{2}p_2 q_1 - 2p_2^2 + p_2)(-q_1 + 2\sqrt{2}p_2) = 0$$

and leads to two possible solutions of the whole system (D.13). One is

$$\{q_1 = 2\sqrt{2}p_2,\ p_1 = \pm(-p_2(3 + 10p_2)/2)^{1/2},\ q_2 = p_1/\sqrt{2}\},$$

where $-3/10 \leq p_2 \leq 0$ because $p_1^2 \geq 0$. The values of F for this solution are

$$m = 3p_2^2; \quad h = -\frac{p_2^2}{4}(9 + 28p_2), \quad -3/10 \leq p_2 \leq 0.$$

We can rewrite this solution in terms of relation between the values m and h of the map F:

$$h = -\frac{m}{12}\left(9 - 28\sqrt{m/3}\right), \quad 0 \leq m \leq 27/100.$$

Another solution corresponds to the system of equations

$$p_1^2 = (p_2 - \sqrt{2}q_1 - q_1^2 - 2p_2^2)/2, \tag{D.14a}$$

$$-3q_1^2 - \sqrt{2}q_1 + 4\sqrt{2}p_2 q_1 - 2p_2^2 + p_2 = 0. \tag{D.14b}$$

Using (D.14b) we can simplify (D.14a) and the system becomes

$$p_1^2 = q_1(q_1 - 2\sqrt{2}p_2), \tag{D.15a}$$

$$-3q_1^2 - \sqrt{2}q_1 + 4\sqrt{2}p_2q_1 - 2p_2^2 + p_2 = 0. \tag{D.15b}$$

As soon as $p_1^2 \geq 0$ the solutions are meaningful only if they belong to a part of the $\{q_1, p_2\}$ plane given by inequalities

$$\{q_1 \geq 0, \quad q_1 \geq 2\sqrt{2}p_2\}, \quad \{q_1 \leq 0, \quad q_1 \leq 2\sqrt{2}p_2\}. \tag{D.16}$$

Thus we should solve (D.15b) and retain only those solutions which belong to the region (D.16) specified above. These solutions consist of one isolated point $(0,0) \in \mathbb{R}^4$ and of a line which is outside of U_ϵ.

The $\mathbb{R}^2_{m,h}$ plane image of all critical points of the map $\{F_1, F_2\}$ and of points, where the intersection of σ with regular tori is non-regular (i.e., critical points of the $\{F_1, F_2, F_3\}$ map) is shown in Fig. D.2. In fact, it follows from the implicit function theorem, that eq. (D.14b) defines in some neighborhood Θ of point $q_1 = p_2 = 0$ a smooth curve which is tangent to the line $\{q_1 = p_2/\sqrt{2}\}$ at that point. Thus, the system (D.14) has no such solutions (p_1, q_1, p_2) that $(q_1, p_2) \in \Theta$. Otherwise, we have proved that for sufficiently small ϵ U_ϵ belongs to a small neighborhood of the union of two planes $\{q_1 = \sqrt{2}p_2\}$ and $\{q_1 = -\sqrt{2}p_2\}$ in σ. Both corresponding lines in the (q_1, p_2) plane intersect sector (D.16) in the zero point $(q_1, p_2) = 0$ only.

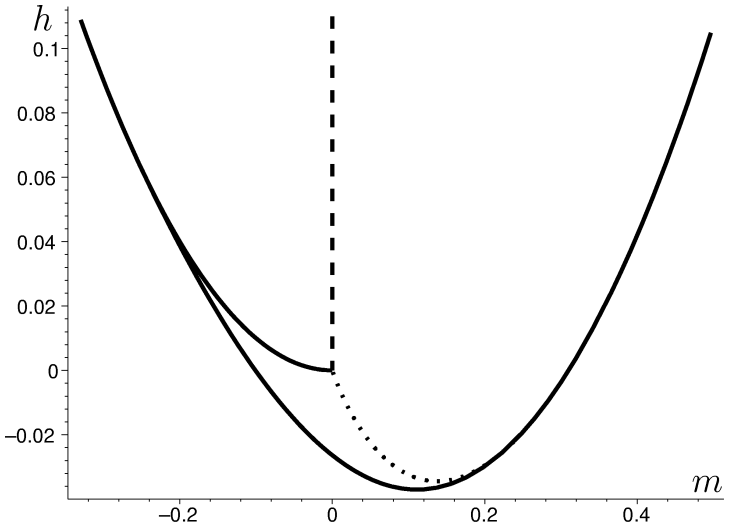

FIGURE D.2. Image of the critical points of the $\{F_1, F_2, F_3\}$ map in the plane of the (m, h) values. Solid lines represent critical values of the $\{F_1, F_2\}$ map; dotted and dashed lines correspond to non-regular intersections of regular tori with σ.

Thus, if $(q_1, p_2) \notin \Theta$, the system (D.14) does not have the solutions $(p_1, q_1, p_2) \in U_\epsilon$ which are of interest to us. Thus, Lemma D.6 is completely proven. □

We can now prove Lemma 5.2 formulated in Sec. 5.2 of the main text.

Proof. Points where surfaces $\Lambda_{m.h}$ are not smooth correspond to points where the Jacobian matrix $\frac{\partial(F_1,F_2)}{\partial(p,q)}$ has non-maximal rank. All points where surfaces $\Lambda_{m,h}$ intersect the hyperplane $\sigma = \{p_1 - \sqrt{2}q_2 = 0\}$ non-transversally correspond to points where the rank of the Jacobian matrix $\frac{\partial(F_1,F_2,F_3)}{\partial(p,q)}$, with $F_3 = p_1 - \sqrt{2}q_2$ is not maximal. All such points for sufficiently small $|m|$ and $|h|$ are described in Lemma D.6.

In order to verify that the plane tangent to surface $\Lambda_{m,h}$ at any point χ on p_1^σ and on θ (with exception of $0 \in \mathbb{R}^4$) belongs to hyperplane σ, we only need to verify that both conditions

$$\{dF_3(X_{F_1}) = 0, \quad dF_3(X_{F_2}) = 0\}$$

take place at any point lying on p_1^σ and on θ in U_ϵ except for $0 \in \mathbb{R}^4$.

This proves Lemma 5.2. □

D.2. Analysis of the intersection $\Lambda_{m,h} \cap \sigma$. Case $m_1 = 1, m_2 = 2$.

Let us now describe the intersection $\Lambda_{m,h} \cap \sigma$ in the case of the 1:(−2) resonance. Restriction on $\sigma = \{p_1 - \sqrt{2}q_2 = 0\}$ enables one to reduce the number of variables to three. The remaining variables are p_1, q_1, p_2, which we change for convenience (see Lemma D.5) to x, y, p_1. In what follows below we will describe the behavior of the intersection line $\lambda_{m,h} := \Lambda_{m,h} \cap \sigma$ in σ using these coordinates x, y, p_1.

Figure D.2 shows the image of the energy momentum map $F = (F_1, F_2)$ together with the curves of critical values. The same figure shows projections of critical points of the (F_1, F_2, F_3) map on the plane (F_1, F_2). Near $0 \in \mathbb{R}^2$ this projection consists of three curves (disregarding the boundary), one of which is the line of critical values of the map $F = (F_1, F_2)$. These three curves split the domain of allowed values into three regions. We need to study all these 2D and 1D strata, but the most important again is to study the $m = 0$ case because it in some sense "organizes" the behavior of $\lambda_{m,h}$ for small positive and negative m.

So we start again with the $m = 0$ case. The analysis of eqs. (D.8) defining curves $\lambda_{0,h}$ is more complicated in the 1:(−2) case than in the case 1:(−1). It enables us to find the following facts which we formulate first using a graphical representation.

The behavior and the number of components depends on the sign of h. For $h < 0$ the situation is simpler. The intersection $\lambda_{0,h}$, for $h < 0$ has four connected components. Three lie in the $y = 0$ plane. They are described by the equation

$$3p_1^2 x/2 - x^3/4 + (2p_1^2 + x^2)^2/4 = h. \tag{D.17}$$

The fourth component lies in the $x = 0$ plane. Its equation in the p_1, y variables

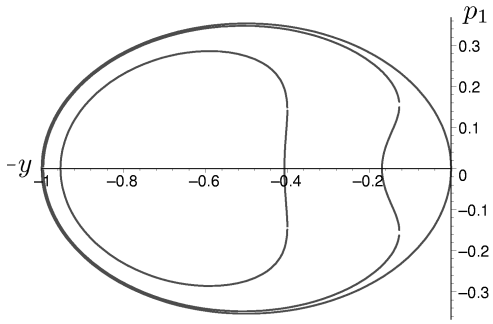

FIGURE D.3. Planar component of the $\lambda_{0,h}$, $h \leq 0$ curves lying in the $x = 0$ plane. This component is shown for $h = -0.01$, $h = -0.001$, and $h = 0$.

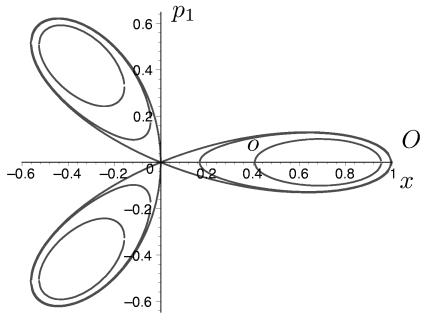

FIGURE D.4. Planar components of the $\lambda_{0,h}$, $h \leq 0$ curves lying in the $y = 0$ plane. These components are shown for $h = -0.01$, $h = -0.001$, and $h = 0$.

takes the form

$$p_1^2 y/2 + y^3/4 + (2p_1^2 + y^2)^2/4 = h. \tag{D.18}$$

For $\lambda_{0,h}$, $h > 0$ the intersection line is the union of two planar curves lying in the planes $\{y = 0\}$ and $\{x = 0\}$. In each plane there is only one component and the two planar curves have two common points which belong to axis p_1.

Figure D.3 shows planar components of the $\lambda_{0,h}$, $h \leq 0$ curves lying in the $x = 0$ plane for three different values of h. Three components lying in the plane $y = 0$ are shown in Fig. D.4 for the same three values of $h \leq 0$.

For $h = 0$ all four components have one common point $x = y = p_1 = 0$. For positive h (but keeping always $m = 0$) we get the union of two planar curves shown separately in Fig. D.5 for the $x = 0$ component and in Fig. D.6 for the $y = 0$ component.

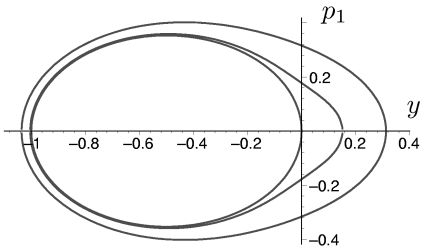

FIGURE D.5. Planar component of the curves $\lambda_{0,h}$ with $h \geq 0$ lying in the $x = 0$ plane for $h = 0.01$, $h = 0.001$, and $h = 0$.

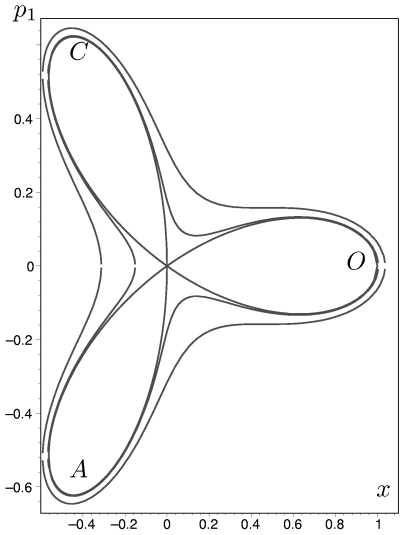

FIGURE D.6. Planar components of the curves $\lambda_{0,h}$ with $h > 0$ lying in the $y = 0$ plane for $h = 0.001$, $h = 0.01$ and $h = 0$.

The 3D-view of the intersection curves for $m = 0, h > 0$ is shown in Fig. D.7. As in the case of the 1:(−1) resonance we name these curves *skeleton curves*. They correspond to the point Γ_5 (see Fig. 6) on the contour Γ and this is precisely the point around which we will study the evolution of cycle $2\gamma_0$ by constructing a homotopically equivalent cycle and deforming it along the contour Γ.

As soon as we have the skeleton curves corresponding to $\lambda_{0,h}$, $h > 0$, we look at the intersection $\Lambda_{m,h} \cap \sigma$ for $h > 0$ and small $|m| \ll h_{\max}$. In coordinates (x, y, p_1) on σ the function F_1 has extremely simple form $F_1 = xy$. This means that for $m \neq 0$ components of the intersection belong to two sheets of cylindrical hyperboloid surfaces. If $m > 0$ these two sheets lie in the first and third cylindrical quadrant. If $m < 0$ they lie in the second and fourth cylindrical quadrant. We

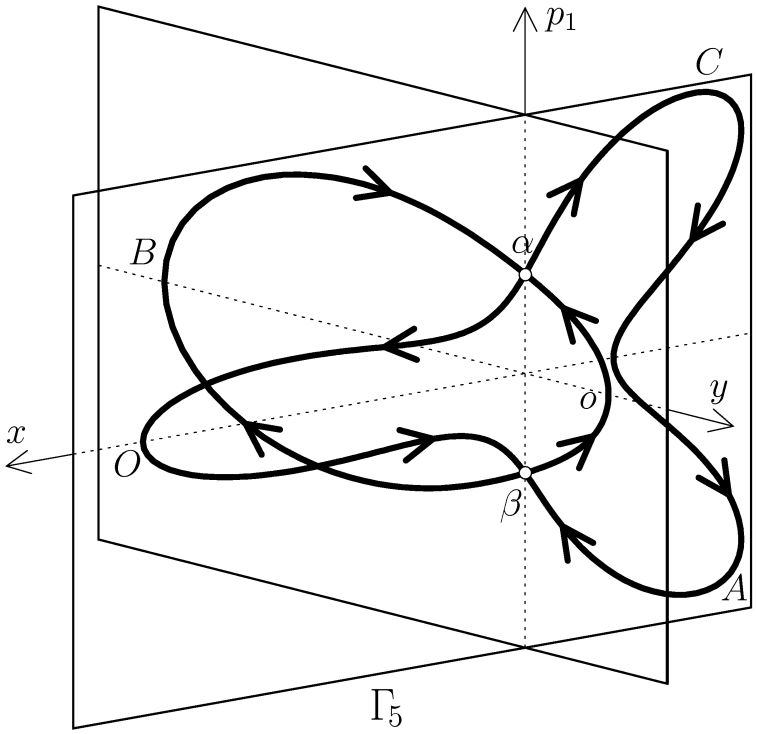

FIGURE D.7. Skeleton curves with orientation defined by the intersection $\Lambda_{m,h} \cap \sigma$. Closed curve $O\beta AC\alpha O$ belongs to plane $y = 0$. Closed curve $B\alpha o\beta B$ belongs to plane $x = 0$. Each planar curve consists of two fragments with different orientation.

denote as $s^k_{m,h}$ the union of components of the intersection curve which belong to the k-th quadrant. For the sake of simplicity we will speak also about k-th hyperboloid, meaning the part of the $F_1 = xy$ hyperboloid which belongs to the k-th quadrant. Examples of curves $s^3_{m,h}$ and $s^1_{m,h}$ with $h > 0$ and small positive m are shown in Fig. D.8. Figure D.9 shows curves $s^2_{m,h}$ and $s^4_{m,h}$ for $m < 0$ and $h > m^2 > 0$.

The precise statements about the form of the skeleton curves $\lambda_{0,h}$ and intersection lines $s^k_{m,h}$, $(m, h) \in \Gamma$ are given in Lemmas D.7 and D.8, which follow next.

Lemma D.7. *The skeleton curve $\lambda_{0,h}$ is the union of two planar curves: $\lambda_{0,h} = \lambda^x_{0,h} \cup \lambda^y_{0,h}$ which lie in the respective planes $\{x = 0\}$ and $\{y = 0\}$ within σ. Each of these planar curves is symmetric in its plane with respect to the coordinate axis $\{p_1 = 0\}$. The curve $\lambda^x_{0,0}$ is a union of three loops with common point at zero*

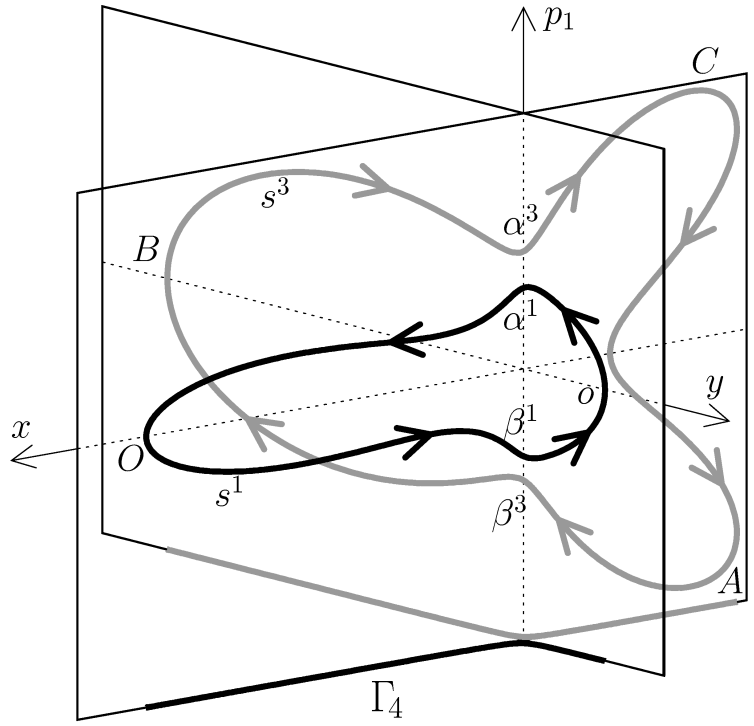

FIGURE D.8. Bold lines show two components $s^1_{\Gamma_4}$ (black) and $s^3_{\Gamma_4}$ (grey) of the intersection $\Lambda_{m,h} \cap \sigma$ at point $\Gamma_4 = (m, h)$. s^1 and s^3 belong respectively to the hyperboloid sheets situated in the first and third quadrant. α^1, α^3 (β^1, β^3) are points of the intersection which are closest to the branching point α (β) of the skeleton curve in Fig. D.7. Projections of the intersection curves on the plane (x, y) are shown at the bottom of the plot.

$p_1 = x = 0$. *The three loops are smooth everywhere except at this point and are situated as shown in Fig.* D.4. *In the neighborhood of the origin* $p_1 = x = 0$ *the curve* $\lambda^x_{0,0}$ *has the form of the union of three smooth curves intersecting at that point* (*see Fig.* D.4). *For small* $h > 0$ *the curve* $\lambda^x_{0,h}$ *is obtained from* $\lambda^x_{0,0}$ *by "inflation"* (*see Fig.* D.6) *and for small* $-h > 0$ *by "deflation"* (*see Fig.* D.4).

Curve $\lambda^y_{0,0}$ *is a smooth curve lying in the half-plane* $y \leq 0$ *and tangent to coordinate axis* p_1 *at zero* $p_1 = y = 0$. *For small* $|h|$ *curve* $\lambda^y_{0,h}$ *is obtained from* $\lambda^y_{0,0}$ *by "inflation" or "deflation" depending on the sign of* h (*see Figs.* D.5 *and* D.3).

Curves $\lambda^x_{0,h}$ *and* $\lambda^y_{0,h}$ *intersect at two points of the coordinate axis* p_1 *in* σ *with coordinates* $x = y = 0$ *and* $p_1 = \pm(h)^{1/4}$, *see Fig.* D.7.

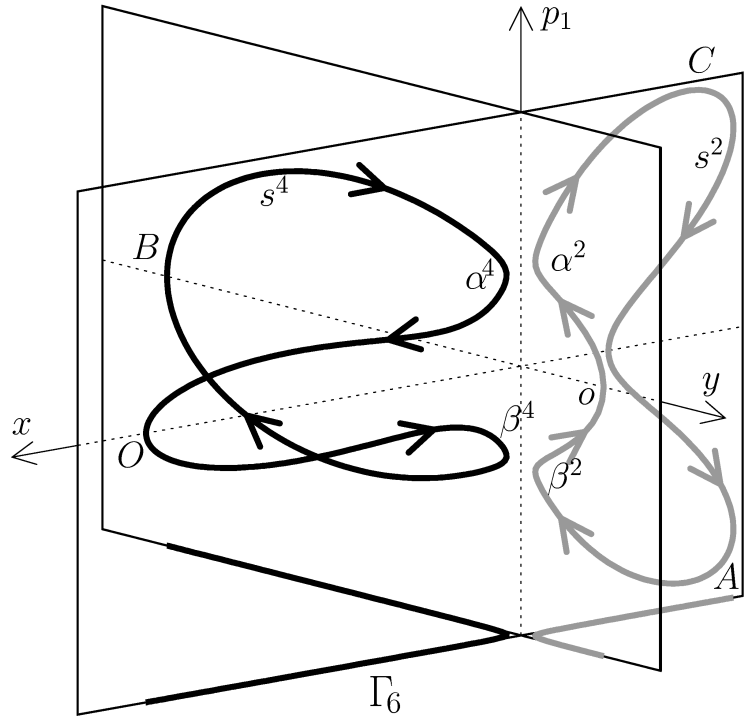

FIGURE D.9. Bold lines show two components $s^2_{\Gamma_6}$ (grey) and $s^4_{\Gamma_6}$ (black) of the intersection $\Lambda_{m,h} \cap \sigma$ at point $\Gamma_6 = (m, h)$. s^1 and s^3 belong respectively to the hyperboloid sheets situated in the first and third quadrant. $\alpha^4, (\alpha^2)$ and $\beta^4, (\beta^2)$ are points of the intersection which are closest to the branching points α and β of the skeleton curves in Fig. D.7. Projections of the intersection curves on the plane (x, y) are shown at the bottom of the plot.

Proof. We start by analyzing curve $\lambda^x_{0,h}$ defined by eq. (D.17). By substitution $z = p_1^2$ and $u = x/2$ we transform this equation into

$$z^2 + bz + c = 0, \quad \text{where} \quad b = 4u^2 + 3u, \quad \text{and} \quad c = 4u^4 - 2u^3 - h.$$

Let us set $h = 0$ and analyze roots $z_{1,2}(u)$ of this quadratic equation for $u \in \mathbb{R}$. We get:
i) $u \in (-\infty, -9/32)$, $\Delta = b^2 - 4c = u^2(32u + 9) < 0$, there are no real roots;
ii) $u = -9/32$, $\Delta = 0, c > 0, b < 0$, there is one multiple root $z_1 = z_2 > 0$;
iii) $u \in (-9/32, 0)$, $\Delta > 0, c > 0, b < 0$, $z_1 > z_2 > 0$;
iv) $u = 0$, $\Delta = 0, c = b = 0$, $z_1 = z_2 = 0$;
v) $u \in (0, 1/2)$, $\Delta > 0, c < 0$, $z_1 > 0 > z_2$;

vi) $u = 1/2,\ \Delta > 0, c = 0, b > 0,\quad z_1 = 0,\ z_2 < 0;$
vii) $u \in (1/2, +\infty),\ \Delta > 0, c > 0, b > 0,\quad$ there are no non negative real roots.
As a leading part of eq. (D.17) in the neighborhood of point $p_1 = x = 0$ we can take $p_1^4 + 3p_1^2 x/2 - x^3/4 = 0$. Solving this equation with respect to p_1, we find that the curve $\lambda^x_{0,0}$ has the form described in the statement of the lemma. In particular, in the neighborhood of the origin $\lambda^x_{0,0}$ has the form of the union of three smooth curves intersecting at the origin and having there tangents $\{p_1 = \pm x/6\}$ and $\{x = 0\}$.

The relation between curves $\lambda^x_{0,h}$ for $h \neq 0$ and $\lambda^x_{0,0}$ and the proof of the fact that $\lambda^x_{0,h}, h \neq 0$ is smooth everywhere including points of the intersection with axis p_1 is completely similar to the case 1:(-1) (see Lemma C.4).

We turn to the analysis of the curve $\lambda^y_{0,h}$. After changing variables $z = p_1^2, u = y/2$ in eq. (D.18) we get:

$$z^2 + bz + c = 0, \quad \text{where} \quad b = 4u^2 + u, \quad \text{and} \quad c = 4u^4 + 2u^3 - h.$$

Let us set $h = 0$ and analyze roots $z_{1,2}(u)$ of this equation for $u \in \mathbb{R}$. We have $\Delta = u^2 \geq 0$ and:
i) $u \in (-\infty, -1/2),\ c > 0, b > 0\quad$ there are no non-negative real roots;
ii) $u = -1/2,\ c = 0, b > 0,\quad z_1 = 0, z_2 < 0;$
iii) $u \in (-1/2, 0),\ c < 0,\quad z_1 > 0 > z_2;$
iv) $u = 0,\ c = b = 0,\quad z_1 = z_2 = 0;$
v) $u > 0,\ c > 0, b > 0,\quad$ there are no non-negative real roots.

In the neighborhood of the origin $p_1 = y = 0$, the leading part of equation (D.18) has the form $p_1^4 + p_1^2 y/2 + y^3/4 = 0$. This ensures that $\lambda^y_{0,0}$ is smooth in the neighborhood of the origin. Further analysis repeats exactly the proof in the case of the curve $\lambda^x_{m,h}$. Thus all statements of the lemma are proved. □

The next lemma provides exact correspondence between the intersection lines $s^k_{m,h}$ and skeleton curves $s^k_{0,h}$. As compared to the 1:(-1) case (see Lemma C.5) we need to treat different cylindrical quadrants separately and we need to study special one-dimensional strata.

Lemma D.8. *There exists such $h_0 > 0$ that for all $\epsilon > 0$ and $\eta > 0$ there is $\delta = \delta(h_0, \epsilon, \eta) > 0$ with the following property. For m and h such that $|h| < h_0$ and $|m| < \delta$*

1. *The distance between $s^1_{m,h}$ and $s^1_{0,h}$ does not exceed ϵ: $\rho_0(s^1_{m,h}, s^1_{0,h}) < \epsilon$. Here the distance $\rho_0(A, B)$ between subset A and subset B is defined in a standard way: $\rho_0(A, B) = \max_{\xi \in A} \rho_0(\xi, B)$, where ρ_0 is the distance induced by the coordinates (p, q) in $\mathbb{R}^4$.*
2. *$\rho_1(s^1_{m,h} \setminus \mathcal{V}_\eta,\ s^1_{0,h} \setminus \mathcal{V}_\eta) < \epsilon$, where ρ_1 is the distance similar to ρ_0, but with C^1 norm, rather than C^0, i.e., the norm takes into account both the distance between points and between directions of lines tangent at these points to curves $s^1_{m,h} \setminus \mathcal{V}_\eta$, and $s^1_{0,h} \setminus \mathcal{V}_\eta$. In other words, curves $s^1_{m,h}$ and $s^1_{0,h}$ are almost parallel each other outside the cylinder $\mathcal{V}_\eta$.*

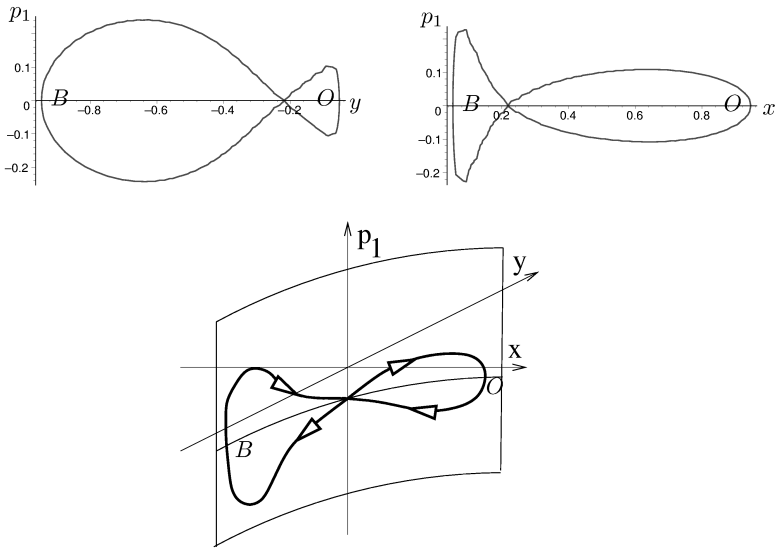

FIGURE D.10. Parts of the intersection $\Lambda_{m,h} \cap \sigma$ at point Γ_8 lying in the 4th quadrant. Projections on the (y, p_1) and (x, p_1) planes are shown on the top; schematic 3D-view of the intersection situated on the hyperboloid surface is shown on bottom.

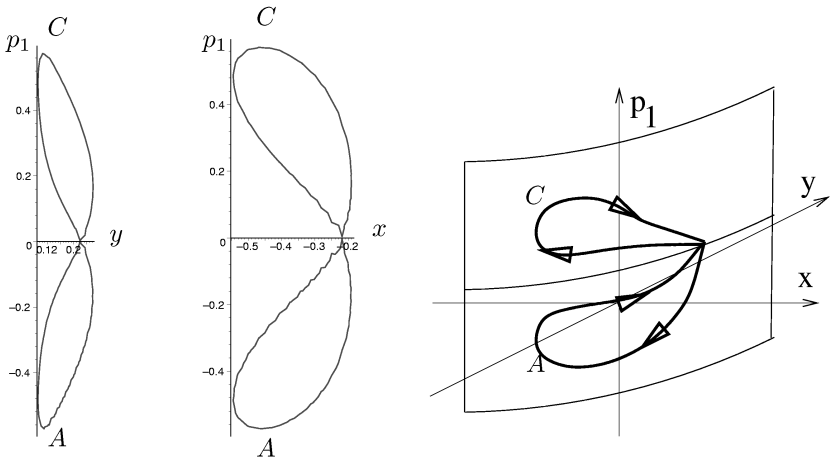

FIGURE D.11. Part of the intersection curves at point Γ_8 lying in the 2nd quadrant. Projections on the (y, p_1) and (x, p_1) planes are shown left and center. Schematic 3D-view of the intersection curve lying on the hyperboloid surface is shown in the rightmost plot.

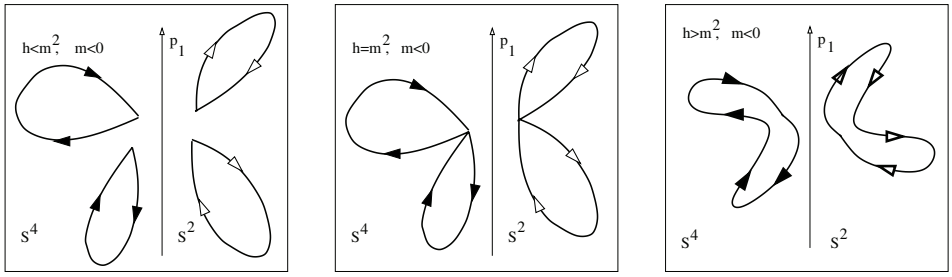

FIGURE D.12. Rearrangement of the components of intersection line near the singular fiber (curled torus).

3. *Let us consider the mapping ϕ between the curve $s^1_{m,h} \setminus \mathcal{V}_\eta$ and the part of the curve $s^1_{0,h}$ which sends each point from $s^1_{m,h} \setminus \mathcal{V}_\eta$ to the nearest point of the curve $s^1_{0,h}$. Then ϕ is a diffeomorphism.*
4. *Curves $s^1_{m,h}$ and $s^1_{0,h}$ are homeomorphic to each other. The curve $s^1_{m,h}$ for $m \neq 0$ and the curve $s^1_{0,h} \setminus \{x = y = 0\}$ are smooth. For $h = m^2$ and $0 < -m \ll 1$ the curve $s^2_{m,h}$ ($s^4_{m,h}$) has the form of figure eight which lies close to $s^2_{0,0}$ (respectively to $s^4_{0,0}$) and is homeomorphic to this curve (see Figs.* D.11, D.10*). For $0 < h - m^2 \ll m^2 \ll 1$ and $m < 0$, the $s^2_{m,h}$ ($s^4_{m,h}$) curve is produced by "inflation", and for $0 < m^2 - h \ll m^2 \ll 1$ and $m < 0$ by "deflation" of s^2_{m,m^2} (s^4_{m,m^2}) (see Fig.* D.12*). Curve $s^3_{m,h}$ for $(m,h) \in \theta$ has the form of a "double figure eight" shown in Fig.* D.13*, centre. If point (m,h) moves from curve θ to higher (lower) h values without changing m, the corresponding curve $s^3_{m,h}$ results from $s^3_{m,h}$, $(m,h) \in \theta$, after "inflation" ("deflation") of the latter (see Fig.* D.13*, right (left)).*

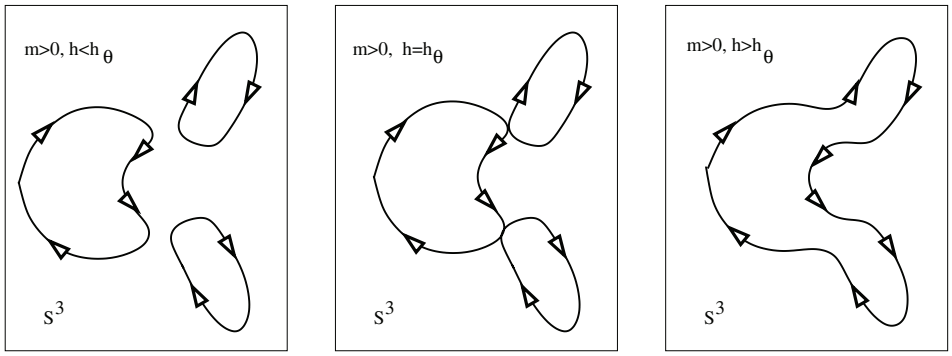

FIGURE D.13. Rearrangement of the s^3 components of the intersection curve near the critical line of the $\{F_1, F_2, F_3\}$ map.

Proof. Similar to Lemma C.5, statements i), ii), iii) of Lemma D.8 as well as statement iv) in the case of the first quadrant follow from the implicit function theorem and Lemmas D.6 and D.7. We omit the standard proof of these statements.

In order to prove statement iv) in the case of quadrants $k = 2, 3, 4$ we need to study curves $s^k_{m,h}$, $k = 4, 2$ for $h = m^2, m < 0$ and for close values of (m, h), as well as curve $s^3_{m,h}$ for $(m, h) \in \theta$ and for close values of (m, h).

Let us start with $s^k_{m,h}$, $k = 4, 2$ for $|h - m^2| \ll m^2 \ll 1$ and $m < 0$. Substituting $\mathcal{F}_1 = m, \mathcal{F}_2 = h$ in (D.7) and solving the first of these equations with respect to p_2 we get $p_2 = \pm\sqrt{-m + q_1^2/2}$. Let us treat both cases.

1) $p_2 = -\sqrt{-m + q_1^2/2}$. (Analysis of curves $s^4_{m,h}$ for $|h - m^2| \ll m^2 \ll 1$, $m < 0$.) Substituting this expression for p_2 into the second equation in (D.7) and changing to variables $z = p_1^2$, $q = q_1$, we get

$$z^2 + bz + c = 0$$

$$b = \sqrt{-m + q^2/2} + \sqrt{2}q + 2q^2 - 2m, \quad c = q^2(-\sqrt{-m + q^2/2} + q^2 - 2m).$$

Let us analyse roots $z_{1,2}(q)$ of this equation for all $q \in \mathbb{R}$.

Resolving $c(q) = 0$ we get four roots $q_{1,2} = 0, q_{3,4} = \pm\alpha$, with $\alpha = 1/\sqrt{2} + \beta$, $\beta > 0$ and $\beta(m) \to 0$ for $-m \to 0$. It is easy to verify that for $|q| > \alpha$ and $m < 0$, we have $c(q) > 0$ and $b(q) > b_0 > 0$, and for $0 < |q| < \alpha$, we have $c(q) < 0$. If $q = 0$, then $c = 0$ and $b > 0$. Thus for roots $z_{1,2}(q)$ we have:
$q \in (-\infty, -\alpha)$, no real non-negative roots;
$q = -\alpha$, $z_1 = 0, z_2 < 0$;
$q \in (-\alpha, 0)$, $z_1 > 0 > z_2$;
$q = 0$, $z_1 = 0, z_2 < 0$;
$q \in (0, \alpha)$, $z_1 > 0 > z_2$;
$q = \alpha$, $z_1 = 0, z_2 < 0$;
$q \in (\alpha, +\infty)$, no real non-negative roots.

This information proves the statement about the form of the curves s^4_{m,m^2} at small $-m > 0$. Taking into account how h enters in the solution of (D.7) with respect to p_1, we get equally the form of $s^4_{m,h}$ for small $|h - m^2| \ll m^2 \ll 1$ and $m < 0$.

2) $p_2 = -\sqrt{-m + q_1^2/2}$. (Analysis of curves $s^2_{m,h}$ for $|h - m^2| \ll m^2 \ll 1$, $m < 0$.) Substituting this expression for p_2 into the second equation of (D.7) and changing variables $z = p_1^2$, $q = q_1$, we obtain

$$z^2 + bz + c = 0$$

$$b = -\sqrt{-m + q^2/2} + \sqrt{2}q + 2q^2 - 2m, \quad c = q^2(\sqrt{-m + q^2/2} + q^2 - 2m).$$

We have $c > 0$ for $q \neq 0$ and $c(0) = 0$, with function $c = c(q)$ being even and $c'(q) > 0$ for $q > 0$.

Let us find roots of the equation $b(q) = 0$. If $|q| \ll 1$ the leading part of this equation is $P(q) = 0$ where $P(q) = -\sqrt{-m + q^2/2} + \sqrt{2}q$. The only solution of $P(q) = 0$ is $\alpha = \sqrt{-2m/3}$. As soon as $P'(\alpha) > 0$ the initial equation $b(q) = 0$

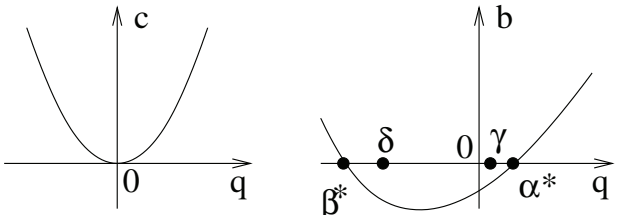

FIGURE D.14. Geometric representation of $c(q)$ and $b(q)$.

for $|q| \ll 1$ also has unique solution α^*, with α^* being close to α, namely $\alpha^* = \alpha + o(\sqrt{-m})$ for small $-m$ and $|q|$.

For $|q| \gg \sqrt{-m}$ the leading part of equation $b(q) = 0$ is $\sqrt{2}q + 2q^2 = 0$. Its solution gives the only acceptable root, $\beta = -1/\sqrt{2}$. The derivative of the left-hand side of this shorten equation in point β is negative. Thus, the initial equation $b(q) = 0$ for all $|q| \gg \sqrt{-m}$ has the only solution $\beta^* = \beta + o(1)$ close to β for $(-m) \to 0$. Taking into account that $b(0) < 0$, we can verify that the graphics of functions $c(q)$ and $b(q)$ have the form, shown in Fig. D.14.

Let us analyze now the discriminant $\Delta = \Delta(q) = b^2(q) - 4c(q)$ of equation $z^2 + bz + c = 0$. It is clear that $\Delta(0) > 0$, $\Delta(\alpha^*) < 0$ and $b'(q) > 0$ if $q \in [0, \alpha^*]$. From this and from inequality $c'(q) > 0$ for $q > 0$ we get that $\Delta'(q) < 0$ for $q \in (0, \alpha^*]$. Thus, equation $\Delta(q) = 0$ has on the interval $(0, \alpha^*)$ the only solution, which we denote by γ (see Fig. D.14). To analyze $\Delta = \Delta(q)$ on the closed interval $[\beta^*, 0]$ we start with the complete expression of $\Delta(q)$ and reduce it to the shortened expression

$$S := \left(\sqrt{-m + q^2/2} - \sqrt{2}q\right)^2.$$

For $m < 0$ and $q < 0$ we have $S > -m + q^2 > 0$. Now it follows easily that

$$\Delta = S + o(S) \quad \text{for small positive } (-m) \text{ and } (-q), \tag{D.19}$$

and consequently, the choice of $S(q)$ as a leading part of $\Delta(q)$ for these m and q is justified. From (D.19) it follows that equation $\Delta(q) = 0$ for $0 < -m + q^2 \ll 1$ and $m < 0, q < 0$ has no solutions.

For $-q \gg \sqrt{-m}$ the leading part of $\Delta(q) = 0$ can be taken as $Q(q) = 0$, where $Q = 9q^2/2 + 8\sqrt{2}q^3$. On the semi-open interval $[\beta^*, 0)$ equation $Q(q) = 0$ has the only solution $q = -9\sqrt{2}/32$. Since $Q'(\beta^*) < 0$, the $\Delta(q) = 0$ equation for $\sqrt{-m} \ll -q \le -\beta^*$ also has a unique solution, which should be close to $-9\sqrt{2}/32$ and which we denote as δ. Then, $\Delta(\delta) = 0$ and $\delta \in (\beta^*, 0)$, as illustrated in Fig. D.14.

Analysis of the coefficients $b(q)$ and $c(q)$ and of the discriminant $\Delta(q)$ of the quadratic equation $z^2 + bz + c = 0$ enables us to make the following conclusion about the roots $z_{1,2}(q)$ of this equation.

$q \in (-\infty, \delta)$: no real non-negative roots (because either $c > 0, b > 0$, or $\Delta < 0$);

$q = \delta$: $z_1 = z_2 > 0$, $(c > 0, b < 0, \Delta = 0)$;

$q \in (\delta, 0)$: $z_1 > z_2 > 0$, $(c > 0, b < 0, \Delta > 0)$;
$q = 0$: $z_1 > 0, z_2 = 0$, $(c = 0, b < 0, \Delta > 0)$;
$q \in (0, \gamma)$: $z_1 > z_2 > 0$, $(c > 0, b < 0, \Delta > 0)$;
$q = \gamma$: $z_1 = z_2 > 0$, $(c > 0, b < 0, \Delta = 0)$;
$q \in (\gamma, \infty)$: no real non-negative roots (either $\Delta < 0$, or $c > 0, b > 0$).

The form of curves s^2_{m,m^2} which was described for small $m < 0$ in Lemma D.8 follows from this analysis. Taking into account the way h enters into the solution of eq. (D.7) with respect to p_1, we get also the form of curves $s^2_{m,h}$ for small $|h - m^2| \ll m^2$.

To prove the statement of Lemma D.8 about the form of curves $s^3_{m,h}$ for (m, h) lying on θ and situated close to it, we need to follow the same scheme of the analysis of roots of the biquadratic equation. As soon as this statement is not needed for the proof of Theorem 2, we omit it here. □

Lemma D.8 and the analysis of the skeleton curves (Lemma D.7) enable us to precise the number of components $s^i_{m,h}$ of the intersection $\Lambda_{m,h} \cap \sigma$ lying on each sheet of the hyperboloid for all three regions which exist near the singular value $(0, 0)$ of the map F. (See Fig. D.15.) Note, that in the lower region the total number of components is always four, but their distribution between different sheets of the hyperboloid changes at $m = 0$.

To complete the understanding of the evolution of the components of the intersection curves we also need to define their orientations (according to the con-

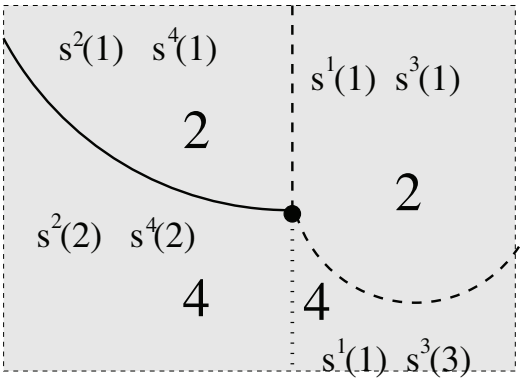

FIGURE D.15. Regions of the image of the energy momentum map F near $(0, 0)$ and the number of components (big numbers) of intersection $\Lambda_{m,h} \cap \sigma$ in each region. Solid line shows critical values of map F. Dashed lines show images of points with nonregular intersection under F. Dotted line corresponds to the degeneration of the two-sheet hyperboloid into two intersecting planes. Symbols $s^i(K)$ indicate that there are K components on the sheet of the hyperboloid lying in the i-th quadrant.

struction described earlier in Sec. 5). This orientation is indicated in all Figs. D.7–D.13. One can easily verify that the orientation is chosen in such a way that under reorganization of the intersection curves the orientation of each fragment is conserved.

The next step in the proof of the monodromy theorem in the case of the 1:(−2) resonance is the analysis of the deformation of cycles in σ as we follow along Γ. To simplify the analysis and to visualize better the deformation of cycles we establish in the next lemma the correspondence between the intersection curves on σ and on the universal covering of the tori in the special point Γ_5 (i.e., for $m = 0, h > 0$) of the contour Γ.

Lemma D.9. *Let us consider torus* $\Lambda_{\Gamma_5}(\Gamma_5 = (m,h)\,|_{m=0,h>0})$ *(see Fig.* 6*).*

On this torus there exist continuous "angle coordinates"

$$\psi \bmod 2\pi = (\psi_1 \bmod 2\pi, \psi_2 \bmod 2\pi)$$

with the following properties:

Parallel "coordinate" circles $\{\psi_2 \bmod 2\pi = c\}$ *coinside with trajectories of vector field* X_{F_1} *and circles* $\{\psi_1 \bmod 2\pi = d\}$ *are homotopic to the cycle* $\gamma_0^{\Gamma_5} \subset \Lambda_{\Gamma_5}$*, which is obtained by a continuous deformation of cycle* $\gamma_0 = \gamma_0^{\Gamma_0} = s^1_{\Gamma_0}$ *associated with the displacement of point* (m,h) *from* Γ_0 *to* Γ_5 *along the right part of the contour* Γ*, i.e., along* $\Gamma \cap \{m \geq 0\}$*. Function* ψ_1 *increases along the curve* $\{\psi_2 \bmod 2\pi = c\}$ *in the direction corresponding to the direction of evolution of points on* Λ_{Γ_5} *under the action of the phase flow of field* X_{F_1}*. Natural orientation defined on cycle* $\{\psi_1 \bmod 2\pi = d\}$ *agrees with the orientation defined on cycle* γ_0*. Moreover, in "coordinates"* $\psi \bmod 2\pi$ *the intersection* λ_{Γ_5} *has the form of contour constructed from straight segments as shown in Fig.* D.16*. More exactly, let us interpret the square shown in Fig.* D.16 *as a fundamental region on the* $\mathbb{R}^2$ *covering of torus* Λ_{Γ_5} *with coordinates* ψ*. Then the planar component* $\lambda^x_{0,h} = \lambda_{0,h} \cap \{y = 0\} \subset \sigma$ *of intersection* $\lambda_{0,h}$ *on the covering* $\mathbb{R}^2_\psi$ *is given by equation* $\psi_2 = 3\psi_1 + 1/3$*. Another planar part* $\lambda^y_{0,h} = \lambda_{0,h} \cap \{x = 0\} \subset \sigma$ *is given by equation* $\psi_2 = \psi_1$*. [Remind, that* $\lambda_{0,h} = \lambda^x_{0,h} \cup \lambda^y_{0,h}$*.]*

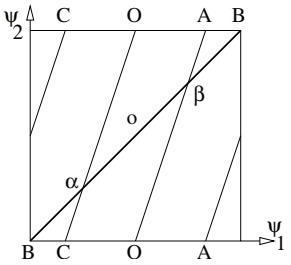

FIGURE D.16. Schematic representation of the intersection curves on the covering of the torus Λ_{Γ_5} in the (ψ_1, ψ_2) coordinates.

Proof. Let us consider smooth "coordinates" $\varphi \bmod 2\pi$, $\varphi = (\varphi_1, \varphi_2)$ on torus Λ_{Γ_5} such that circles $\{\varphi_2 \bmod 2\pi = c\}$ coinside with trajectories of vector field X_{F_1} and circles $\{\varphi_1 \bmod 2\pi = d\}$ are homotopic to cycle $\gamma_0^{\Gamma_5}$ and at each point of torus Λ_{Γ_5} the direction of vector $\frac{\partial}{\partial\varphi_1}$ coinsides with the direction of vector X_{F_1} at that point. The existence of such coordinates follows, for example, from the Liouville–Arnol'd theorem [54].

Intersection of the planar skeleton component λ^x with the plane given in σ by equation $p_1 = 0$ consists of two points. We denote by O the point lying in the half-space $x > 0$, i.e., the point which is farthest from the origin among these two points (see Figs. D.4, D.6, and Lemma D.7).

We take as a circle $\phi_2 \bmod 2\pi = 0$ the trajectory of the field X_{F_1} which goes through the point $O \in \lambda_{\Gamma_5}$. It follows from Lemma D.3 that this trajectory contains three other points lying on λ_{Γ_5}. We denote these points in the order of increasing time as A, B, C. From Lemma D.3 we conclude that point A belongs to quadrant $y = 0, x < 0, p_1 < 0$, point B belongs to ray $x = p_1 = 0, y < 0$, and point C belongs to quadrant $y = 0, x < 0, p_1 > 0$ (see Fig. D.7).

Let us consider cycle $O\beta o\alpha O$ lying on the curve $s^1_{\Gamma_5} \subset \Lambda_{\Gamma_5}$ (see Fig. D.7) and show that this cycle is homotopic to the curve $\gamma_0^{\Gamma_5} \subset \Lambda_{\Gamma_5}$. We notice first, that tori $\Lambda_{m,h}$ form a locally trivial fibration of the part U of the phase space $\mathbb{R}^4_{p,q}$, which lies above some small neighborhood $\mathcal{V} \subset \mathbb{R}^2_{m,h}$ of the right part $\Gamma \cap \{m \geq 0\}$ of the contour Γ: $U = F^{-1}(\mathcal{V})$, $\Gamma \cap \{m \geq 0\} \subset \mathcal{V}$. From Lemmas 5.2, D.7, and D.8 it follows that for $(m, h) \in \Gamma \cap \{m \geq 0\}$, except the final point $(m, h) = \Gamma_5$, the intersection $s^1_{m,h}$ is the connected component of the intersection $\Lambda_{m,h} \cap \sigma = \lambda_{m,h}$ of torus $\Lambda_{m,h}$ with hyperplane σ. Moreover, this component does not include any exceptional points of the intersection. Thus it follows that for such (m, h) the intersection $s^1_{m,h}$ can be obtained from $\gamma_0 = s^1_{\Gamma_0}$ by a smooth deformation in σ. At point Γ_5 the continuity in σ of the deformation of curve $s^1_{m,h}$ follows from Lemma D.8. All these facts give the homotopy of cycles $\gamma_0 \subset \Lambda_{\Gamma_0}$ and $O\beta o\alpha O \subset \Lambda_{\Gamma_5}$ respecting the orientation and corresponding to the displacement from Γ_0 to Γ_5 along the right part of the contour Γ.

Let us show now that on the covering of the Λ_{Γ_5} torus in coordinates $\varphi = (\varphi_1, \varphi_2)$ the cycle $O\beta o\alpha O$ belongs to a half-band $\Pi := \{0 \leq \varphi_2 \leq 2\pi\}$ and connects point O with its 2π-shift "up", i.e., with point $O + (0, 2\pi)$. Moreover, the cycle $O\beta o\alpha O$ on $\mathbb{R}^2_\varphi$ behaves similarly to the oriented "polygonal" line $O\beta o\alpha O$ represented in Fig. D.16 in the following sense. The line $O\beta o\alpha O \subset \mathbb{R}^2_\varphi$ consists of three smooth generic curve segments. The first segment $[0, \beta]$ "goes up" from point O to point β which is situated below the upper boundary of the band Π. The second segment $[\beta, \alpha]$ goes down to the left of the first segment without touching the lower boundary of the band Π. The third segment $[\beta, O + (0, 2\pi)]$ is situated farther to the left and goes up to point $O + (0, 2\pi)$.

The fact that cycle $O\beta o\alpha O$ on the covering of the torus $\Lambda := \Lambda_{\Gamma_5}$ consists of three smooth segments follows from the smoothness of torus Λ and "coordinates" $\varphi \bmod 2\pi$ on it, and from the smoothness of the curve $O\beta o\alpha O \subset \sigma$ in σ except

points β and α. On each of these smooth segments, "moving up" along coordinate φ_2 cannot change to "moving down" and vice versa, because the internal parts of these segments do not intersect the plane $\{q_1 = 2\sqrt{2}p_2\} \subset \sigma$ (see Lemma D.4). Recall that curves $\lambda_{m,h}$ are tangent to trajectories of the vector field X_{F_1} only at that plane.

The fact, that "moving up" to point β on the segment $[O, \beta]$ should change to "moving down" on the segment $[\beta o \alpha]$ to the left of $[O, \beta]$ follows from Lemma D.4, see Fig. D.1. In fact, the position of curves $[O, \beta]$, $[\beta o \alpha]$, and positive coordinate semi-axis φ_1 in the neighborhood of the point β on the covering $\mathbb{R}^2_\varphi$ of torus Λ should correspond respectively to positions of coordinate semi-axes x and y and vector $X_{F_1}(\beta)$ in the neighborhood of point β on σ, see Fig. D.1. Taking into account that $p_1(\beta) < 0$ we conclude that vector $X_{F_1}(\beta)$ has direction opposite to that shown in Fig. D.1. Thus, going on the torus chart Λ near point β from segment $[\beta o \alpha]$ along the straight lines $\{\varphi_2 = c\}$ in the direction of increasing coordinate φ_1 should almost immediately lead to the curved segment $[O, \beta]$. This results in "going down" in φ_2 after leaving point β along segment $[\beta o \alpha]$.

Completely similar analysis shows that "going down" along $[\beta o \alpha]$ when approaching point α changes to "going up" in φ_2. Thus we get the "zigzag" form of the cycle $O\beta o \alpha O$ on the covering $\mathbb{R}^2_\varphi$ of torus Λ.

Let us now show that the "zigzag" curve, with exception of its initial point O and its final point $O + (0, 2\pi)$, belongs to the internal part of band Π. In fact, the boundary $\partial\Pi$ of $\Pi \subset \mathbb{R}^2_\varphi$ is given by equations: $\varphi_2 = 0$ and $\varphi_2 = 2\pi$. But the subset $\lambda = \lambda_{\Gamma_5} \subset \Lambda_{\Gamma_5}$ intersects trajectories of vector field X_{F_1}, which coinside with circles $\{\varphi_2 \bmod 2\pi = 0\}$ only in four points O, A, B, and C. None of these points belong to the curve $O\beta o \alpha O \subset \sigma$ except the initial (and at the same time the final) point O. Hence the internal part of the "zigzag" curve belongs to $\Pi \backslash \partial\Pi$.

Just above we have shown that the circle $s^1_{\Gamma_5} \subset \Lambda_{\Gamma_5}$ corresponding to the "zigzag" curve is homotopic to cycle $\gamma_0^{\Gamma_5}$. By the definition of the angle "coordinate" φ_1, the circle $\{\varphi_1 \bmod 2\pi = 0\}$ is also homotopic to the same cycle. This

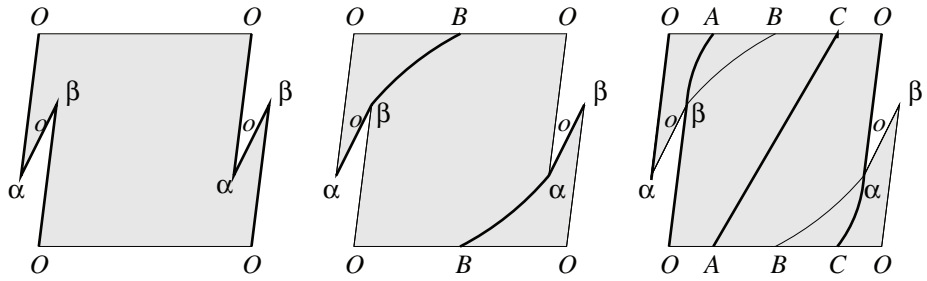

FIGURE D.17. Schematic representation of skeleton curve on the Λ_{Γ_5} torus map. Left: The loop $(O{-}\beta{-}\alpha{-}O)$ on the torus covering together with the choice of the fundamental region (shadow part). Center: Loop $\alpha o \beta B \alpha$. Right: Loop $\alpha O \beta A C \alpha$.

means that the final point of the "zigzag" curve is shifted with respect to its initial point by the vector $(0, 2\pi) \in \mathbb{R}^2_\varphi$, i.e., the final point coinsides with $O + (0, 2\pi)$.

Let us now consider the fundamental region of the torus covering which is bounded from below and above by trajectories of the field X_{F_1} lying respectively on lines $\varphi_2 = 0$ and $\varphi_2 = 2\pi$. On the right and on the left, this region is bounded by the zigzag curve $(O\beta o\alpha O)$ (see Fig. D.17, left).

Let us now take a smooth loop going along λ^y on the skeleton starting at point α: $(\alpha o\beta B\alpha)$. The first segment $(\alpha o\beta)$ is represented on the torus covering and we go along it to higher values of φ_2. This means that values of φ_2 should increase along the whole loop and on the torus we come back to point α. On the torus covering the final point is different from the initial one. Because the rest of the loop $(\beta B\alpha)$ does not intersect the zigzag curve $(O\beta\alpha O)$ and λ^y intersects cycle $\{\varphi_2 \bmod 2\pi = 0\}$ only in point B, the $(\beta B\alpha)$ part of the loop should intersect the straight line $\varphi_2 = 2\pi$ at $0 < \varphi_1 < 2\pi$ and the intersection point should coincide with point B (see Fig. D.17, center).

It is easy to see that the final point of the loop $(\alpha o\beta B\alpha)$ is displaced on the torus covering with respect to the starting point O by vector $(2\pi, 2\pi)$. In fact, the orbit $\varphi_2 \bmod 2\pi = 0$ of the field X_{F_1} intersects the loop $(\alpha o\beta B\alpha)$ only in point B. Thus the value of coordinate φ_2 in the final point should be between 2π and 4π. On the other hand, the main part of the loop $(\beta B\alpha)$ has no common points with the zigzag curve corresponding to the loop $(O\beta o\alpha O)$ except its ends. Thus the final point of the smooth loop $(\alpha o\beta B\alpha)$ on the torus covering can either return back to the continuation of the initial zigzag curve or come to a zigzag curve shifted to the right by 2π, i.e., the zigzag shifted by the vector $(2\pi, 0)$. But the curve representing the loop $(\alpha o\beta B\alpha)$ cannot come back to the same zigzag because in such a case the increase of φ_2 has to be followed by a decrease (see Fig. D.17, center). This contradicts the behaviour of the zigzag curve which was already proven earlier.

Let us consider now other planar part of the skeleton lying on λ^x. We take point α as a starting point and move along $(\alpha O\beta AC\alpha)$. We look for the form of this curve on the torus covering with coordinates (φ_1, φ_2). The part $(\alpha O\beta)$ was studied earlier. The rest does not contain points α, β of the intersection of planar parts of the skeleton. Using similar arguments we get that the curve representing the loop $(\alpha O\beta AC\alpha)$ on the torus covering always goes up (to higher values of φ_2) and its final point is displaced with respect to the starting point by vector $(2\pi, 6\pi)$, (see Fig. D.17, right). We note that the value $\Delta\varphi_2 = 6\pi$ is due to the fact that the loop $(\alpha O\beta AC\alpha)$ intersects trajectories $\varphi_2 \bmod 2\pi = 0$ in three points, O, A, C.

We prove now the statement ii) about the existence of the homeomorphism straightening the planar parts λ^x, λ^y of the skeleton on the torus covering, i.e., the existence of "angle coordinates" $(\psi_1 \bmod 2\pi, \psi_2 \bmod 2\pi)$ with required properties on torus Λ_{Γ_5}. As it was mentioned earlier both curves λ^x, λ^y represented in smooth coordinates (φ_1, φ_2) are smooth and intersect themselves only in points α and β.

Let us pose $\psi_2 = \varphi_2$ and construct the "angular coordinate function" $\psi_1 = \psi_1(\varphi_1, \varphi_2)$ separately on each circle $\{\varphi_2 \bmod 2\pi = c\}$. From the facts proven

earlier it follows that the points of intersection $l_c = \lambda \cap \{\varphi_2 \bmod 2\pi = c\} \subset \Lambda \subset \sigma$ in coordinates φ appear on circle $\{\varphi_2 \bmod 2\pi = c\}$ in the same order as points of the intersection with circle $\{\psi_2 \bmod 2\pi = c\}$ of the polygonal line composed of straight segments as shown in Fig. D.16.

At the same time and in contrast to Fig. D.16, under the variation of c the intersection points l_c in coordinates $\varphi \bmod 2\pi$ move on curved rather than on straight lines. To improve this deficiency of coordinates $\varphi \bmod 2\pi$ we construct for each $c \bmod 2\pi$ a homeomorphism $\mathcal{F}_c\colon \{\varphi_2 \bmod 2\pi = c\} \to \{\varphi_2 \bmod 2\pi = c\}$, which transforms points of l_c in "coordinates" $\varphi \bmod 2\pi$ into corresponding points of intersection of the polygonal line in Fig. D.16 with circle $\{\psi_2 \bmod 2\pi = c\}$.

It is not hard to see that such homeomorphism exists. Moreover, the corresponding functions F and G, where $F(\varphi_1, \varphi_2) := \mathcal{F}_{\varphi_2}(\varphi_1)$ and $G(\psi_1, \varphi_2) := \mathcal{F}^{-1}_{\varphi_2}(\psi_1)$, can be chosen continuous over all arguments (φ_1, φ_2) and (ψ_1, φ_2) respectively. Then mapping $(\varphi_1, \varphi_2) \mapsto (\psi_1, \psi_2)$, where $\psi_1 = F(\varphi_1, \varphi_2), \psi_2 = \varphi_2$ is the homeomorphism straightening the intersection $\lambda = \lambda_{\Gamma_5}$ as formulated in the statement of Lemma D.9. This proofs the lemma. □

D.2.1. Curve fragments used for construction of deformation of $2\gamma_0$. First of all we need to choose properly the cycle which can be deformed along Γ. The obvious restriction imposed on this choice is due to the fusion (splitting) of loops lying on the same hyperboloid surface which occurs when we pass through the singular curled torus fiber. From Figs. D.10, D.11, D.12 it is clear that only the cycles formed by two loops can continuously pass through this singular fiber. Consequently, we need to take a double loop to construct the monodromy map associated with the closed path δ_Γ.

In order to simplify the crossing of the θ line, associated with the fusion of three loops on the 3-rd hyperboloid sheet, we take the double loop situated at $m = 0, h < 0$ in the $y = 0$, $x > 0$ half-plane as a $2\gamma_0$ cycle. For positive m this loop is situated on the hyperboloid in the first quadrant, whereas three other loops for $m > 0$ are on the hyperboloid in the third quadrant. The chosen s^1 loop can be deformed smoothly as (m, h) crosses the θ curve. As soon as we take it to be a double loop, it passes continuously across the "curled torus" singular fiber as well. The only point to be verified is the deformation of the chosen $2\gamma_0$ cycle at the $m = 0, h > 0$ line.

To cross the $m = 0, h > 0$ line we will replace the $2\gamma_0$ cycle by the homotopically equivalent cycle which we construct from the following fragments.

- Fragments of curves $s^k_{m,h}$.
- Trajectories γ_f of the system with Hamiltonian F_1.
- Shadow fragments $\mathcal{I}_{m,h}[\xi_1\xi_2]$, which belong to surfaces $\Lambda_{m,h}$. Each such fragment belongs to a small neighborhood $U \subset \mathbb{R}^4$ of a nonzero point on the axis p^σ_1 and connects some points ξ_1 and ξ_2, which belong to $\Lambda_{m,h} \cap \sigma \cap U$ and are close to each other on $\Lambda_{m,h}$.

In fact, we realize the construction of the homotopically equivalent cycle on σ which repeats the construction realized in Sec. 5 (see especially Fig. 9) where we use

the same notation for characteristic points as on figures representing intersection curves on σ (see Figs. D.7, D.8, D.9).

D.2.2. Deformation of cycle $2\gamma_0$ along contour Γ. In this section we repeat the analysis of deformation of the $2\gamma_0$ cycle along Γ which was described in Sec. 5.2 by looking directly on surfaces $\Lambda_{m,h}$. Now we study the evolution in σ and use the correspondence between representation on σ and on the torus covering established in Lemma D.9.

The deformation of curve $2\gamma_0$ along contour Γ in counterclockwise direction starting from the point Γ_0 consists of the following steps (see Fig. 6).

- At point $\Gamma_0 = (0, -h_{\max})$ we take $2\gamma_0$ to be represented by the double loop corresponding to a component of the $\Lambda_{0,-h_{\max}} \cap \sigma$ intersection lying in the $\{y = 0, x > 0\}$ half-plane.
- We use deformation $\{2s^1_{m,h}, (m,h) \in [\Gamma_0, \Gamma_4]\}$, where $[\Gamma_0, \Gamma_4]\}$ is part of contour Γ going from Γ_0 to Γ_4 in the counterclockwise direction.
- We replace the closed curve $\{2s^1_{m,h}\}$ by another curve which belongs to torus Λ_{Γ_4}, remains homotopic to $\{2s^1_{\Gamma_4}\}$, and consequently to $2\gamma_0$, but does not belong completely to σ.
- We transfer the constructed curve (homotopic to $2\gamma_0$) along the contour Γ from Γ_4 to Γ_6 thus overcoming the point Γ_5 of non-regular intersection of $\Lambda_{m,h}$ with σ. At Γ_6 the transferred curve becomes the sum of $s^4_{\Gamma_6}$ and the properly oriented closed trajectory $(-\gamma_f)$ of the system with Hamiltonian F_1 which does not vary under further deformations.
- We use deformation $\{s^4_{m,h} \cup (-\gamma_f), (m,h) \in [\Gamma_6, \Gamma_9]\}$, which passes continuously the point Γ_8 where the closed loop $\{s^4_{m,h}\}$ splits into two loops without any modification of the orientation of its fragments.
- Final deformation of $\{s^4_{m,h} \cup (-\gamma_f), (m,h) \in [\Gamma_9, \Gamma_0]\}$ transforms smoothly two components of $\{s^4_{m,h}\}$ into two components of $\Lambda_{0,-h_{\max}} \cap \sigma$, one of which belongs to the $\{y = 0, x > 0\}$ half-plane and another $-$ to the $\{x = 0, y < 0\}$ half plane.

Let us now discuss this deformation in more details.

The chosen cycle $2\gamma_0 = OoOoO = 2s^1_{m,h}, (m,h) \in [\Gamma_0, \Gamma_4]$ corresponds to the component of the intersection which possesses no critical points of the $\{F_1, F_2, F_3\}$ map between Γ_0 and Γ_4, see Fig. D.4. Consequently, the closed curve $2\gamma_0$ depends smoothly on the deformation parameter (m,h) when $(m,h) \in [\Gamma_0, \Gamma_4] \subset \Gamma$.

In order to deform the curve $2\gamma_0$ between Γ_4 and Γ_6 we need to replace the initial curve by homotopically equivalent curve at Γ_4 and then to deform the replacement curve between Γ_4 and Γ_6.

At Γ_4 the double loop $s^1_{m,h}s^1_{m,h}$ represented as $O\beta^1 o\alpha^1 O\beta^1 o\alpha^1 O$ on Fig. D.8 (intersection line $s^1_{\Gamma_4}$ in σ) and as $OoOoO$ on Fig. 9 (intersection line OoO on Λ_{Γ_4} torus chart) is replaced by the cycle

$$r := s^1_{m,h}[O\beta^1] \cup \mathcal{I}_{m,h}[\beta^1\beta^3] \cup s^3_{m,h}[\beta^3 B\alpha^3] \cup \mathcal{I}_{m,h}[\alpha^3\alpha^1] \cup s^1_{m,h}[\alpha^1 O] \cup \gamma^f_{m,h}[\alpha^1\alpha^1]$$

which can be smoothly deformed between Γ_4 and Γ_6. The cycle r belongs to torus $\Lambda_{m,h}$ but it does not belong completely to σ. It consists of fragments $s^1_{m,h}[O\beta^1]$, $s^1_{m,h}[\alpha^1 O]$, and $s^3_{m,h}[\beta^3 B\alpha^3]$ which belong to $\Lambda_{m,h}$ and to σ simultaneously. It includes also two shadow fragments $\mathcal{I}_{m,h}[\beta^1\beta^3]$ and $\mathcal{I}_{m,h}[\alpha^3\alpha^1]$ which lie on $\Lambda_{m,h}$ but not on σ. These two fragments belong to small neighborhood U of axis p_1 and are close to points β and α respectively. Finally, $\gamma^f_{m,h}[\alpha^1\alpha^1] = \alpha^1(-\gamma_f)\alpha^1$ is a properly oriented complete closed trajectory of the system with Hamiltonian F_1 through the point α^1.

The curve r can be obtained from the double loop $s^1_{m,h}s^1_{m,h}$ represented on the torus chart in Fig. 9 as $O\beta^1 o\alpha^1 O\beta^1 o\alpha^1 O$ by cutting the double loop at point α^1 and by introducing the fragment

$$r_0 := s^1_{m,h}[\alpha^1 o\beta^1 O\alpha^1 o\beta^1] \cup \mathcal{I}_{m,h}[\beta^1\beta^3] s^3_{m,h}[\beta^3 B\alpha^3] \cup \mathcal{I}_{m,h}[\alpha^3\alpha^1] \cup \gamma^f_{m,h}[\alpha^1\alpha^1].$$

Thus in order to prove that the double loop $2\gamma_0$ and the curve r are homotopic, it is sufficient to prove that the closed curve r_0 is homotopic to a point on the torus $\Lambda_{m,h}$, $(m,h) = \Gamma_5$.

Let us consider on torus Λ_{Γ_5}, which is close to Λ_{Γ_4}, the closed curve $\tilde{r_0} \subset \Lambda_{\Gamma_5}$ which is close to curve $\gamma_0 \subset \Lambda_{\Gamma_4}$. Using straightening coordinates ψ mod 2π (see Lemma D.9) we construct a closed curve $\overline{r_0} \subset \Lambda_{\Gamma_5}$ which is close to the $\tilde{r_0}$ curve but is composed from straight segments forming the polygonal line, represented in Fig. D.16. Lifting $\overline{r_0}$ up to the covering space $\mathbb{R}^2_\psi$ we see that the lifted curve remains closed. Thus the $\overline{r_0}$ curve and the nearby loops $\tilde{r_0}$ and r_0 are homotopic to zero on respective tori.

Let us now consider the deformation $\{r_{m,h}, (m,h) \in [\Gamma_4, \Gamma_6]\}$ of the curve $r = r_{\Gamma_4}$. For all fragments forming r only index (m,h) is varying. In addition, when passing through $m = 0$, the upper index changes from 1 and 3 to 4. This transformation is obviously continuous. At the end of deformation, the $\mathcal{I}_{m,h}[\alpha^4\alpha^4]$ and $\mathcal{I}_{m,h}[\beta^4\beta^4]$ fragments become points. Consequently, the curve r after such a deformation becomes

$$s^4_{m,h}[O\beta^4] \cup s^4_{m,h}[\beta^4 B\alpha^4] \cup s^4_{m,h}[\alpha^4 O] \cup \gamma^f_{m,h}[\alpha^4\alpha^4]$$

and coincides with $s^4_{m,h} \cup \gamma^f_{m,h}$. This cycle consists at point Γ_6 of two loops represented in Fig. 9 as $OBO - \gamma_f$. Namely, OBO is the connected component of the intersection line λ_{Γ_4} and $-\gamma_f$ is the trajectory of the system with Hamiltonian F_1 taken with proper orientation.

The deformation along $[\Gamma_6, \Gamma_0] \subset \Gamma$ is obviously continuous for $s^2_{m,h}$ and for $s^4_{m,h}$. We are interested only in deformation of the $s^4_{m,h}$ component which is represented at point Γ_6 by the closed loop OBO. Nothing happens with the loop γ_f.

Under the deformation between Γ_6 and Γ_0 the cycle OBO undergoes the non-smooth modification when (m,h) pass the point Γ_8, see Lemma D.7. Namely at this point the loop OBO becomes a figure-eight loop (see Figs. D.10, D.12) due

to the identification of the two points which belong to the Z_2 symmetric trajectory of X_{F_1} and further transforms to two loops OO and BB (see Figs. 8, 7, D.12).

Thus the construction of the continuous deformation of the closed double loop $2\gamma_0$ is completed. After the deformation along directed counterclockwise closed path Γ, the initial cycle $2\gamma_0 = OoOoO$ becomes the cycle $OO + BB - \gamma_f$. Each of the two loops OO and BB is homotopic to the initial loop γ_0. The loop $(-\gamma_f)$ is the properly oriented trajectory of X_{F_1}. Together with the trivial evolution of the cycle γ_f this gives the transformation of cycles corresponding to the basis of the subgroup of the first homology group $H_1(\Gamma_0)$ associated to a closed path Γ

$$(\gamma_f, 2\gamma_0) \to (\gamma_f, 2\gamma_0 - \gamma_f). \tag{D.20}$$

This completes the proof of Theorem 2.

Acknowledgments

We thank Drs. R.H. Cushman and K. Efstathiou for many stimulating discussions and comments. N.N. Nekhoroshev acknowledges CNRS for the six month position at Université du Littoral in Dunkerque in 2002, which made this work possible. B. Zhilinskii thanks IHES, Bures-sur-Yvette, France, and Mathematical Institute, University of Warwick, UK, for support during his sabbatical year 2001–2002. This work is part of the European project *Mechanics and Symmetry in Europe* (*MASIE*), contract HPRN-CT-2000-00113.

Bibliography

[1] Vl.I. Arnol'd, *Mathematical Methods of Classical Mechanics*, vol. 60 of *Graduated Texts in Mathematics*, 2nd edition. Translated by K. Vogtmann and A. Weinstein, Springer-Verlag, New York, 1989. Original Russian edition *Matematicheskie Metody Klassicheskoí Mekhaniki*, Nauka, Moscow, 1974.

[2] Vl.I. Arnol'd, V.V. Kozlov, and A.I. Neíshtadt, *Mathematical Aspects of Classical and Celestial Mechanics. Dynamical Systems III*, volume 3 of *Encyclopedia of Mathematical Sciences* (Springer-Verlag, Berlin, 1988).

[3] M.F. Atiyah, *Convexity and commuting Hamiltonians*, Bull. London Math. Soc., **14** (1982), 1–15.

[4] M.F. Atiyah and R. Bott, *The moment map and equivariant cohomology*, Topology **23** (1984), 1–28.

[5] M. Audin, *Hamiltonian monodromy via Picard-Lefschetz theory*, Commun. Math. Phys. **229** (2002), 459–489.

[6] L. Bates, *Monodromy in the champagne bottle*, J. Appl. Math. Phys. (ZAMP) **42** (1991), 837–847.

[7] L. Bates and M. Zou, *Degeneration of Hamiltonian monodromy cycles*, Nonlinearity **6** (1993), 313–335.

[8] A.V. Bolsinov and A.T. Fomenko, *Geometry and topology of integrable geodesic flows on surfaces*, in Ser. Regular and Chaotic Dynamics, Vol. II, Editorial URSS, Moscow, 1999.

[9] A.V. Bolsinov and A.T. Fomenko, *Integrable Hamiltonian Systems. Geometry, Topology, Classification*, Chapman & Hall/CRC, London, 2004.

[10] A. Bolsinov and V.S. Matveev, *Singularities of momentum maps of integrable Hamiltonian systems with two degrees of freedom*, J. Math. Sci. New York **94**, No. 4 (1999), 1477–1500; translated from Zap. Nauchn. Semin. POMI **235** (1996), 54–86.

[11] S. Brodersen and B.I. Zhilinskiĭ, *Transfer of clusters between the vibrational components of CF_4*, J. Mol. Spectrosc. **169** (1995), 1–17.

[12] M.S. Child, T. Weston, and J. Tennyson, *Quantum monodromy in the spectrum of H_2O and other systems*, Mol. Phys. **96** (1999), 371–379.

[13] Y. Colin de Verdière and S. Vũ Ngọc, *Singular Bohr-Sommerfeld rules for* 2D *integrable systems*, Ann. Ec. Norm. Sup. **36** (2003), 1–55.

[14] R.H. Cushman, *Geometry of the energy momentum mapping of the spherical pendulum*, Centrum voor Wiskunde en Informatica Newsletter **1** (1983), 4–18.

[15] R.H. Cushman and L.M. Bates, *Global aspects of classical integrable systems*, Birkhäuser, Basel, 1997.

[16] R.H. Cushman and J.J. Duistermaat, *The quantum mechanical spherical pendulum*, Bull. Am. Math. Soc. **19** (1988), 475–479.

[17] R.H. Cushman and J.J. Duistermaat, *Non-Hamiltonian monodromy*, J. Diff. Eq. **172** (2001), 42–58.

[18] R.H. Cushman and D.A. Sadovskiĭ, *Monodromy in the hydrogen atom in crossed fields*, Physica D **142** (2000), 166–196.

[19] R.H. Cushman and S. Vũ Ngọc, *Sign of the monodromy for Liouville integrable systems*, Annales Henri Poincaré, **3** (2002), 883–894.

[20] P. Dazord and T. Delzant, *Le problème général des variables action-angles*, J. Diff. Geom. **26** (1987), 223–251.

[21] G. Dhont, D.A. Sadovskiĭ, B.I. Zhilinskiĭ, and V. Boudon, *Analysis of the "unusual" vibrational components of triply degenerate vibrational mode ν_6 of $Mo(CO)_6$ based on the classical interpretation of the effective rotation-vibration Hamiltonian*, J. Mol. Spectrosc. **201** (2000), 95–108.

[22] J.J. Duistermaat, *On global action angle coordinates*, Comm. Pure Appl. Math. **33** (1980), 687–706.

[23] J.J. Duistermaat, G.L. Heckman, *On the variation in the Cohomology of the Symplectic Form of the Reduced Phase Space*, Invent. math. **69** (1982), 259–268.

[24] H. Dullin, A. Giacobbe, and R.H. Cushman, *Monodromy in the resonant swing spring*, Physica D. **190** (2003), 15–37.

[25] K. Efstathiou, R.H. Cushman, and D.A. Sadovskiĭ, *Fractional monodromy in the* $1{:}(-2)$ *resonance*, Adv. Math. in press.

[26] K. Efstathiou, *Metamorphoses of Hamiltonian Systems with Symmetries*, Springer, LNM 1864, 2005.

[27] F. Faure and B.I. Zhilinskiĭ, *Topological Chern indices in molecular spectra*, Phys. Rev. Lett. **85** (2000), 960–963.

[28] F. Faure and B.I. Zhilinskiĭ, *Topological properties of the Born-Oppenheimer approximation and implications for the exact spectrum*, Lett. Math. Phys. **55** (2001), 219–238.

[29] F. Faure and B.I. Zhilinskií, *Topologically coupled energy bands in molecules*, Phys. Lett. A **302** (2002), 242–252.

[30] A. Giacobbe, R.H. Cushman, D.A. Sadovskií, and B.I. Zhilinskií, *Monodromy of the quantum* 1:1:2 *resonant swing spring*, J. Math. Phys. **45** (2004), 5076–5100.

[31] L. Grondin, D.A. Sadovskií, and B.I. Zhilinskií, *Monodromy in systems with coupled angular momenta and rearrangement of bands in quantum spectra*, Phys. Rev. A **142** (2002), 012105-1–15.

[32] M. Gross, Special Lagrangian Fibrations. I. Topology, in: *Integrable Systems and Algebraic Geometry*, Ed. by M.-H. Saito, Y. Shimuzu, and K. Ueno, World Scientific 1998, 156–193.

[33] M. Gross, Special Lagrangian Fibrations. II: Geometry, in: *Surveys in Differential Geometry*, Somerville, MA, International Press 1999, 341–403.

[34] M. Gross, *Topological mirror symmetry*, Invent. math. **144** (2001), 75-137.

[35] V. Guillemin, *Moment Map and Combinatorial Invariants of Hamiltonian T^n-Spaces*, Progress in Mathematics vol. 122, Birkhäuser Boston, 1994.

[36] V. Guillemin, V. Ginzburg, and Y. Karshon, *Moment map, cobordisms, and Hamiltonian group actions,* AMS, Mathematical surveys and monographs, no. 98, Rhode Island, 2002.

[37] V. Guillemin and A. Uribe, *Monodromy in the quantum spherical pendulum*, Comm. Math. Phys. **122** (1989), 563–574.

[38] J.M. Jauch and E.L. Hill, *On the problem of degeneracy in quantum mechanics*, Phys. Rev. **87** (1940), 641–645.

[39] M. Kleman, *Points, Lines and Walls.* (Chichester: Wiley), 1983.

[40] M. Kontsevich and Y. Soibelman, *Affine structure and non-archimedean analytic spaces*, preprint math.AG/0406564 (2004).

[41] I.N. Kozin and R.M. Roberts, *Monodromy in the spectrum of a rigid symmetric top molecule in an electric field*, J. Chem. Phys. **118** (2003), 10523–10533.

[42] E. Kroner, Continuum theory of defects, in *Physics of defects*. Les Houches, Ecole d'été de physique théorique, Elsevier, New York, 1981; pp. 215–315.

[43] L.M. Lerman and Ya.L. Umanskií, *Four dimensional integrable Hamiltonian systems with simple singular points*, Transl. Math. Monographs **176**, American Math. Soc., Providence, R.I., 1998.

[44] Y. Matsumoto, *Torus fibrations over the two sphere with the simplest singular fibers*, J. Math. Soc. Japan **37** (1985), 605–636.

[45] V.S. Matveev, *Integrable Hamiltonian systems with two degrees of freedom. The topological structure of saturated neighborhoods of points of focus-focus and saddle-saddle type*, Sb. Math. **187** No.4 (1996), 495–524.

[46] V.S. Matveev, Integrable Hamiltonian systems with two degrees of freedom: topological structure of saturated neighborhoods of points of focus-focus and saddle-saddle types, in: *Tensor and vector analysis*, pp. 31–56, Gordan and Breach, Amsterdam, 1998.

[47] N.D. Mermin, *The topological theory of defects in ordered media*, Rev. Mod. Phys. **51** (1979), 591–648.

[48] L. Michel, *Symmetry defects and broken symmetry. Configurations. Hidden symmetry*, Rev. Mod. Phys. **52** (1980), 617–651.

[49] L. Michel and B.I. Zhilinskiĭ, *Symmetry, invariants, topology. I. Basic tools*, Phys. Rep. **341** (2001), 11–84.

[50] L. Michel and B.I. Zhilinskiĭ, *Symmetry, invariants, topology. III. Rydberg states of atoms and molecules. Basic group-theoretical and topological analysis*, Phys. Rep. **341** (2001), 173–264.

[51] H. Mineur, *Réduction des systèmes mécaniques a n degrès de liberté admettant n intégrales premières uniformes en involution aux systèmes à variables séparées*, J. Math. Pures Appl. **15** (1936), 385-389.

[52] D. Montgomery and H. Samuelson, *Fiberings with singularities*, Duke Math. J. **3** (1946), 51–56.

[53] N.N. Nekhoroshev, *Two theorems on the action-angle variables*, Uspekhi Mat. Nauk **24** (1969), 237–238; Adv. Math. Sci. (USSR).

[54] N.N. Nekhoroshev, *Action-angle variables and their generalizations*, Trans. Moscow Math. Soc. **26** (1972), 180–198.

[55] N.N. Nekhoroshev, *Theorem of Poincaré-Lyapunov-Liouville-Arnol'd*, Funk. Analiz **28** (1994), 3.

[56] N.N. Nekhoroshev, D.A. Sadovskiĭ, and B.I. Zhilinskiĭ, *Fractional monodromy of resonant classical and quantum oscillators*, C. R. Acad. Sci. Paris, Ser. I, **335** (2002), 985–988.

[57] V.B. Pavlov-Verevkin, D.A. Sadovskiĭ, and B. Zhilinskiĭ, *On the dynamical meaning of the diabolic points*, Europhys. Lett. **6** (1988), 573–578.

[58] B. Rink, *Cantor sets of tori with monodromy near focus-focus singularities*, Nonlinearity, **17** (2004), 347–356.

[59] D. Sadovskiĭ and B. Zhilinskiĭ, *Qualitative analysis of vibration-rotation Hamiltonians for spherical top molecules*, Mol. Phys. **65** (1988), 109–128.

[60] D.A. Sadovskiĭ and B.I. Zhilinskiĭ, *Monodromy, diabolic points, and angular momentum coupling*, Phys. Lett. A **256** (1999), 235–244.

[61] H. Seifert, *Topologie dreidimensionaler gefaster Räume*, Acta Math. **60** (1933), 147–238. H. Seifert, W. Threlfall, *A Textbook of Topology*, Academic Press, New York, 1980.

[62] R.P. Stanley, *Enumerative Combinatorics*, Wadsworth & Brooks/Cole, Montrey, CA, 1986; Vol. 1, Chapt. 4.4.

[63] V. A. Vassiliev, *Applied Picard-Lefschetz Theory*, Amer. Math. Soc. Providence: 2002.

[64] S. Vũ Ngọc, *Quantum monodromy in integrable systems*, Comm. Math. Phys. **203** (1999), 465–479.

[65] S. Vũ Ngọc, *Moment polytopes for symplectic manifolds with monodromy*, Preprint Institut Fourier, 2005; math.SG/0504165.

[66] H. Waalkens and H.R. Dullin, *Quantum monodromy in prolate ellipsoidal billiards*, Ann. Phys. (N.Y.) **295** (2001), 81–112.

[67] H. Waalkens, A. Junge, and H.R. Dullin, *Quantum monodromy in the two-center problem*, J. Phys. A. Math. Gen. **36** (2003), L307–L314; H. Waalkens, H.R. Dullin, and P.H. Richter, *The problem of two fixed centers: bifurcations, actions, monodromy*, Physica D, **196** (2004), 265–310.

[68] B.I. Zhilinskiĭ, *Topological and symmetry features of intramolecular dynamics through high resolution molecular spectroscopy*, Spectrochim. Acta A **52** (1996), 881–900.

[69] B.I. Zhilinskiĭ, *Symmetry, invariants, and topology in molecular models*, Phys. Rep. **341** (2001), 85–171.

[70] B.I. Zhilinskiĭ, *Interpretation of quantum Hamiltonian monodromy in terms of lattice defects*, Acta Appl. Math. **87** (2005), 281–307.

[71] B.I. Zhilinskiĭ, Hamiltonian monodromy as lattice defect, In *Topology in Condensed Matter*, Springer Series in Solid-State Sciences, Vol. 150, 2006, pp. 165–186; arXiv:quant-ph/0303181 (2003).

[72] B.I. Zhilinskiĭ and S. Brodersen, *Symmetry of vibrational components in* T_d *molecules*, J. Mol. Spectrosc. **163** (1994), 326–338.

[73] N.T. Zung, *A note on focus-focus singularities*, Diff. Geom. Appl. **7** (1997), 123–130.

[74] N.T. Zung, *Another note on focus-focus singularities*, Lett. Math. Phys. **60** (2002), 87–99.

Nikolaiĭ N. Nekhoroshev [*] [‡], Dmitriĭ A. Sadovskiĭ, Boris I. Zhilinskiĭ
Université du Littoral
UMR 8101 du CNRS
189A, av. M. Schumann, MREI
F-59140 Dunkerque
France
e-mail: nekhoros@mech.math.msu.su
Nikolai.Nekhoroshev@mat.unimi.it
sadovski@univ-littoral.fr
zhilin@univ-littoral.fr

Communicated by Eduard Zehnder
Submitted: February 25, 2005
Accepted: November 17, 2005

[*]Department of Mathematics and Mechanics, Moscow State University, Moscow 119 992, GSP-2, Russia.
[‡]Dipartimento di Matematica "Federigo Enriques", Universita degli studi di Milano, via C. Saldini 50, I-20133 Milano, Italy.